EXPERIMENTAL MEASUREMENTS OF VESTIBULAR HAIR BUNDLE STIFFNESS IN THE RED EAR SLIDER TURTLE UTRICLE

Jennifer Mary Silverman

Thesis submitted to the Faculty of the
Virginia Polytechnic Institute and State University
in partial fulfillment of the requirements for the degree of

MASTER OF SCIENCE

in

Engineering Mechanics

J.Wallace Grant, Chair
Don H. Morris
Ellengene H. Peterson

July 31, 2002
Blacksburg, Virginia

Keywords: Utricle, Vestibular System, Hair Cell, Stiffness

Copyright 2002, Jennifer M. Silverman

EXPERIMENTAL MEASUREMENTS OF VESTIBULAR HAIR BUNDLE STIFFNESS IN THE RED EAR SLIDER TURTLE UTRICLE

by
Jennifer Mary Silverman
Committee Chairman: J.W. Grant
Engineering Mechanics

(Abstract)

The ear is the organ used for hearing and maintaining equilibrium. In the inner ear, the vestibular system is responsible for the sense of balance. The main organs of the vestibular system are the semicircular canals, the saccule, and the utricle. Within each of the vestibular organs, sensory receptors in the form of hair cells detect motion and send a message to the brain for interpretation. Hair cells found in different parts of the inner ear are structurally different and are mechanically specialized to perform different functions. In this study, the linear and torsional stiffnesses were measured for hair cells located in the red ear slider turtle utricle. The system used to measure the stiffnesses was composed of a glass whisker (attached to a pipette) used to produce a force on the tip of the bundle, an extrinsic Fabry-Perot interferometer (EFPI) to measure the displacement of the pipette, and a photoelectronic motion transducer (PMT) to measure the displacement of the bundle. Using the measured values of whisker stiffness, whisker displacement, and bundle displacement, the stiffness of the bundle was calculated using statics. For each bundle tested, the location of the bundle was determined by measuring its position from a landmark in the utricle, the line of polarity reversal, characterized by a 180^{o} change in direction of the hair bundles. Stiffness results showed that the linear stiffness of a bundle increased in the area surrounding the line of polarity reversal, otherwise referred to as the striolar region (average linear stiffness of 2.27 E-04 N/m). The average linear stiffness value of bundles found lateral to the striolar region was 6.30 E-05 N/m and in the region medial to the striolar region was 1.16 E-04 N/m. A wide range of linear stiffnesses were found in hair cells medial to the striolar region. There was no correlation found between the torsional stiffness of a bundle and its position and the height of a bundle and its linear or torsional stiffness. As the force applied to a hair bundle was increased, the measured linear stiffness of the bundle also increased.

ACKNOWLEDGEMENTS

I would like to thank Dr. J.W. Grant, my advisor and committee chair for advising me throughout my undergraduate and graduate careers at Virginia Tech. I attribute my academic success to his continued support and guidance.

I would also like to thank Dr. E. H. Peterson and Dr. D.H. Morris for their service on my graduate committee. Dr. Peterson was a valuable source for the statistical analysis of my data.

A special thanks to Kirsten Felsted. She came into the lab a few months before the completion of my project and quickly learned the procedure and techniques. Her assistance was greatly appreciated. I would like to thank Joe Silber for keeping me company in the lab and assisting me with any questions I had about the project.

Finally, I would like to thank my family and friends. My parents, Paul and Darlene, and my siblings, Dan, Amy, Sean, Misty, Mike, Moira, and Kristie, provided me with endless support and encouragement. And to my friends, I thank you for your support and for providing an opportunity for me to escape the stresses of school.

TABLE OF CONTENTS

LIST OF FIGURES

LIST OF TABLES

CHAPTER 1: INTRODUCTION

The ear is an important organ animals utilize as a tool for communicating. People immediately recognize the ear as the hearing organ. Another essential function of the ear is sensing and maintaining balance. The term "ear" is used to define the structure that contains the organs responsible for hearing and equilibrium (Geisler, 1998). The anatomy of the human ear (Figure 1.1) includes the outer ear or the pinna, located on the side of the head, the middle ear containing the auditory ossicles (a three-bone structure made up of the malleus, incus, and stapes), and the inner ear. The inner ear houses a membranous labyrinth that contains the sensory organs used in hearing and the vestibular system used in equilibrium (Geisler, 1998).

The following sections will introduce the anatomy and physiology of the inner ear and more specifically, the vestibular system. The background provided will be essential in understanding the work presented in this paper.

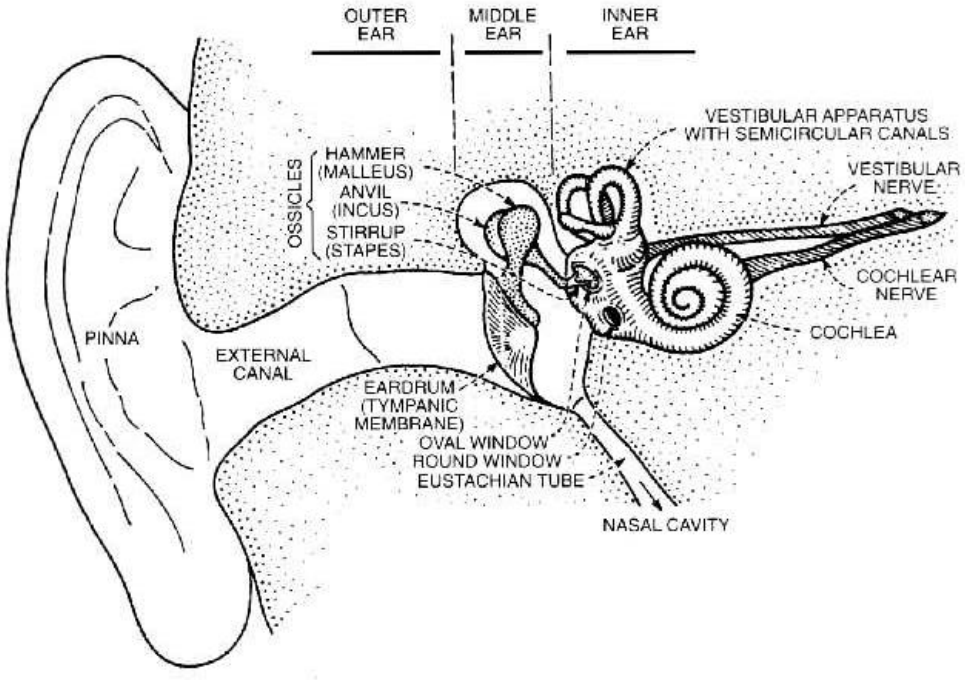

Figure 1.1 Anatomy of the human ear (Flanagan, 1972).
The ear is composed of the outer ear, the middle ear, and the inner ear.

THE INNER EAR

The human inner ear lies within the temporal bone and is composed of the organs of equilibrium or the vestibular system and the organ of hearing or the cochlea (Klinke, 1986). The inner ear is made up of two parts, the bony labyrinth and the membranous labyrinth (Figure 1.2). The bony labyrinth, or the osseous labyrinth, encloses and protects the membranous labyrinth. The tubes of the membranous labyrinth (Figure 1.3), made up of simple epithelium and containing the sensory organs, fit through the cavities of the osseous labyrinth (Kelly, 1981). Fluid that is enclosed by the osseous labyrinth, but is on the outside of the membranous labyrinth is called perilymph. Contained within the membranous labyrinth is another fluid, endolymph. Endolymph is a viscous fluid produced by the stria vascularis of the cochlear duct and has a composition similar to that of intracellular fluid. The vestibule is the middle portion of the osseous labyrinth and houses the vestibular organs, the utricle, saccule, and the semicircular canals. The hearing organ, the cochlea, is a helical tube consisting of two and three fourths turns, resembling the shell of a snail. The organs of hearing and equilibrium are linked and are both supplied by the eighth cranial nerve (Singh, 1980).

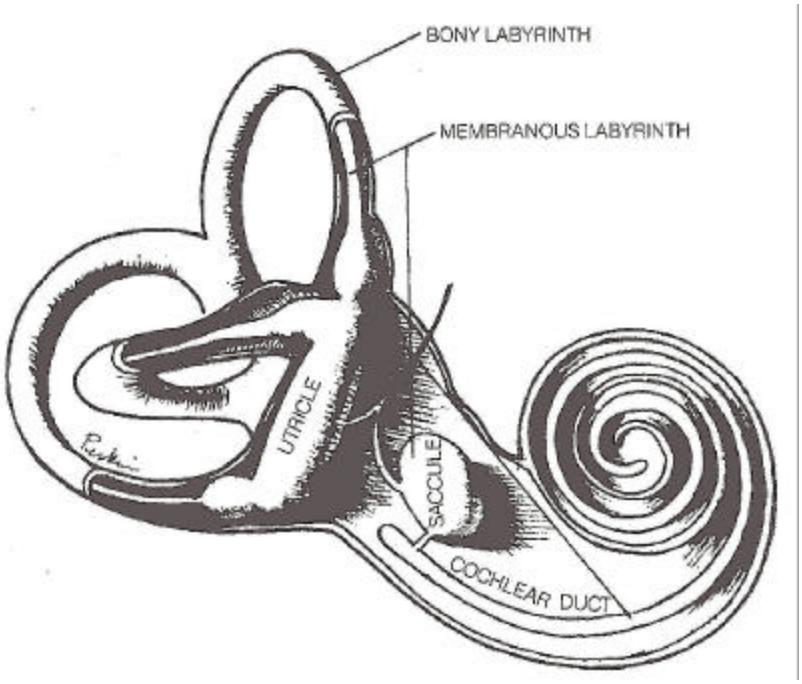

Figure 1.2 Bony and membranous labyrinths in humans (Perkins and Kent, 1986).
The membranous labyrinth of the human inner ear fits into the bony labyrinth.

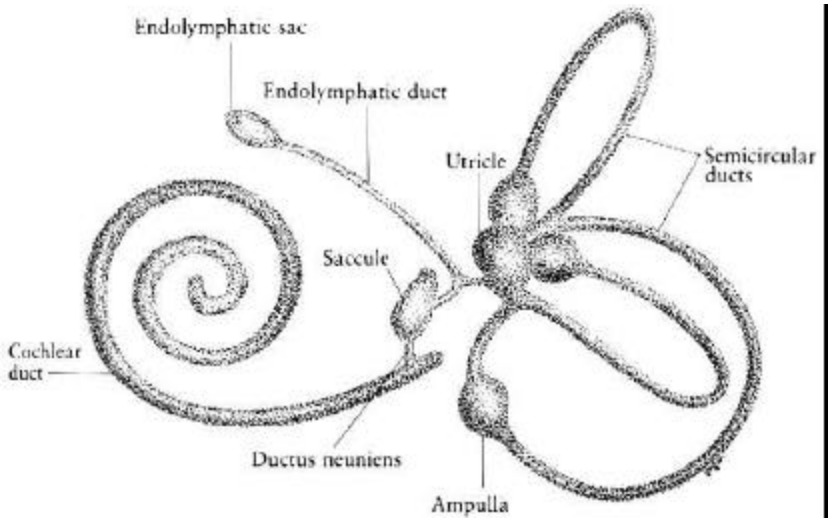

Figure 1.3 The human membranous labyrinth (Singh, 1980).
The human membranous labyrinth is composed of the three semicircular ducts, the utricle, the saccule, and the cochlear duct.

EQUILIBRIUM

The vestibular system, located in the inner ear, is used to maintain equilibrium by coordinating motor responses, eye movements, and posture (Kelly, 1981). By coordinating head and eye movements, the vestibular system allows for the eyes to remain fixed on a point when the head is in motion. The vestibular organs include the otolith organs, the utricle and saccule, and the semicircular canals (Figure 1.4). Located within each of these organs are sensory mechanoreceptors in the form of hair cells. The vestibular hair cells respond to accelerations of the head or accelerations due to gravity (Kelly, 1981). The means by which these different vestibular organs detect motion is quite unique.

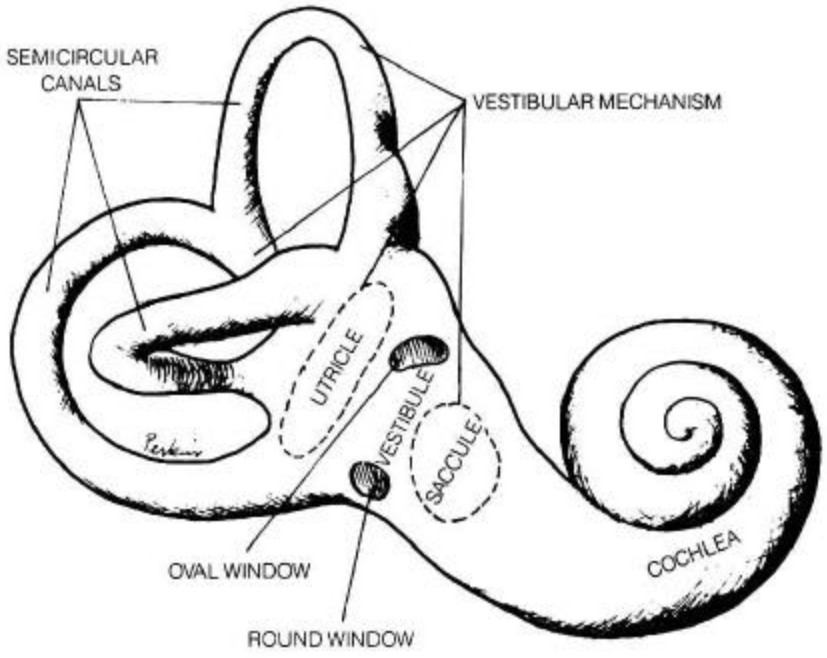

Figure 1.4 Human vestibular organs (Perkins and Kent, 1986).
Human vestibular organs consist of the utricle, the saccule, and the three orthogonal semicircular canals.

SEMICIRCULAR DUCTS

The human semicircular ducts, housed within the semicircular canals, are important in the detection of angular motion and in measuring the head's angular velocity. Three different semicircular ducts are located in different planes. The anterior and posterior ducts are located in the vertical plane at approximately right angles to each other. The lateral duct is in the horizontal plane when the head is tilted down 30^{o} (Singh, 1980) (Figure 1.5). Each duct forms two thirds of a circle and is ampullated at one end. The ampulla contains the sensory hair cells in a region referred to as the ampullary crest or crista (Figure 1.6). The ampullary crest contains the hair bundles embedded in a gelatinous mass, the cupula. When the head undergoes angular accelerations, the viscous endolymph in the semicircular ducts lags behind due to inertia and initiates fluid flow in the duct that results in pressure on the cupula (Figure 1.7). The motion of the cupula elicits a response in the hair cells (Kelly, 1981). Once again, this response is sent to the brain via the VIII cranial nerve for interpretation.

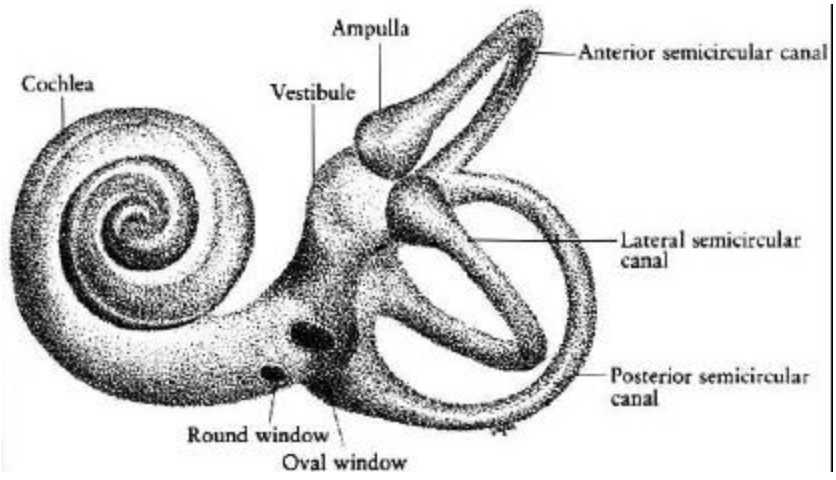

Figure 1.5 Orientation of the human semicircular canals in the vestibular system (Singh, 1980).

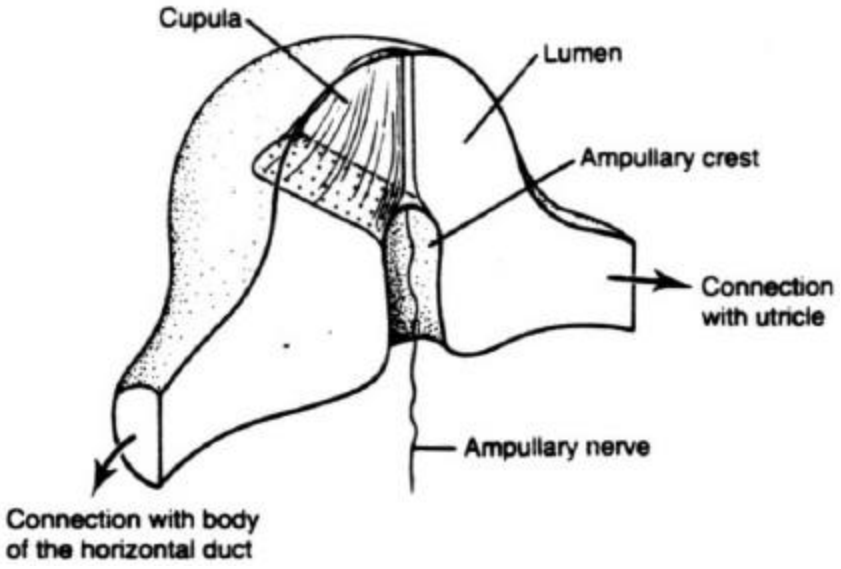

Figure 1.6 The ampulla of the semicircular ducts (Kelly, 1981).
The ampullary crest contains hair cells embedded in a gelatinous layer, the cupula.

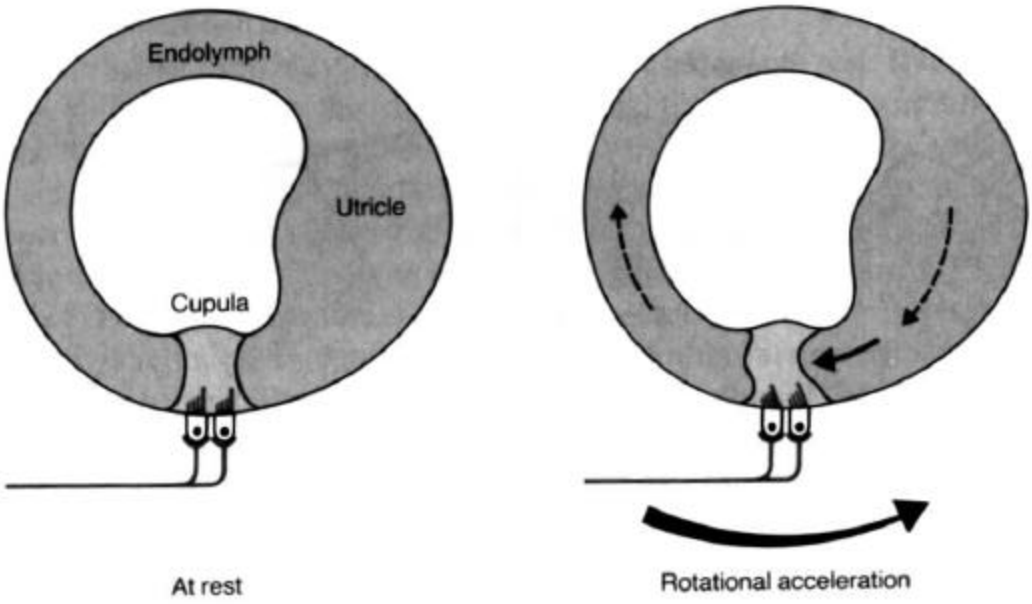

Figure 1.7 Positioning of the cupula during angular accelerations (Klinke, 1986).
During angular accelerations, the endolymph causes a force on the cupula resulting in a displacement of the cupula and the hair cells embedded in it.

UTRICLE AND SACCULE

The otolith organs, or the oval shaped utricle and the round shaped saccule, detect linear accelerations and help to determine the absolute position of the head in space during static conditions (Kelly, 1981). The principal receptor region of the otolith organs are the maculae. The maculae consists of neuroepithelial hair cells covered with a gelatinous layer, which is then covered with a layer of calcium carbonate crystals, otoconia, that are embedded in the gel (Figure 1.8). The entire substance and its contents are referred to as the otolith membrane (Klinke, 1986). The epithelium is connected to the otolithic membrane by a 5-8 μm thick column filament layer (Kachar et al, 1989). When the head is tilted, gravity will displace the otoconia, causing a disturbance in the gelatinous layer (Figure 1.9). This disturbance stimulates the hair cells to send a signal to the brain. Any acceleration of the head will displace the otoconial layer.

While both the utricle and the saccule contain the macula region, it is orientated in different directions. In the concave saccule, the macula it is orientated vertically, allowing the detection of motion in the vertical direction. The long axis of the macula is oriented in the anterior-posterior direction (Lewis, 1985). The saccular macula contains two populations of oppositely oriented hair cells. In the utricle, the macula is located horizontally, is somewhat concave, and allows the detection of motion in the horizontal direction (Lewis, 1985). There are two populations of oppositely orientated hair cells in the utricular macula. The boundary between these sets of cells is located in the striola region of the utricle and is referred to as the line of polarity reversal (Figure 1.10). The region lateral to the striolar region is the rampa and the region medial to the striolar region is the cotillus (Figure 1.11). The utricle will be the focus of this research project.

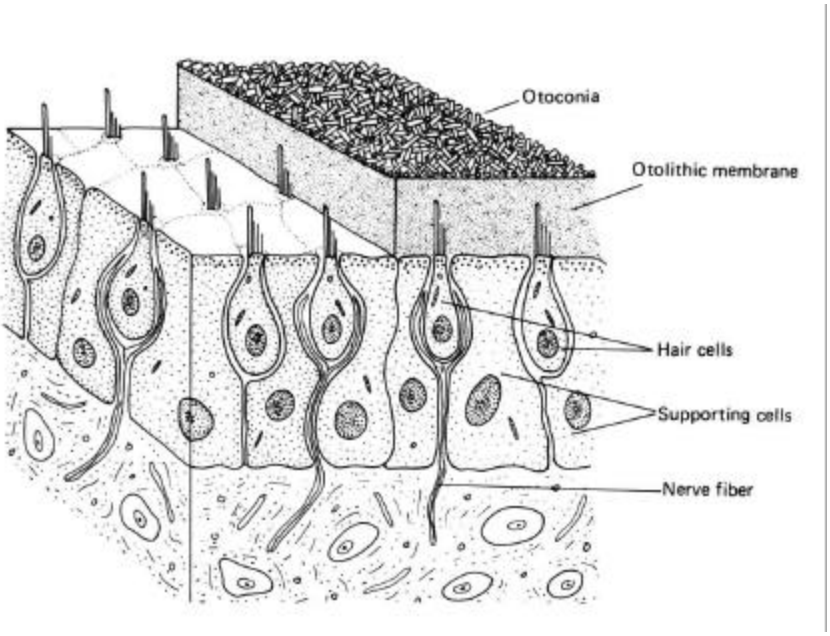

Figure 1.8 The otolithic membrane (Iurato, 1967).
The hair bundles are embedded in the otolithic membrane that is made up of a gel layer with otoconia crystals resting on top.

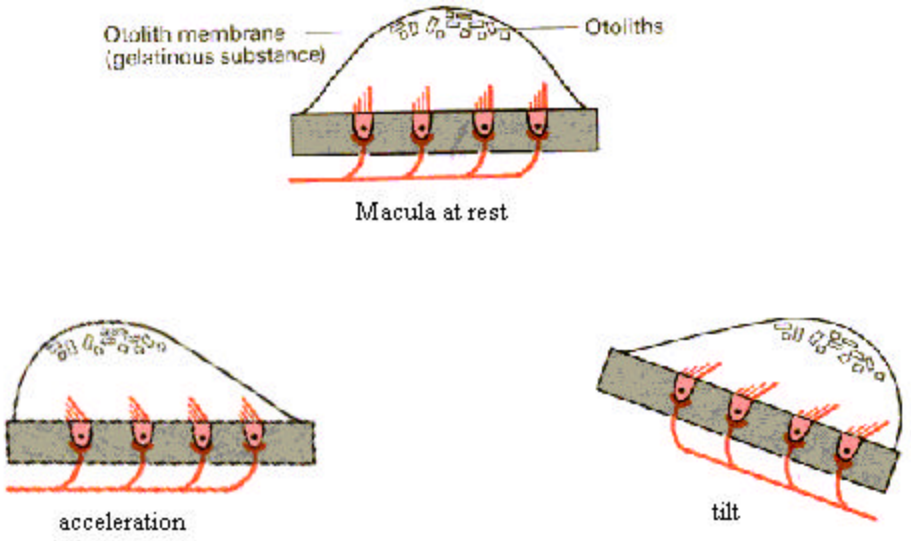

Figure 1.9 Displacement of the macula during motion (Klinke, 1986).
As the head is accelerated, the otoconia lag behind causing a disturbance in the gelatinous layer. As the head is tilted, gravity pulls the otoconia down, also causing a disturbance in the gelatinous substance, which in turn stimulates the hair cells.

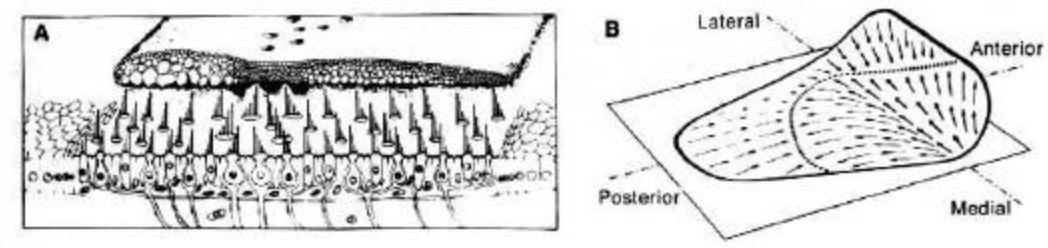

Figure 1.10 Hair bundle orientation in the utricle (Lindeman, 1973).
A. The utricular macula consists of two sets of oppositely oriented hair bundles. The imaginary boundary between them is referred to as the line of polarity reversal. **B.** The diagram shows the direction of hair cell polarization of the two populations of hair cells.

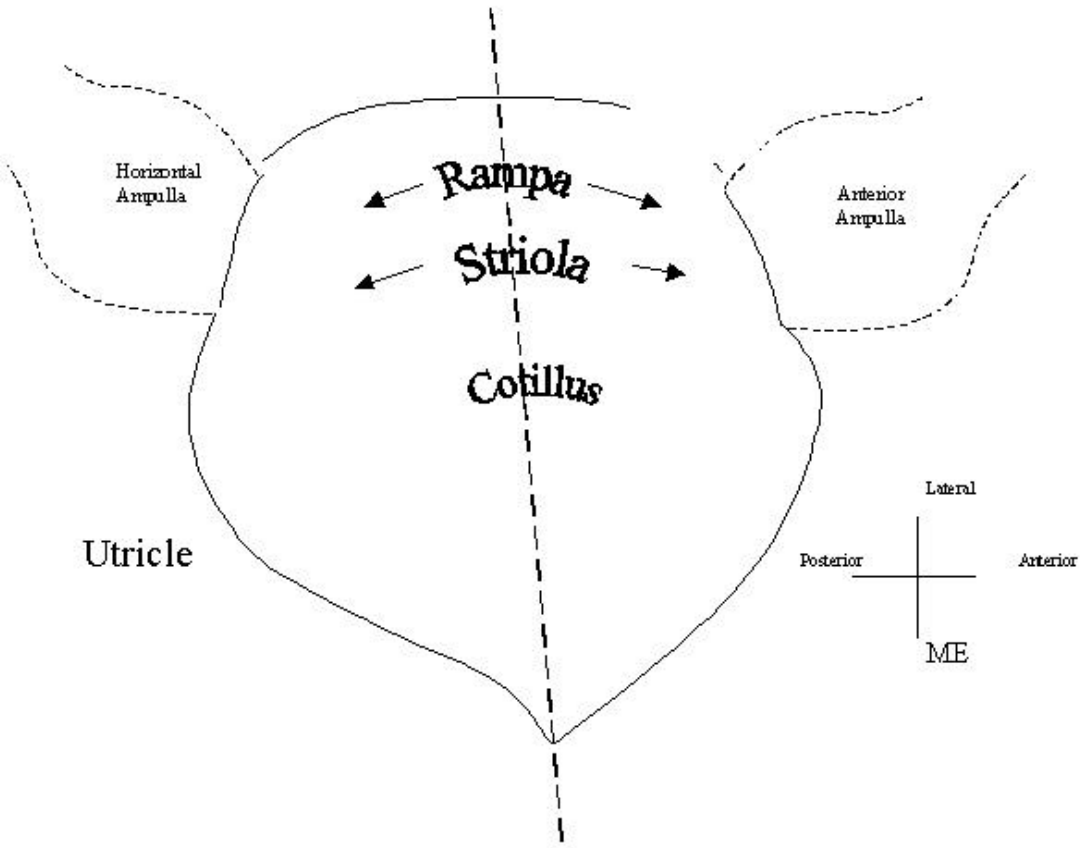

Figure 1.11 The regions of the utricle (Merkle, 2000).
The three main regions of the utricle are the rampa, the striola (the location of the line of polarity reversal), and the cotillus.

HAIR CELLS

The receptor responsible for detecting motion is called the hair cell. The hair cell consists of a cell body and an extending hair bundle, a group of hair-like projections that extend in to the surrounding fluid or gelatinous material (Hudspeth, 1983).

STRUCTURE

In the sensory epithelium there are two basic cell types, hair cells and supporting cells (Lewis, 1985). The hair cells of the inner ear are separated by supporting cells (Figure 1.12). Although the specific structure of a hair bundle differs among different species (Figure 1.13) and also differs within different areas of the organs of the inner ear, the basic structure is the same (Hudspeth, 1983). Each bundle is made up of 10-220 closely packed stereocilia, located in the cuticular plate (Figure 1.14), a dense filamentous mass beneath the surface, and usually one kinocilium, not located in the cuticular plate (Figure 1.15) (Lewis, 1985). The individual stereocilia are cylindrical shaped microvilli, composed of actin filaments tightly packed in hexagonal arrays. The stereocilia range in diameter from 0.2 micrometer to one micrometer (Figure 1.16). Each stereocilia is covered by a sheath membrane, the plasmalemma (Hudspeth, 1983). The stereocilia are connected to other adjacent stereocilia by tip links and lateral links (Figure 1.17). Each bundle includes a single kinocilium, with a diameter of approximately 0.25 micrometer (Geisler, 1998). Stereocilia lengths differ within a bundle and decrease as the distance from the kinocilium increases. The function of the kinocilium is not completely understood and its removal does not impair the transduction properties of the bundle (Geisler, 1998). The kinocilium is rigidly linked to adjacent stereocilia with lateral links.

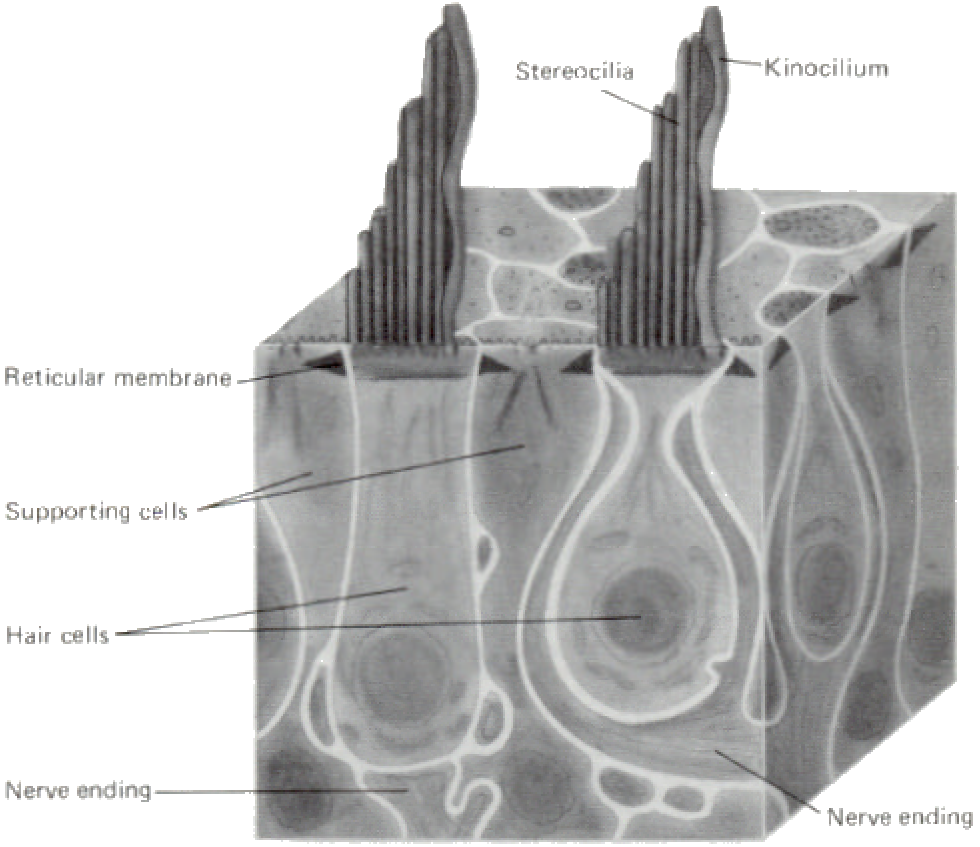

Figure 1.12 Hair cells are separated by supporting cells (Spoendlin, 1966).

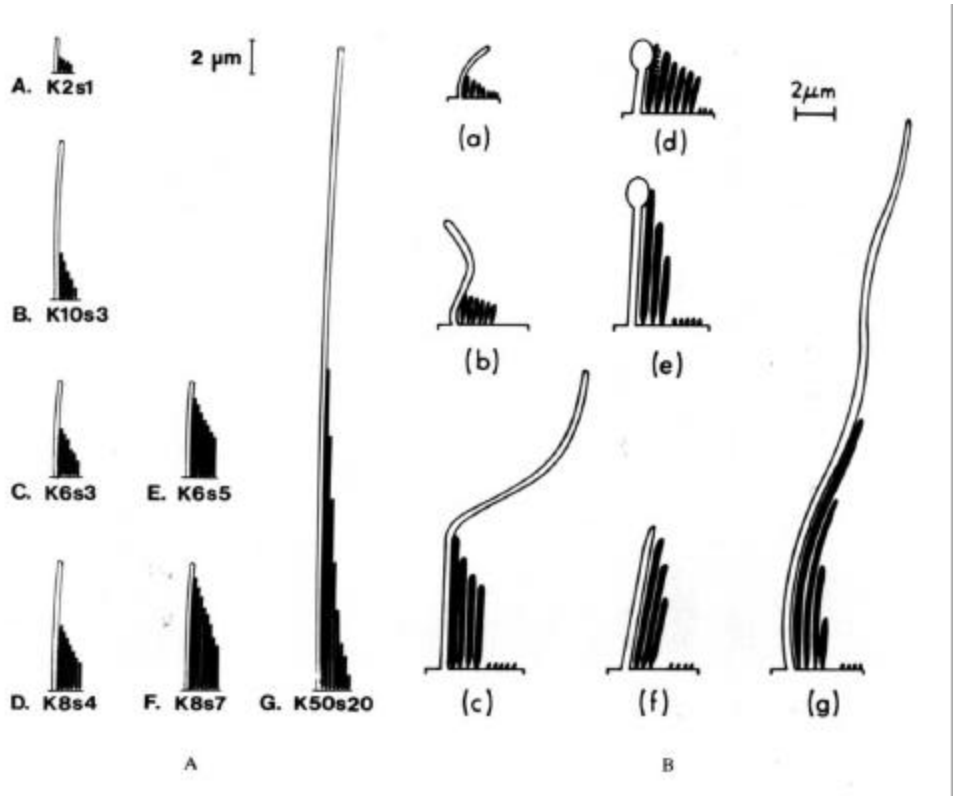

Figure 1.13 Different species of fish have different hair bundle structures (Lim, 1976).

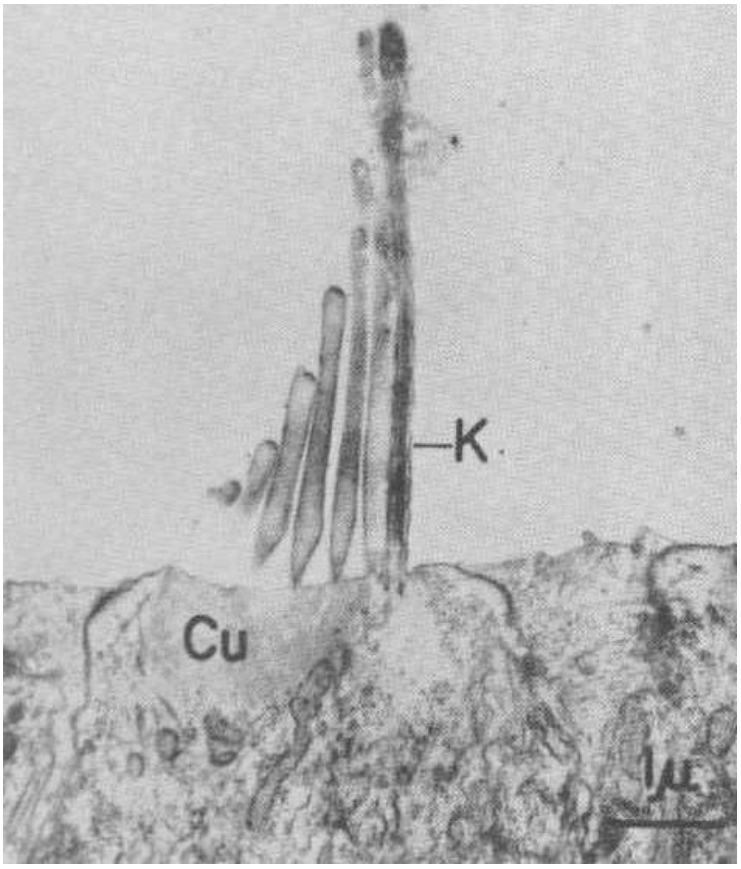

Figure 1.14 Location of the stereocilia and kinocilium within a hair bundle (Flock, 1965).
The stereocilia are located in the cuticular plate (**Cu**), while the kinocilium (**K**) is not.

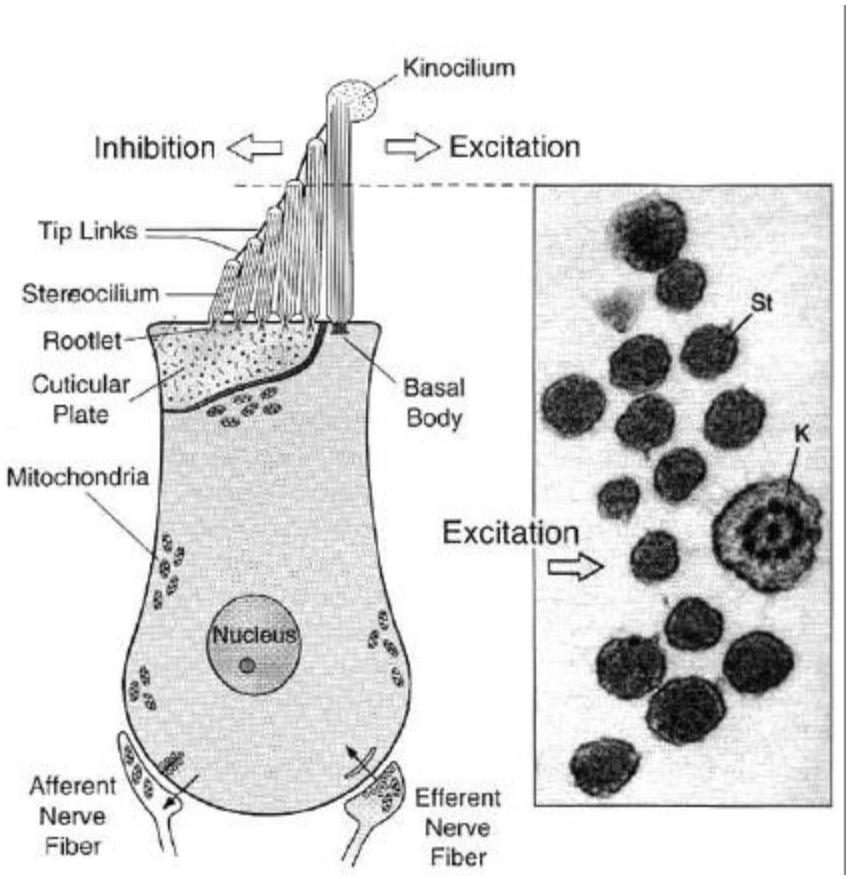

Figure 1.15 Structure of a bullfrog hair bundle (Geisler, 1998).
A typical hair bundle consists of a group of stereocilia and one kinocilium. Shown in this diagram is the direction of excitation and inhibition of a hair cell.

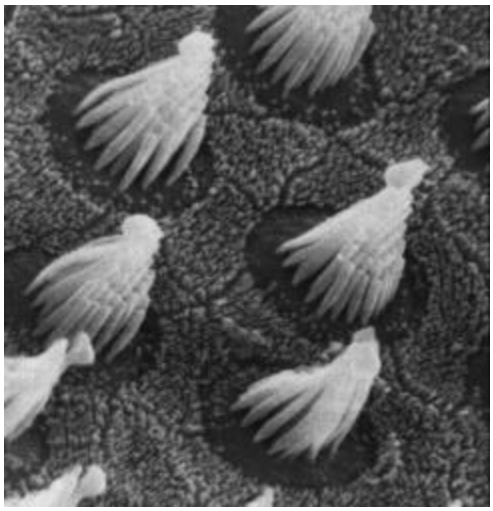

Figure 1.16 The stereocilia of a bullfrog hair bundle (Lewis, 1985).
Stereocilia are cylindrical shaped and are arranged in a hexagonal array.

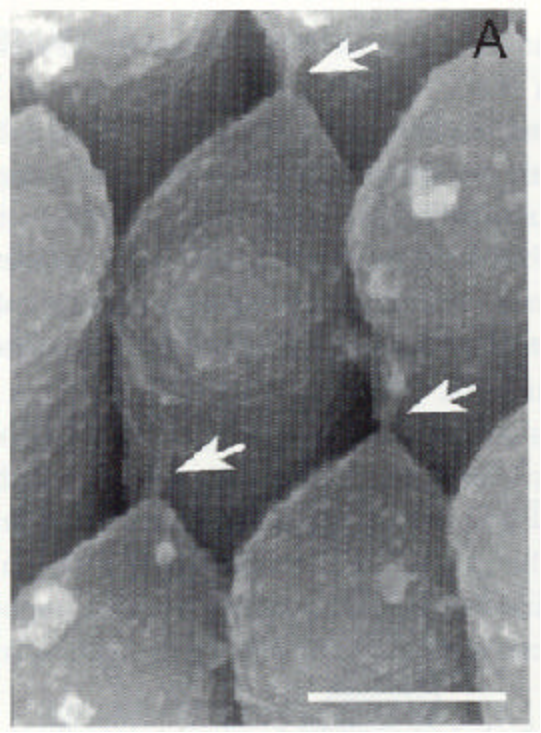

Figure 1.17 Tip links (Geisler, 1998).
Tip links connect the tips of adjacent stereocilia.

CLASSIFICATION

Each sensory organ of the vestibular system has a specific distribution of different types of hair cells. Hair cell types I and II are distinguished by the structure of their cell body (Figure 1.18). Type I hair cells have a flask shaped cell body. The type I cell body is innervated by an afferent nerve fiber. Type II hair cells (Figure 1.19) are cylindrical shaped with a rounded lower end. The type II cell body is innervated by both afferent and efferent nerve fibers. Both cell types have hair bundles that vary in length (Lewis, 1985).

In mammalian utricles, approximately two thirds of the striolar hair cells (Figure 1.20) are classified as Type I and one half of the extrastriolar hair cells are Type I. Turtle Type I hair cells are all located in elevated striolar belt (Lewis, 1985). The elevated striolar belt has been observed during this study.

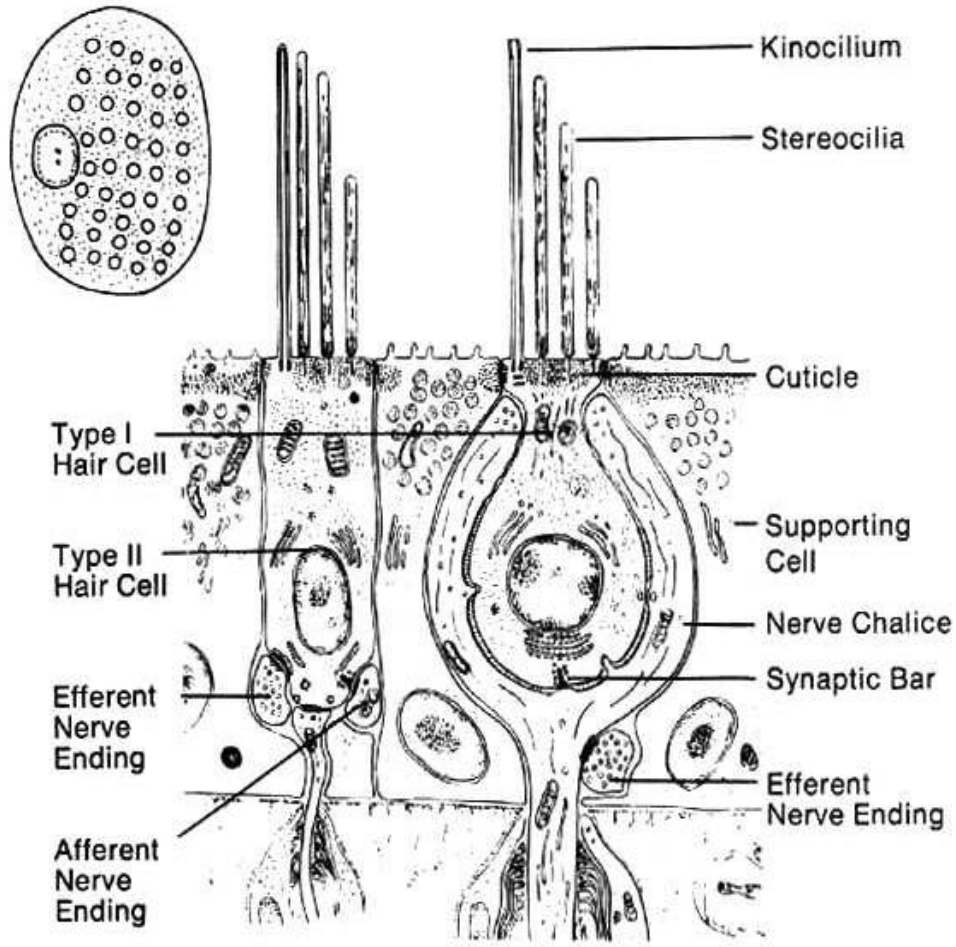

Figure 1.18 Hair cell types (Wersall et. al, 1974).
The two hair cell types found in the vestibular system are Type I (rounded bottom) and Type II (cylindrical bottom).

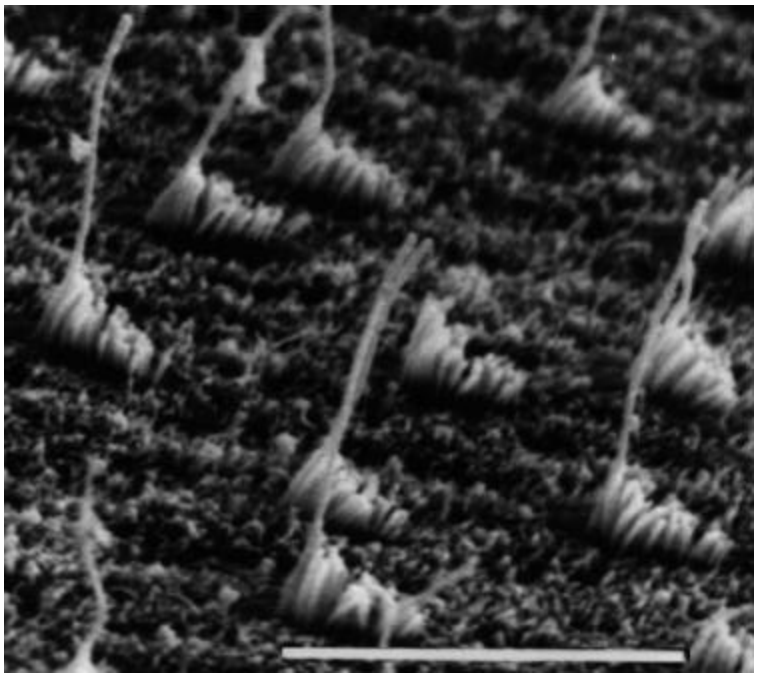

Figure 1.19 Turtle utricular media type II hair cell bundles (Peterson).
Type II hair bundles are characterized by a cylindrical shaped cell body as well as a long kinocilium and shorter stereocilia.

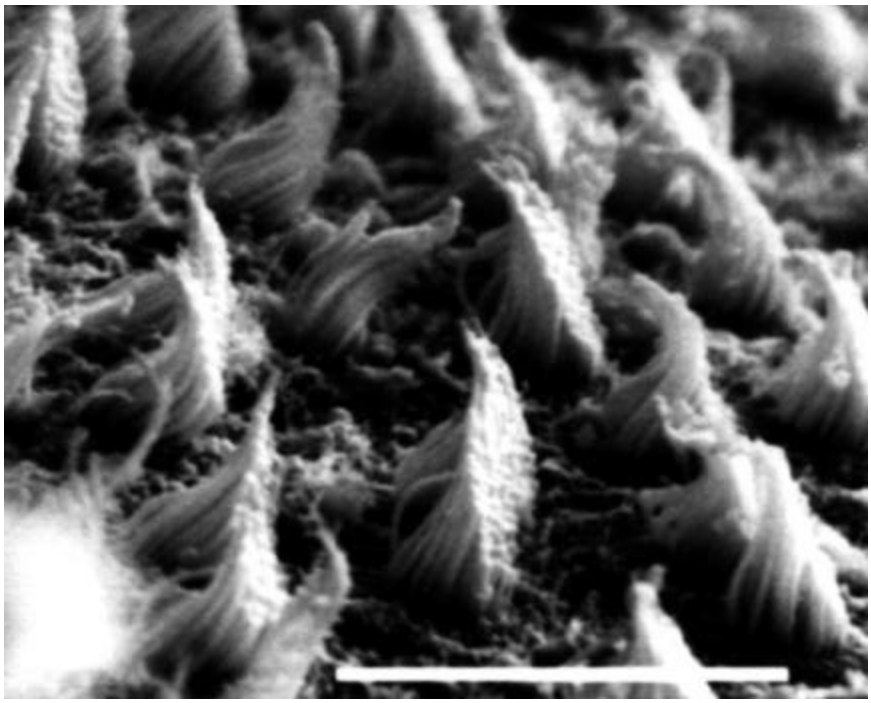

Figure 1.20 Turtle utricular striolar region hair bundles (Peterson).

MECHANOELECTRIC TRANSDUCTION

Individual hair cells within an organ are only responsible for a very limited range of stimuli. Therefore, it is important for the responses from thousands of hair cells to be combined to determine information about the motion of an animal or its surroundings (Hudspeth, 1983). Hair cells are stimulated when a force displaces the bundle in the direction opposite that of a given acceleration (Hudspeth, 1983). The resulting output is a mechanoelectric transduction that is sent to the brain via the VIII cranial nerve.

Each hair bundle has an axis of polarization, the axis of bilateral symmetry that runs from the shortest stereocilium to the kinocilium. Movement of the stereocilia towards the kinocilium results in an electrical depolarization of the cell. Movement in the opposite direction, away from the kinocilium, results in a slight hyperpolarization of the cell. Moving the stereocilia at right angles to these directions produces no response. If the hair bundle is displaced along an intermediate axis, the cell will resolve the forces into two components, one along the axis of bilateral symmetry and the other perpendicular to it. The first component results in a depolarization or hyperpolarization of the cell, depending on the direction of the stimulus and the second component, on the perpendicular axis, results in no response (Hudspeth, 1983). Figure 1.21 shows that as the direction of the stimulus moves away from the axis of bilateral symmetry, the response by the cell decreases.

The difference in the potential between the inside of the cell and the outside of the cell is referred to as the membrane potential. Decreasing of the membrane potential results in depolarization and increasing of the membrane potential results in hyperpolarization (Hudspeth, 1983). The "trapdoor" model is used to describe the transduction of hair cells. Changes in the tension of tip links of the hair bundles are thought to change the conduction probabilities of cation conducting channel openings in the plasmalemma (Hudspeth, 1983). During displacements towards the kinocilium, the tip link is stretched; increasing the probability of the trapdoor opening, causing an influx of positively charged ions into the cell leading to depolarization. During displacements away from the kinocilium, the tip links are relaxed and the trapdoor theory states that some of the channels close, reducing the influx of positive ions, leading to a

hyperpolarization of the cell. Positively charged potassium ions, occurring in high concentrations within the endolymph, flow into the trap doors by strong electrical potentials that exist between the positively charged endolymph and the negatively charged interior of the cell (Geisler, 1998). Molecular pumps in the plasmalemma maintain the internal concentration of ions in the cell. When the membrane potential increases or decreases, calcium channels in the cell body open or close, respectively. As calcium ions enter the cell, they assist in releasing vesicles containing neurotransmitters. The neurotransmitter causes a depolarization of the neuron, resulting in an action potential that travels along the nerve to the brain (Hudspeth, 1983).

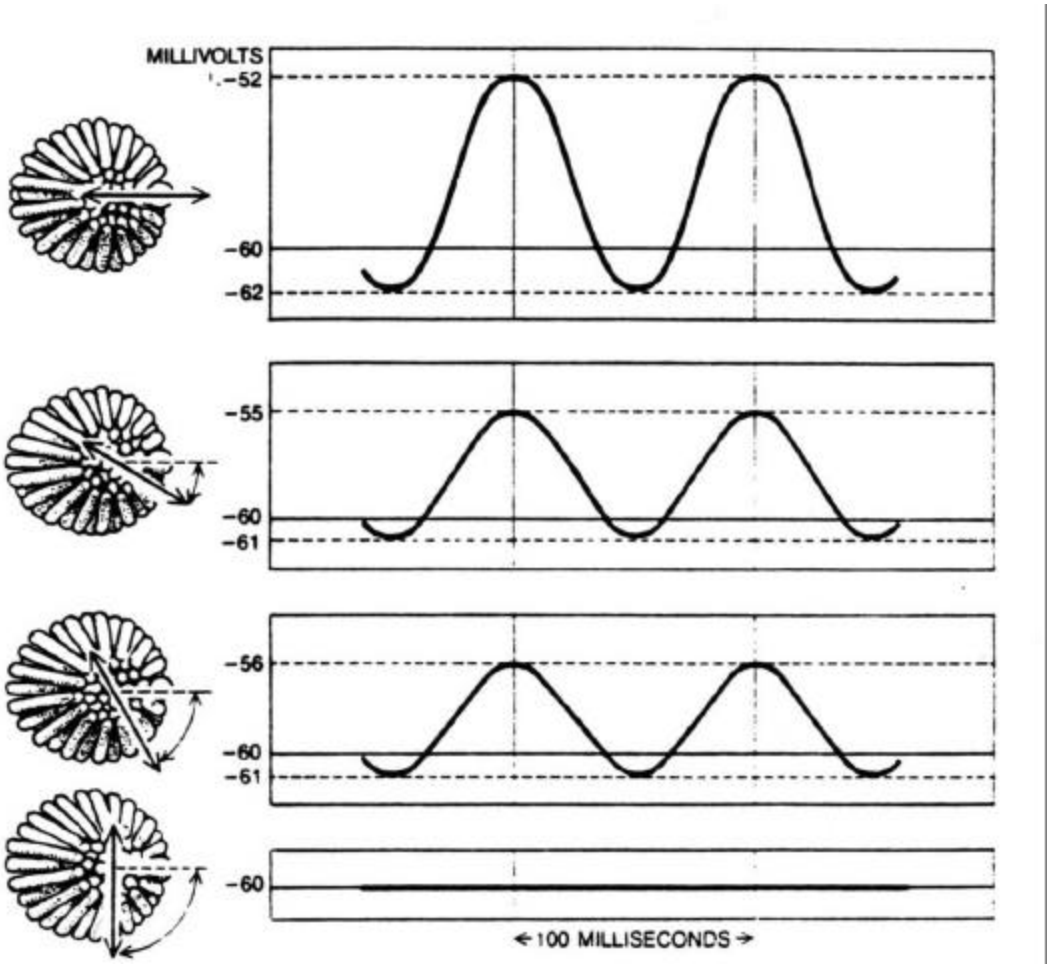

Figure 1.21 Directional sensitivity of a hair cell (Hudspeth, 1983).
As the direction of the stimulus diverges away from the axis of symmetry, the response decreases. The closer the direction of the stimulus is to the axis of symmetry of a hair cell, the larger the response. The cell does not respond to stimuli in a direction perpendicular to the axis of symmetry.

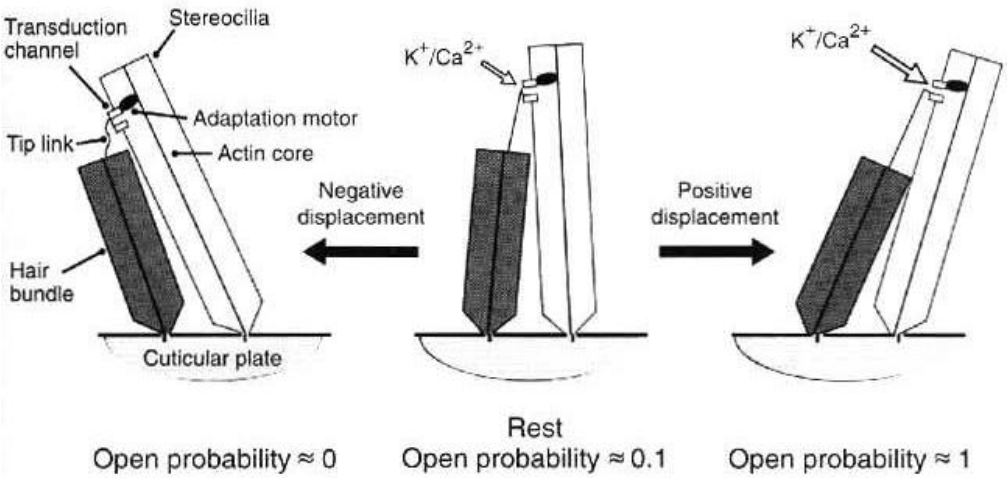

Figure 1.22 "Trapdoor" theory of hair cell excitation (Gillespie, 1995).

HAIR CELL MECHANICS

There is very limited research in the area of inner ear hair cell mechanics. Different techniques have been used to determine the mechanical stiffness of hair bundles. Glass whiskers are used to deflect hair bundles and the deflection is measured with video microscopy (Strelioff & Flock, 1984) or with photodiodes (Crawford & Fettiplace, 1985). Using simple statics, the stiffness of the hair bundle can be calculated when the whisker stiffness is known (see Chapter 3 for details). Another method used to deflect the bundles involves using the stream from a water jet (Szymko, et al, 1991).

The resulting stiffness values from previous works are shown in Table 1.1. These average stiffness values are for different animals and are from different parts of the vestibular and auditory systems. One study showed the relationship between different types of hair bundles in the utricle and their stiffness values. It was found that the striolar hair bundles (stiffness of 2.83-27.1x10^{-5} N/m) had a higher stiffness value than the nonstriolar bundles (stiffness of .26-2.62x10^{-5} N/m) (Merkle, 2000). There has been no research to date comparing the measured location of the hair bundle within the utricle to its stiffness.

Table 1.1 Experimental stiffness values (Szymko, 1991).

INVESTIGATOR	**STIFFNESS (x 10^{-4} N/m)**	**HAIR CELL ORGAN**
Ashmore (1984)	1.32	frog sacculus
Flock and Streiloff (1984)	7.8 to 34.7	guinea pig cochlea
Streiloff and Flock (1984)	1 to 97.2	guinea pig cochlea
Crawford and Fettiplace (1985)	6	turtle cochlea
Howard and Ashmore (1986)	2.56	frog sacculus
Howard and Hudspeth (1988)	6.3	bullfrog sacculus
Denk, Webb, and Hudspeth (1989)	3.41	frog sacculus
Russell, Richardson and Kossl (1989)	16 to 35	mouse cochlea
Szymko, Dmitri and Saunders (1992)	5.04	chick cochlea

MOTIVATION FOR THIS STUDY

The vestibular system is important to animals of every kind. Being able to stand upright and control our motions is a skill we often take for granted. Malfunctioning of the vestibular system leads to unpleasant sensations such as dizziness and nausea (Kelly, 1981). More recently it has been discovered that vestibular dysfunction is important when studying elderly people and their propensity for falling. Problems encountered while flying, including sickness and loss of the sense of orientation, both controlled by the vestibular system, can results in accidents and fatalities (Engstrom et al, 1981).

The motivation behind this research is a need to understand the mechanics of the vestibular system and more specifically, of the hair cells. The functions of the vestibular system can be better understood by determining the mechanical specialization of hair cells to perform certain tasks. Hair cells may have different functions based on their location or physical characteristics.

OBJECTIVE

The primary objective of this research is to develop a technique for locating cells within the utricle and finding their corresponding stiffness. The results will show a relationship between the positioning of a cell within the utricle, the physical dimensions of the cell bundle, and the stiffness of the bundle. This will allow for a better understanding of the mechanical specialization of hair cells.

The specific objectives of this research are as follows:

- dissect and isolate the utricle from a turtle, *Trachemys (Pseudemys) scripta*
- make and calibrate glass whiskers to be used as a hair bundle stimulus
- calculate the stiffness of the glass whiskers
- develop a method for preserving the viability of the hair cells for extended periods of time
- use piezoelectric micromanipulators to hold the glass whisker and to control the motion of the whisker
- utilize an Extrinsic Fabry-Perot Interferometer (EFPI) to measure the distance the glass whisker is moved

- calibrate and employ a photoelectric motion transducer (PMT) to measure the distance the bundle is displaced
- develop a method for determining the location of a specific hair bundle within the utricle
- perform experimental trials by applying a force from the glass whisker to the hair bundle and measuring the resulting displacements
- calculate the stiffness of the hair bundles
- develop a relationship between the location of the bundle and its stiffness

OVERVIEW

The following chapter will present the experimental setup and the equipment used in this research. Chapter three will detail the procedure utilized for preparing the specimen and collecting data. Chapter four will explain the testing and calibrations used during the research. Chapter five includes the results and a discussion of the results. Finally, chapter six will provide a conclusion as well as recommendations for future work.

CHAPTER 2: EXPERIMENTAL SETUP AND EQUIPMENT

This chapter will introduce the experimental setup and the equipment used to locate and measure a hair bundle's stiffness.

EXPERIMENTAL SETUP

Once the vestibular system is dissected out of the red-eared slider turtle (*Pseudemys (Trachemys) scripta*), the utricle is separated from the rest of the membranous labyrinth. The utricle is then placed in a petri dish partially filled with sylgard and viewed under a Zeiss Stemi 2000-C microscope for further dissection. Next, the utricle is pinned onto a cover slip and viewed under a high power microscope, the Zeiss Axioskop FS. During the dissections and testing, the utricle is constantly kept in a pre-made solution (Table 2.1). The specimen is viewed under a water immersion objective (Zeiss 40x Acroplan; N.A. 0.75) and magnified by a 1.6x optivar slide. The image is viewed either through 10x oculars or through a video imaging system (Merkle, 2000).

Once the utricle is setup on the microscope, the hair bundles are brought into focus. The microscope is used to locate the line of polarity reversal. When the location of the line of polarity reversal can be determined, a random hair cell is selected and its distance from the line of polarity reversal is measured using the Imagen XR2001 Marking and Measurement System. Measurements of the dimensions of the bundle are made using the same measurement system. A prefabricated glass whisker is aligned with the bundle using a micromanipulator (Burleigh PCS-5000). A Fabry-Perot system (Luna Innovations AFSS-PC v3) is used to measure the displacement of the pipette by the micromanipulator. The image of the bundle travels through a beam splitter onto a photodiode pair (EG&G UV 140-2) and to a video camera (Dage-Mti DC 200). The image from the video camera is viewed on a Sony Triniton Color Video Monitor. The input voltage to the photodiode pair is supplied by a dual power supply (HP E6360A) and the output voltage is monitored with both a digital storage oscilloscope (Tektronix 2220) and a digital multimeter (Keithley 197). Once all equipment is setup and the bundle is focused under the microscope, the whisker is used to apply a force to the bundle resulting in a displacement of the bundle. The displacement of the bundle is measured using the

photodiode pairs while the displacement of the pipette on which the whisker is attached is measured using the Fabry-Perot system. This information is ultimately used to calculate the stiffness of the bundle (Merkle, 2000).

SOLUTIONS

A solution was developed to preserve the viability of the hair cells during testing. After measuring the extracellular fluid, or perilymph, in the inner ear of the turtle, it was determined that the fluid had a solute concentration of approximately 300 mOsm. Osmolality measurements were conducted using a VAPRO Vapor Pressure Osmometer 5520. An artificial perilymph (AP) solution was then developed to contain the same osmolality as the actual biological fluid. The solutes in Table 2.1 were added to one liter of deionized water. Also added were 10 mL of vitamins and 20 mL of amino acids. Once the AP solution was properly mixed, the pH was then measured. In order to get the pH close to the normal pH of blood and most extracellular fluids, the AP solution was titrated with hydrochloric acid until the pH was approximately 7.3-7.4. The AP solutions were stored in 100-mL aliquots, then frozen and thawed upon use (Felsted, 2002).

Table 2.1 Solute concentrations mixed into a solution to be used during dissection and testing (Felsted, 2002).

Solute	**milliMolar (mM) Values**	**Mass (grams)**
NaCl	144.0	8.415
NaH_2PO_4	0.7	0.084
KCl	5.8	0.432
CaCl2	1.3	0.144
MgCl2	0.9	0.086
HEPES	10.0	2.383
D-Glucose	5.6	1.001

EQUIPMENT

WHISKER FABRICATION

Whiskers are made in a two step process from borosilicate glass rods pulled with a micropipette puller and microforge (Steolting Co.) to a tip diameter of 1-2 μm. Glass whiskers were used because of they were simple to manufacture with the equipment available and it was possible to produce whiskers with a very small stiffness value. The whisker is designed to be less stiff than the bundle so the pipette displacement is greater than the bundle displacement.

The glass rods are first placed in the micropipette puller and a piece of clay is placed on the end of the rod. The coils are heated until the pipette begins to elongate due to the weight of the clay. Once the pipette is drawn to approximately 4 μm, the heat is turned off. The rod is then placed in a microforge (Steolting Co.) where it is heated again by a nickel-chromium filament. Another weight is attached to the bottom of the pipette and it is again drawn until the diameter is now 1-3 μm. Another pipette that has already been pulled to approximately 25 μm by the micropipette puller and shaped by the microforge to fit the contour of the slides is aligned perpendicular to the smaller pipette. Using a light sensitive adhesive, the smaller pipette is bonded to the tip of the larger pipette. The smaller pipette is then trimmed to a length of 600-900 μm. The smaller pipette is now referred to as the glass whisker (Figure 2.1) (Merkle, 2000).

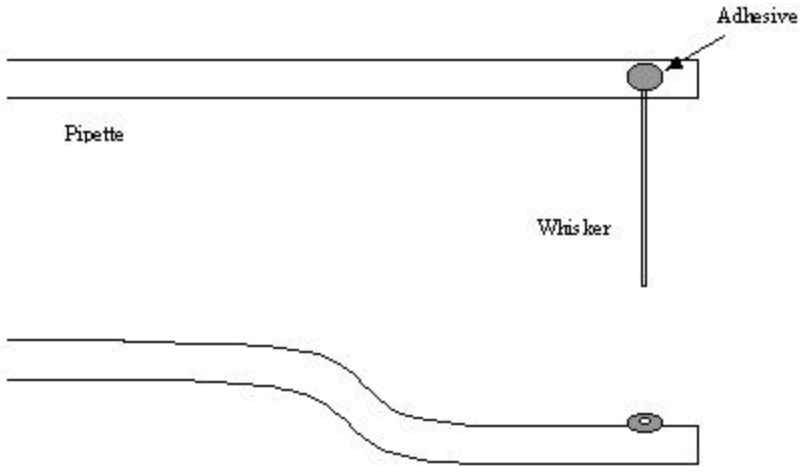

Figure 2.1 Pipette with attached whisker (Merkle, 2000).
The glass pipette is shaped to fit the contour of the slides on which the utricle is mounted. A small amount of adhesive is used to attach the whisker to the pipette.

MICROMANIPULATOR

The Burleigh PCS-5100 was used to hold and manipulate the motion of the pipette. The micromanipulator (Figure 2.2) utilizes piezoelectric (PZT) actuators to make very small, precise movements. Three actuators allow for motion in three orthogonal directions, up and down, left and right, and forward and backward. An Axis Control Unit (ACU) controls the actual movement. Three knobs on the ACU correspond to the three different directions and are used to move the pipette in those directions (Burleigh manual). The PZT actuators and the ACU are used to position the whisker on the bundle and to produce a force on the bundle. In order to position the whisker in the vicinity of the bundle, screws located on the side of the stage are turned. The screws allow for greater movement, while the actuators and the ACU allow for smaller movements of up to 300 μm. The pipette is held by placing it in a groove on the micromanipulator and another plate is screwed on top to clamp it down (Figure 2.3).

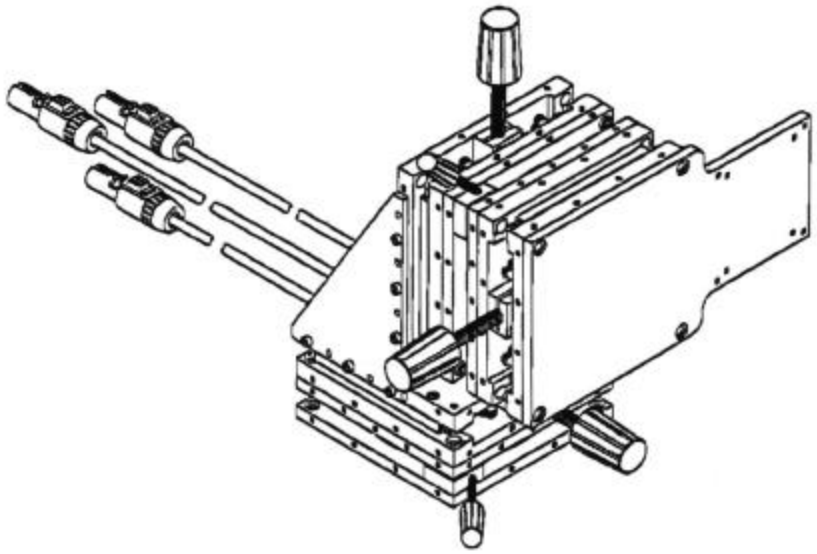

Figure 2.2 Micromanipulator (Burleigh manual).
The three large knobs on the micromanipulator are used to maneuver the pipette in three orthogonal directions.

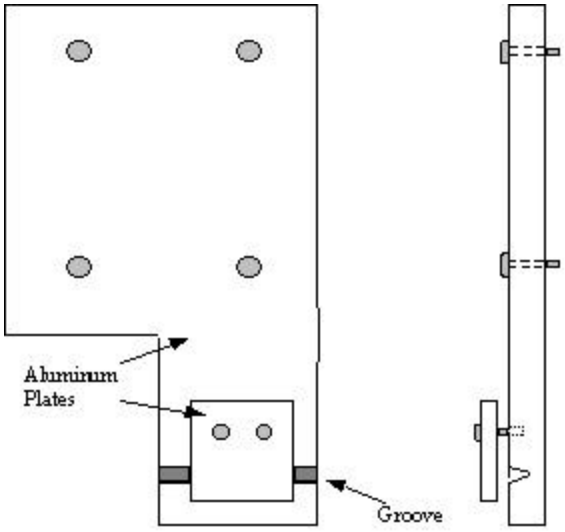

Figure 2.3 Pipette holder (Merkle, 2000).
The groove in the large aluminum plate holds the pipette when the smaller aluminum plate is screwed in to clamp down on the pipette.

EXTRINSIC FABRY-PEROT INTERFEROMETER

The Fabry-Perot configuration is used to detect information, such as displacement, from a perturbation (i.e. strain or temperature). The extrinsic Fabry-Perot interferometer (EFPI) used in this research (AFSS-PC by Luna Innovations) (Figure 2.4) is used to detect the motion of the pipette in the nanometer range. The term phase sensor refers to the two signals used, a sensing and reference signal.

The optical source is a broadband light-emitting diode (LED) (F&S, Inc., 1999). A light signal is sent from the optical source and travels through an input/output fiber to the sensor head. When the light reaches the end of the fiber, a portion of the light is reflected off the internal face of the fiber. This signal is referred to as the reference reflection. The remaining portion of the light is transmitted through the end of the fiber until it hits another fiber, the reflector fiber. The signal off of the reflector fiber is referred to as the sensing reflection. The sensing reflection then enters back into the original optical fiber and interferes with the existing reference reflection. Both fibers are aligned in a hollow sleeve to ensure proper positioning and to eliminate outside interference (Barrett, 1995).

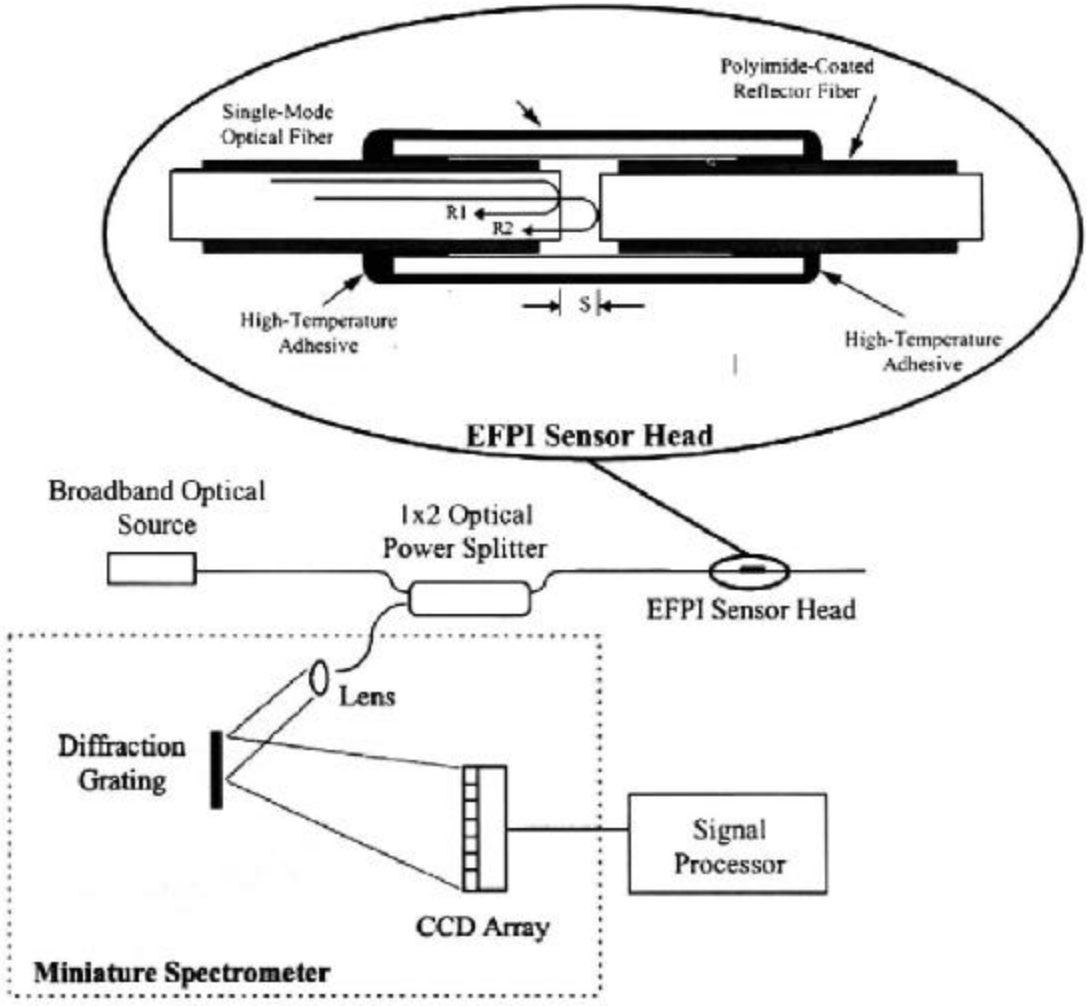

Figure 2.4 Extrinsic Fabry Perot Interferometer (Luna Manual, 1999).

As the knobs on the micromanipulator are moved, the distance between the two fibers increases or decreases. The distance is measured when the new signal is sent back to the AFSS-PC system where it is run through a signal-processing algorithm. A personal computer installed with LabView is used to do the computations for the signal processing and displays the gap distance. A good spectrum plot is used to determine the quality of the signal (Figure 2.5) (F&S, Inc., 1999). In order for the signal to be a quality signal, it must be ensured that the ends of both the optical fiber and the reflector fiber are flat. The system works best when the gap distance is at least 30 µm.

In this research the optical fiber is kept stationary, while the reflecting fiber is fixed to the same stage as the pipette containing the glass whisker. Therefore the

reflecting fiber moves with the pipette and the EFPI system is used to measure the distance the pipette moves.

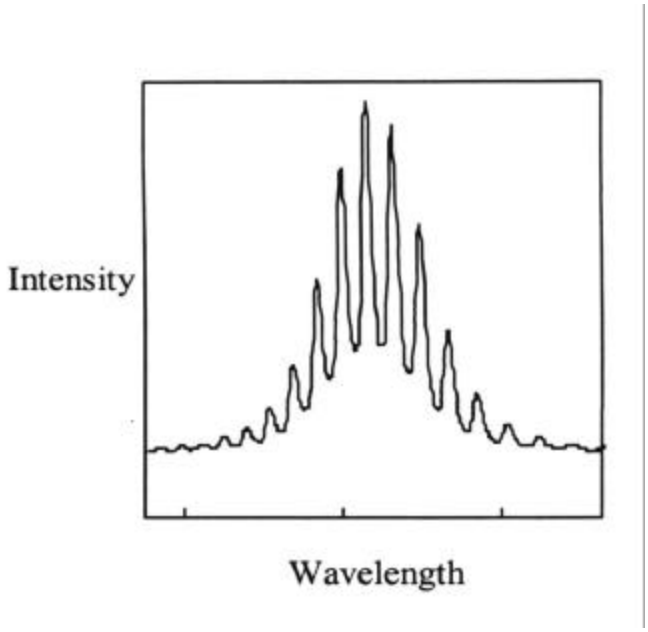

Figure 2.5 Spectrum plot of AFSS-PC signal (F&S Manual, 1999)**.**
A good spectrum plot is essential in assuring that the measurements are accurate.

PHOTOELECTRONIC MOTION TRANSDUCER (PMT)

Silicon photodiodes are semiconducting devices used to detect light and convert it to an electrical signal (current) (EG&G Catalog). The amount of current generated by the photodiodes is proportional to the intensity of the light that it is exposed to. A linear relationship can be developed between the amount of light on the diode and the output voltage. The dual diode array used in this research consists of two diodes mounted side by side. If the two diodes are equally illuminated, then they will have the same output voltage. If the two diodes are not equally illuminated, the output voltages will be different. A dual power supply provides a DC voltage to the photodiode array. A differential amplifier is used to amplify the output signal and to calculate the difference between the two signals. The output signal is sent to a multimeter where the voltage difference can be read. If the light is equal on the two diodes the difference in the output voltages will be zero. If the difference in the output voltages is not zero (when light is

not equal on the two diodes), then the voltage difference will be read on the multimeter (Merkle, 2000).

By moving the glass whisker in the field of the two diodes, light reflected off the whisker will hit the diodes, resulting in a differential voltage. Using the distance the whisker was moved, measured with the EFPI, and the corresponding differential voltages, a linear relationship can be developed. This relationship assigns a ratio between the voltage changes and the distance the whisker was moved. During testing, the PMT is used to measure the distance the tip of the whisker moves, which is also the distance the hair bundle moves.

OPTICS AND IMAGING

The light microscope used to view the hair bundles utilizes a 12-volt DC, 100-Watt halogen filament lamp for illumination. The microscope is equipped with DIC optics and bright field settings. A field diaphragm is used to control the amount of light that reaches the specimen. The DIC optics include an analyzer, polarizer, and a prism. The optics allow a thick tissue specimen, such as the utricle in this research, to be viewed clearly instead of using phase-contrast examination.

There are a few different lenses used while examining the utricle. The Zeiss Acroplan 4x/0.10 Numerical Aperture (NA) and the Zeiss Acromat 10x/0.25 NA are used to position the utricle in the viewing field. The Zeiss Acroplan 40x/0.75 NA water-immersion lens is then used to bring the hair bundles into focus and to align the glass whisker with the bundle.

The entire microscope assembly is mounted on a vibration isolation table (Technical Manufacturing Corporation). The isolation table reduces the vibrations from outside noises or floor vibrations.

CHAPTER 3: EXPERIMENTAL PROCEDURE

TISSUE PREPARATION

The hair cells used for this research are located in the utricle of the *Pseudemys (Trachemys) scripta*, or the red-eared slider turtle. The following sections will describe the process by which the utricle is dissected and the hair cells are located and tested.

ANESTHETIZATION

The first step in the dissection process is the anesthetization of the turtle. The standards followed were set forth by the Virginia Tech Animal Care Committee. The turtle is injected with 0.5 mL of Euthasol. The injection is done intramuscularly into the hind leg. Following the injection, the turtle sits for approximately 10-20 minutes until it is determined that it no longer has eyelid reflexes and the dissection can begin. While waiting, the carapace length of the turtle is measured to use for size comparisons of the results. The carapace length is characterized by the long axis of the turtle shell, from head to tail.

EXTRACTION OF THE LABYRINTH

The extraction begins by separating the head from the body of the turtle by decapitating the turtle. Loose tissue, such as skin, is removed from the head with scissors. The jawbone is also separated from the rest of the head, exposing the skull bones. The head is then split into two halves. The two halves are placed in a petri dish filled with the solution described in Chapter 2.

The two sides of the head are moved to a stereomicroscope (Zeiss Stemi 2000C). Using the microscope, the brain tissue is removed from one of the halves. This exposes the area where the labyrinth is located. The location of the labyrinth is shown in Figure 3.1. The squamosal, quadrate, parocipital, and pre-optic bones are all removed (Figure 3.2) allowing easier access to the labyrinth (Barrett, 1995). Once these bones are removed, the labyrinth is in full view. It is covered by a thin piece of cartilage. Using sharp forceps, the cartilage is carefully removed, ensuring that the labyrinth is not damaged or punctured. The three semicircular canals are then pulled slightly from their

place in the bone and snipped with scissors. The VIII cranial nerve is also cut away from the labyrinth. At this point, the labyrinth can be easily pulled from the head. The same procedure is carried out on the other half of the head, resulting in two vestibular labyrinths.

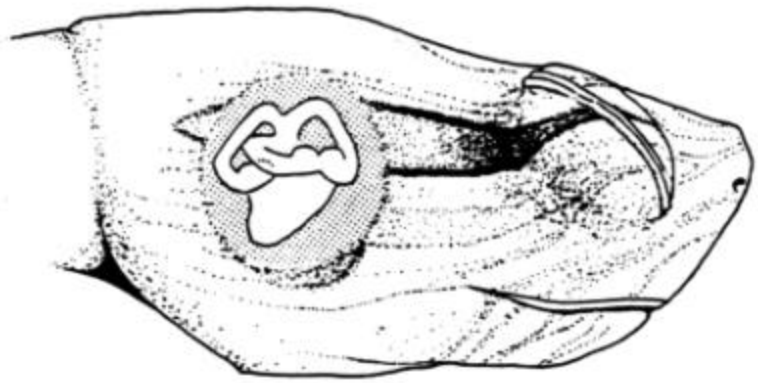

Figure 3.1 Location of the vestibular system in the red-eared slider turtle (Brichta and Peterson, 1994).

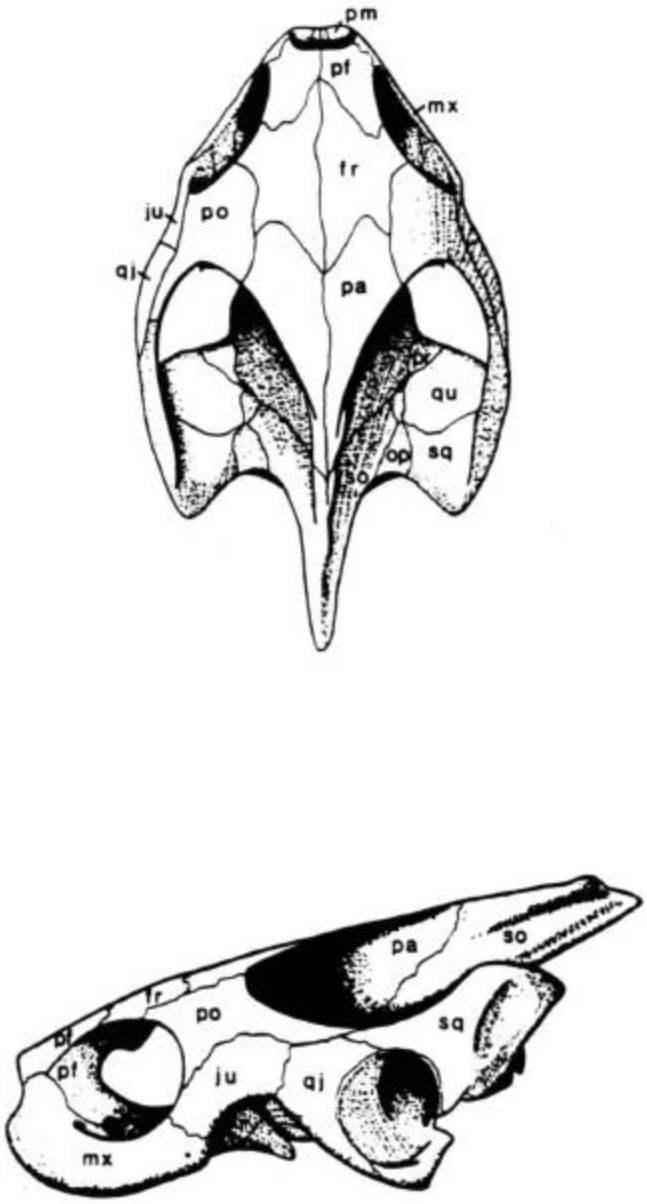

Figure 3.2 Skull bones of a *Pseudemys (Trachemys) scripta* (Gibbons, 1990).
The top drawing shows the dorsal skull bones while the bottom drawing shows the lateral skull bones. **fr**, frontal; **ju**, jugal; **mx**, maxillary; **op**, paroccipital; **pa**, parietal; **pf**, prefrontal; **pm**, premaxillary; **po**, postorbital; **pr**, pre-optic; **qj**, quadratojugal; **qu**, quadrate; **so**, supraoccipital; **sq**, squamosal.

DISSECTION AND MOUNTING OF THE UTRICLE

The following sections will detail the dissection of the utricle from the rest of the labyrinth and the positioning of it on a slide for testing.

DISSECTION OF THE LABYRINTH

Once removed from the head, the labyrinth is placed in a petri dish filled with the AP solution. The petri dish contains a thick layer of sylgard to allow easier access to the labyrinth during dissection. The canals and the saccule are cut away from the labyrinth. This leaves the utricle, portions of two canals, and the nerve. The canals are cut away below the ampulla (Figure 3.3). The nerves on the utricle are peeled off using very sharp forceps. This is a very delicate process and if not done carefully, can cause damage to the sensory epithelium in the utricle.

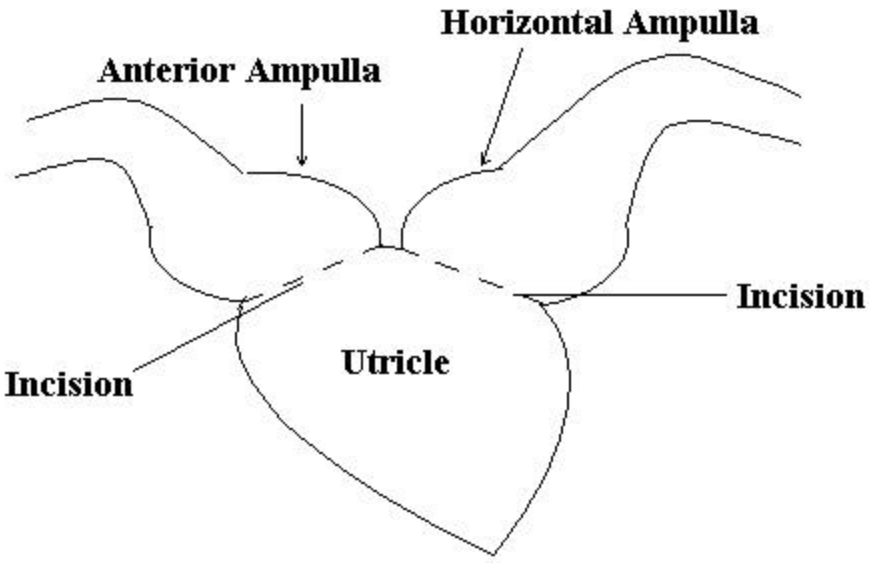

Figure 3.3 Dissection of the labyrinth.
The horizontal and anterior ampulla are cut away from the utricle.

With the nerve side facing down, the utricle resembles a scallop shell. The lateral wall of the utricle is then removed. The remaining portion of the utricle contains the macula. A shelf like piece of tissue is removed very carefully from the utricle. The shelf covers the striolar region. The final step is the removal of the otolith membrane. Using a small pin, the membrane is gently teased off of the surface of the sensory epithelium. Again, this is a delicate process and must be done with precision as to not destroy the underlying hair cells.

MOUNTING OF THE UTRICLE

Following the dissection of the utricle from the rest of the labyrinth, it is carefully transferred from the petri dish to a slide. During all the dissection and testing processes, the tissue is always kept in the AP solution. The utricle is gently placed face down and an insect pin is used to hold one edge of the tissue. A pair of forceps is used to grab the unpinned side of the utricle and fold it over. It is folded along a transect shown in Figure 3.4. The original pin is then used to clamp both edges together to be held in place during testing. This set up leaves the hair bundles sticking out the side of the folded utricle. Testing can then be done on the profile of the bundle.

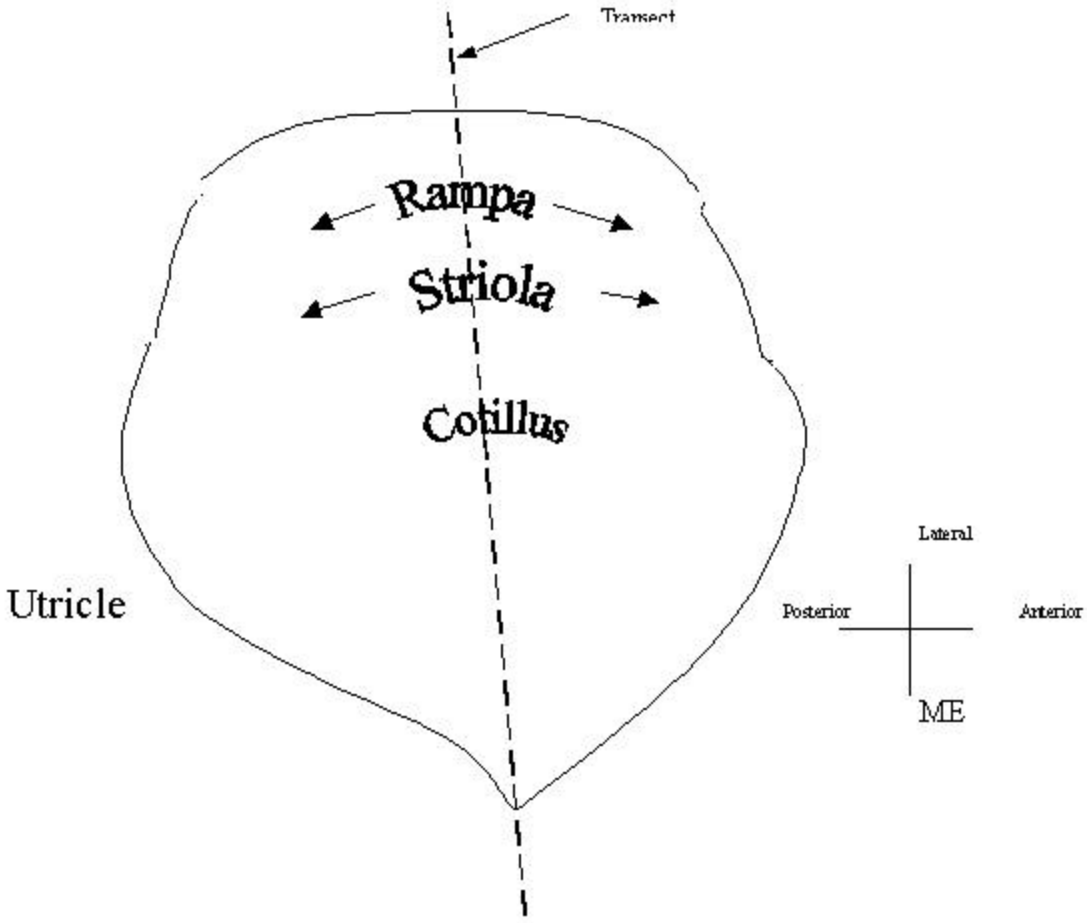

Figure 3.4 Utricle transect (Merkle, 2000).
Once the utricle has been cut away from the membranous labyrinth it is folded along a transect and placed on a slide to be viewed under a high power microscope.

TISSUE TESTS

PRE-TEST PREPARATION

Prior to testing a hair bundle, the dimensions of the bundle must be measured as well as the location. The photoelectric motion transducer must also be calibrated.

CRITERIA FOR BUNDLE SELECTION

Once the folded edge of the utricle has been located under the 40x water immersion lens, the profile of the hair bundle is focused upon. The edge of the utricle is scanned until the line of polarity of reversal is identified. The line of polarity reversal is characterized by a change in the direction of the hair cells by 180^{o} (Figure 3.5). Once the line of polarity reversal is located, measurements are made from the line along the transect until no more hair bundles can be seen. The measurements are made with the Imagen XR2001 Marking and Measurement System. Since the entire transect cannot be viewed on the video screen at one time, measurements are made by measuring to a landmark, such as another hair bundle, and then moving down the transect, picking up measurements from that landmark. A new landmark is chosen and a new measurement is made. Measurements are done in both directions from the line of polarity reversal.

When a hair bundle has been selected for testing, its dimensions are measured using the same marking and measurement system. The height of the kinocilium is measured. Also measured is the height of the tallest stereocilia. Attempts to measure the base width of the bundle were made, but these measurements were inaccurate due to the entire base potentially not oriented in the same plane on the monitor. These dimensions, the height of the kinocilium and the height of the tallest stereocilia, and a constant base width of 5 μm were used to create profiles of the hair bundles. Next, the distance from the hair bundle to the line of polarity reversal is measured using the same technique described above.

Figure 3.5 Line of polarity reversal (Lindeman, 1973).
The line of polarity reversal, located in the striolar region of the utricle, is characterized by a 180° change in the direction of the hair bundles.

CALIBRATING THE PMT

Once the hair bundles have been focused upon, the glass whisker attached to a pipette is positioned with the micromanipulator in the same plane of the hair cells (Figure 3.6). Testing cannot be done until the photoelectronic motion transducer is calibrated. A calibration curve will establish a relationship between the distance the end of the whisker moves and the PMT output voltage.

The calibration begins by moving the whisker back from the hair bundles until the whisker can be focused upon on the monitor and the whisker is out of view of the hair bundles. The Fabry-Perot interferometer (EFPI) is turned on and the reflecting fiber is adjusted until a good spectrum plot is obtained. After turning on the dual power supply to the PMT and turning on the multimeter to show output voltages, the whisker is moved with the micromanipulator across the field of the two diodes. When the whisker reaches the gap between the two diodes, the output voltage will read zero. The region around the gap is where a linear relationship exists between the voltage and the displacement (between positions 4 and 5.5 in Figure 3.7). As the whisker is moved in this region, the output voltage from the multimeter and the corresponding displacement from the EFPI are recorded. These two values are be plotted to produce a curve. The slope of this line is the ratio between the displacement and the output voltage. This value will be used to determine the displacement of the kinocilium during stiffness testing. As the kinocilium

is displaced, a change in voltage from the PMT will exist. Using the ratio, the distance the kinocilium moved can be calculated (Merkle, 2000).

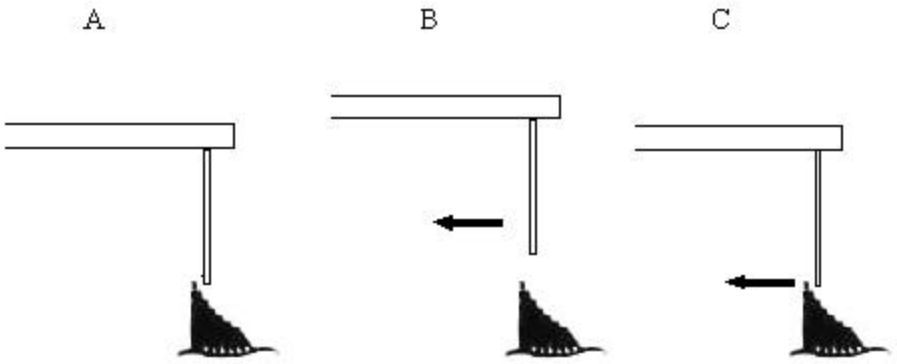

Figure 3.6 Whisker position for calibrations and testing (Merkle, 2000).
A. The whisker is positioned in the same plane as the hair bundle. **B.** The whisker is moved away from the bundle to perform the calibrations on the PMT. **C.** The whisker is moved back to the position adjacent to the bundle so the tip of the whisker is in contact with the end of the kinocilium.

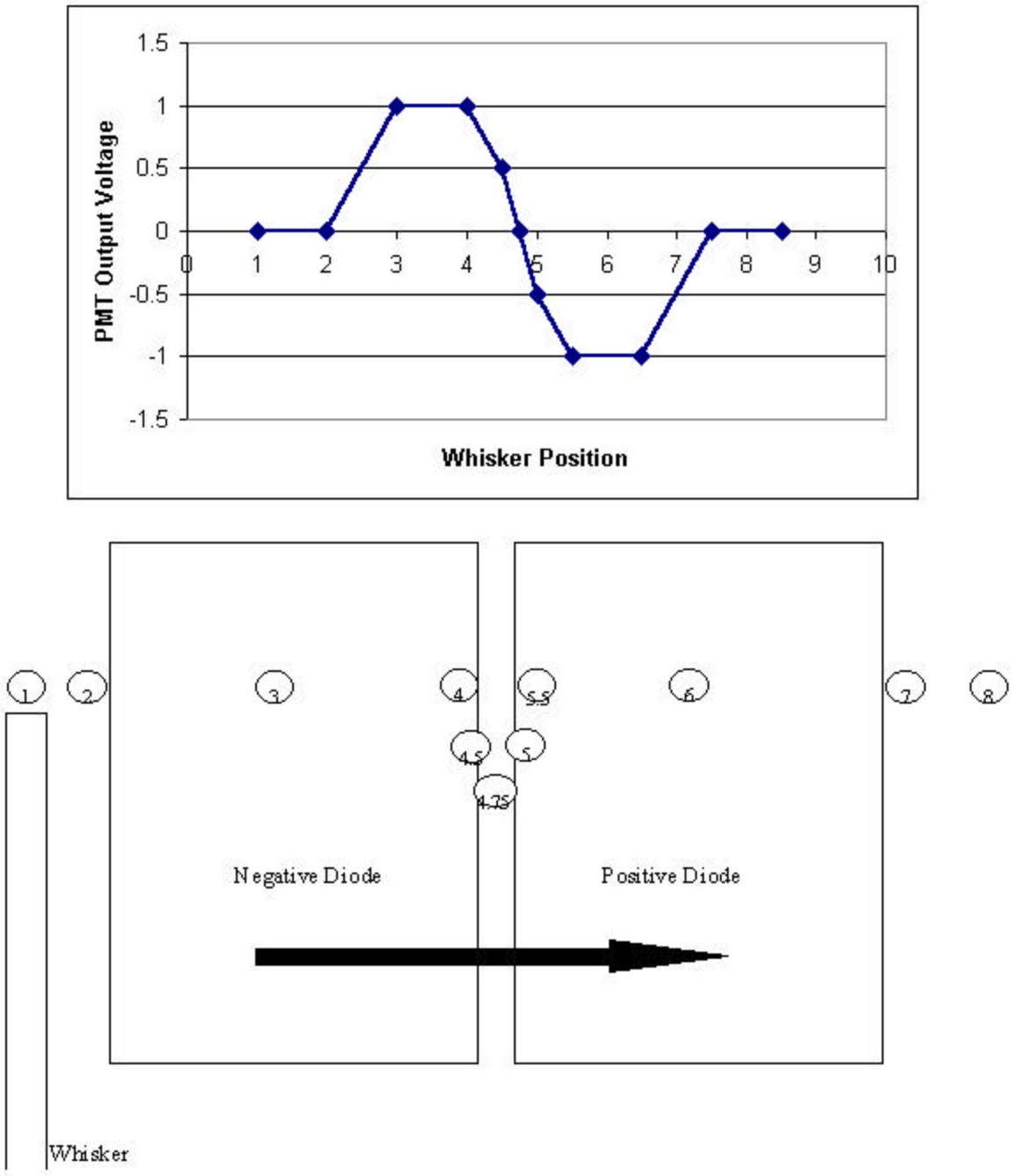

Figure 3.7 Photodiode response (Merkle, 2000).
As the whisker is moved across the field of the dual diode array, the output voltages are recorded and plotted. The linear region of the plot is used to develop a ratio between the distance the whisker moves and the output voltage.

The calibrating of the PMT must be done before testing each utricle since the testing conditions (i.e. lighting, focus, etc.) may not be the same in each test. Therefore, only the hair bundles that are in focus at the instant the PMT is calibrated are tested. In order for the calibrations to be accurate, the whisker must be oriented horizontally, allowing the entire whisker to be in focus at one time. If the whisker is not entirely focused upon, the reflections from parts of the whisker not in focus will hit the diodes producing false results. The whisker must also be aligned parallel to the edges of the diodes so that at an instant the whisker is either completely on the diode or completely off of the diode (Merkle, 2000). Mapping of the diodes is described in Chapter 4.

STIFFNESS TESTS

Following the calibration of the PMT, stiffness testing is ready to begin. Using the micromanipulator, the whisker is moved until it is aligned with the tip of the kinocilium of a selected bundle (Figure 3.6C). The EFPI gap distance and the PMT output voltage are both recorded. The whisker is displaced horizontally approximately 1 μm using the micromanipulator. The displacement of the whisker will cause a force to act on the hair bundle, resulting in a displacement of the kinocilium. The final EFPI gap distance and the final PMT output voltage are recorded. The change in the gap distance is the distance the pipette was moved and the change in the output voltage corresponds to the distance the kinocilium moved. The displacement procedure is repeated 8-10 times. The resulting stiffness values from the numerous tests are averaged to obtain a stiffness value for the selected hair bundle.

CALCULATING BUNDLE STIFFNESS

The force applied to the bundle by the whisker can be related to the stiffness of the bundle by the simple equation

$$k=F/\delta \qquad [3.1]$$

where k is the stiffness, F is the force, and δ is the displacement. During testing, the initial position of the end of the whisker (the end attached to the pipette) is determined using the EFPI and the initial position of the tip of the whisker (the end hitting the kinocilium) is determined using the PMT output voltage. Following the deflection of the

hair bundle (Figure 3.8), the final position of the end of the whisker is also determined using the EFPI and the final position of the tip of the whisker or the kinocilium is determined using the PMT output voltage. The distance the end of the whisker moved, Δx_P, can be calculated by finding the difference in the initial and final positions. The distance the bundle moved, Δx_B, can be calculated with the equation

$$\Delta x_B\ (\mu m) = \frac{\text{change in PMT output voltage (V)}}{\text{calibration factor (V/}\mu m)} \qquad [3.2]$$

The whisker displacement, Δx_W, is found finding the difference between the displacements of the bundle and the pipette

$$\Delta x_W = \Delta x_P - \Delta x_B \qquad [3.3]$$

By knowing the whisker displacement and the whisker stiffness (Chapter 4), the force acting on the whisker can be calculated using Equation 3.1. Because the force acting on the bundle, F_B, is considered equal and opposite to the force acting on the whisker, F_W, it is concluded that

$$F_B = F_W \qquad [3.4]$$

Equation 3.4 can be rewritten using Equation 3.1 as

$$k_B \Delta x_B = k_W \Delta x_W \qquad [3.5]$$

where k_B and k_W are the stiffness of the bundle and the whisker, respectively. Solving Equation 3.5 for Δx_W and substituting it into Equation 3.3, the bundle stiffness is calculated with the equation

$$k_B = k_W \left(\frac{\Delta x_P}{\Delta x_B} - 1 \right) \qquad [3.6]$$

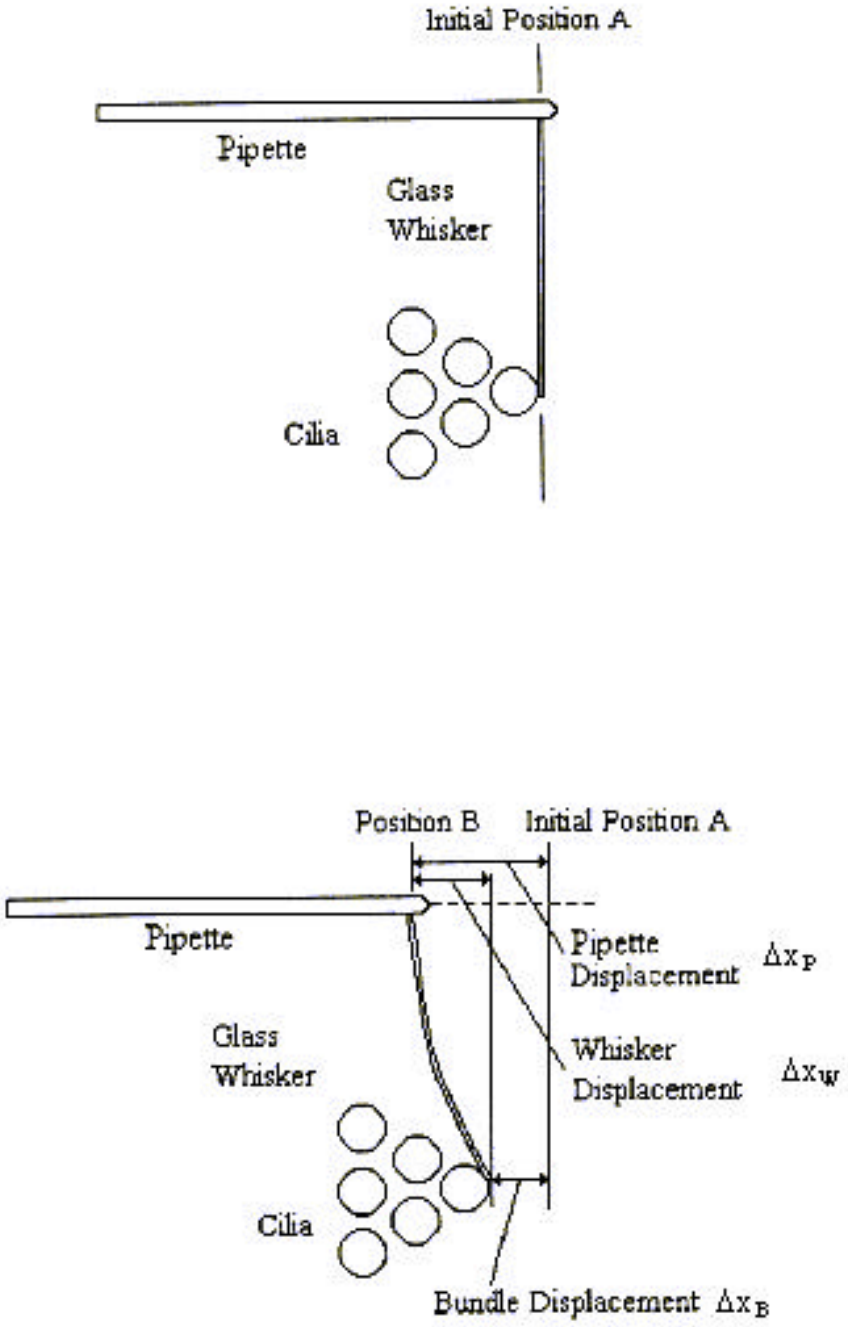

Figure 3.8 Whisker and bundle displacement during testing (Barrett, 1995).
The top drawing shows the initial position of the whisker against the bundle. The bottom drawing shows the final position of the bundle and the whisker following deflection. The whisker displacement, pipette displacement, and the bundle displacement are labeled on the drawing. Note that this picture show s the bundles in top view.

CHAPTER 4: CALIBRATIONS

WHISKER CALIBRATION

Prior to testing a bundle and calculating the stiffness of the bundle, the stiffness of the glass whisker must be determined. The pipette containing the glass whisker is placed in the microforge in a vertical position with the whisker in a horizontal position (Figure 4.1a). A small spoon containing macro beads (Bangs Laboratories) is moved up to the whisker. The beads will attach electrostatically to the whisker. The microforge is gently tapped until all but one of the beads fall off. This should be done very carefully so the whisker is not broken. The whisker will bend with the added weight of the bead (Figure 4.1b). Using a calibrated reticule located in the eyepiece of the microforge, the diameter of the bead is measured and recorded. Next, the deflection of the whisker and the length of the whisker are measured and recorded (Merkle, 2000). The biggest error in calculating the stiffness of the whisker can be attributed to the measurement of the diameter of the bead (since this value is cubed in the final equation).

The whisker stiffness is calculated using the equation for the deflection of a cantilever beam due to an applied force, assuming that the whisker is homogenous and isotropic and the measured deflections are small. Since not all of the beads will attach to the tip of the whisker, a correction factor is included for forces not applied at the end of the beam (Beer and Johnston, 1992). The equation for the deflection of the beam becomes

$$d = \frac{W}{6EI}\left(2l^3 - 3l^2 a + a^3\right) \qquad [4.1]$$

where δ is the beam deflection (Figure 4.2), W is the weight of the bead, l is the length of the whisker, a is the distance of the bead from the tip of the whisker, E is the elastic modulus of the whisker, and I is the moment of inertia.

The moment of inertia can be found using the equation

$$k = F/d = 6EI/2l^3 = 3EI/l^3 \qquad [4.2]$$

where F and δ are the force and deflection, respectively, that occur at the end of the beam (a=0). By solving equation [4.1] for $3EI/l^3$ and plugging into equation [4.2], the following equation is obtained:

$$k = \frac{W\left(1 - \frac{3}{2}\frac{a}{l} + \frac{1}{2}\frac{a^3}{l^3}\right)}{d}. \qquad [4.3]$$

Equation 4.3 is used to calculate the stiffness of the glass whisker. The weight of the bead is calculated with the following equations:

$$W = mg \qquad [4.4]$$

$$W = rVg \qquad [4.5]$$

$$W = \frac{4}{3}pr^3 rg \qquad [4.6]$$

where m is the mass, g is the acceleration due to gravity, V is the volume, r is the radius (a constant value), and ρ is the known density of the beads, 1.030 g/cm^3 (Merkle, 2000).

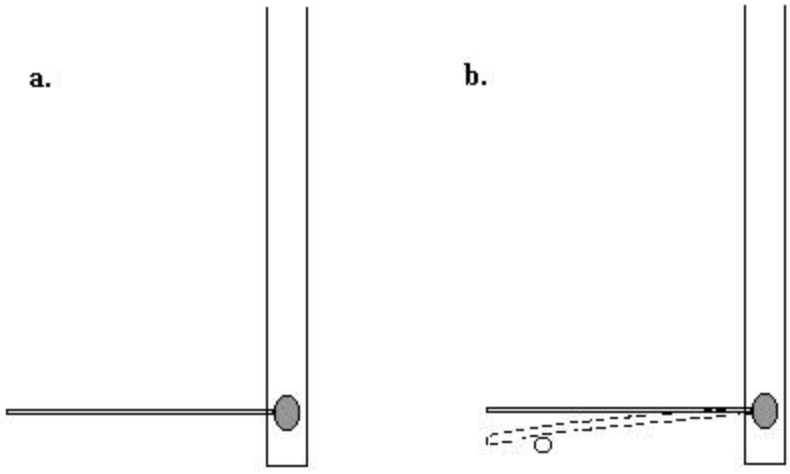

Figure 4.1 Positioning of the whisker during calibrations (Merkle, 2000).
a. During calibrations, the pipette is placed so the whisker is horizontal. b. The whisker deflects with the added weight of a bead.

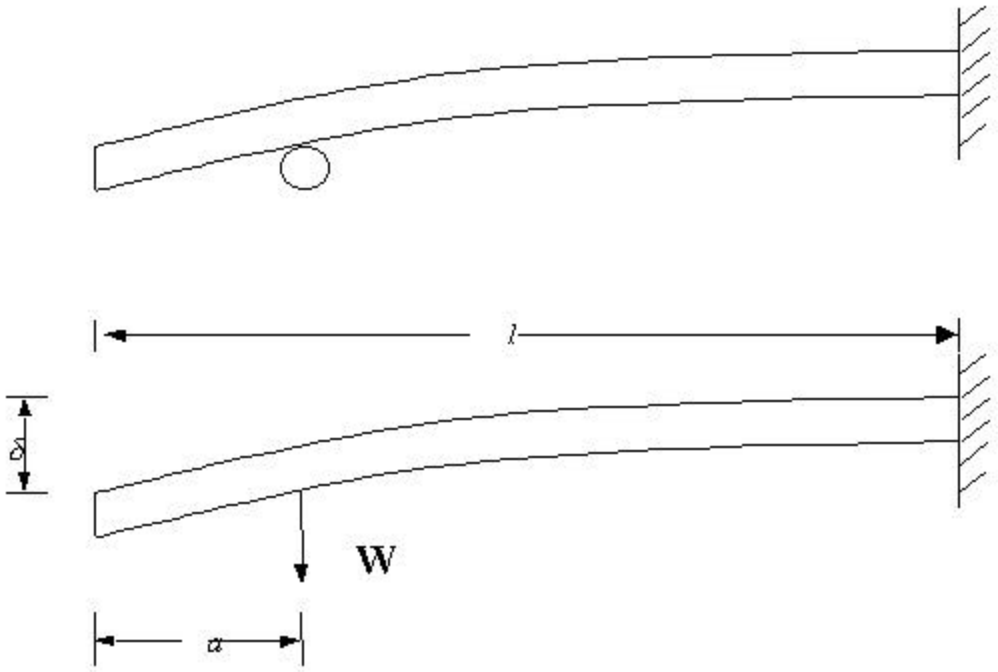

Figure 4.2 Deflection of the glass whisker during calibrations (Merkle, 2000).
The glass whisker will deflect a distance of δ with the added weight of the bead.

MAPPING OF THE PHOTODIODE

In order to align the glass whisker up within the boundaries of the dual diode array during testing, the positioning of the diodes must be determined. Since both the photodiodes and the monitor are connected to the same beam splitter, the same image is relayed to each device. Therefore, the mapping of the diodes can be done on the monitor. The boundaries can be located by moving a particle across the diode array and recording the position of the particle when there is a change in the output voltage. The mapping is done by placing a small bead (.05mm-.1mm diameter) on a slide and moving the particle across the field of vision on the monitor. The bead reflects the light at a point and results in a voltage change read by the multimeter. For each new position, the position of the bead is marked on a piece of clear plastic placed on the monitor and then the output voltage is recorded. The output voltage will be positive on one diode and negative on the other. When the particle is moved along the boundary between the two diodes, the output differential voltage will read zero. Plotting the position of the bead and the output voltages on the clear plastic sheet insures that the whisker will be properly positioned during testing (Merkle, 2000).

CHAPTER 5: RESULTS, DISCUSSION, AND FUTURE WORK

WHISKER STIFFNESS RESULTS

When making and calibrating a whisker to use during testing, it is essential to make a whisker that has a small enough stiffness so that the whisker will bend before it displaces a bundle. This is achieved by having the whisker stiffness less than the smallest expected bundle stiffness. By having the whisker bend before displacing the bundle, the displacement of the whisker will be greater than the displacement of the bundle, leading to an accurate calculation of bundle stiffness. The displacement of the bundle, the displacement of the whisker, and the stiffness of the whisker is used to calculate the bundle stiffness. Whiskers used during this study ranged in stiffness from 9.21 E-06 N/m to 3.61 E-05 N/m. These whiskers ranged in diameter from 2-3.6 μm and ranged from 0.855-3.42 μm in length.

HAIR BUNDLE STIFFNESS RESULTS

While choosing a hair bundle to test, there are a few considerations to make. Only hair bundles that are in focus on the monitor are chosen for testing because these bundles will have the same lighting conditions that were used to calibrate the PMT for a particular utricle. The entire kinocilium must be in focus at one time to ensure that the bundle is in the same plane as the tip of the glass whisker. This also allows for an accurate measurement of the height of the kinocilium and the height of the tallest stereocilia. The order of testing for hair bundles within a given utricle was random and varied from utricle to utricle. All tests were completed with the glass whisker in contact with the tip of the kinocilium. During the testing of a hair bundle, several trials were completed resulting in a range of stiffnesses for that bundle. The mean and the median of the trials were computed to determine the final stiffness value. Overall, there were 121 hair bundles tested from 20 different utricles. Not all of the bundle test data was used in the final results due to errors during testing. Reasons for discarding data will be discussed later in this chapter.

The data collected, including location of the bundle from the line of polarity reversal (μm), height of the kinocilium (μm), height of the tallest stereocilia (μm), utricle number, turtle number, order the bundle was tested within a given utricle, and carapace length (cm) of the turtle (not determined in earlier experiments) is shown in Appendix A. Also shown in the table are the calculated values for the mean linear and torsional stiffnesses with corresponding standard deviations and median linear and torsional stiffnesses with corresponding interquartile ranges for each bundle.

LINEAR STIFFNESS

Due to the large number of measurements and the variety in the position of the bundles collected within a single utricle, utricle 12 will be presented as an example. This utricle was chosen as representative of all tested as it contained a variety of bundles from different parts of the utricle, including medial, striolar, and lateral. Figure 5.1 shows PMT calibration curve for utricle 12 and the testing trials used to determine the linear and torsional stiffnesses of test 12-9 (utricle 12, test 9). Based on the calibration curve the calibration factor is the slope of the curve, 0.0965 V/μm. The calibration factor is used to calculate the bundle displacement from the absolute PMT voltage change value. The values of the absolute PMT voltage change contain only one significant figure. This was due to constraints on the multimeter from where the output voltages were read. The mean linear stiffness for test 12-9 is 3.181 E-04 N/m and the median linear stiffness 2.56 E-04 N/m. This calculation procedure was done for each bundle tested. Figure 5.2 shows the position from the line of polarity reversal versus the mean linear stiffness (with standard deviations) and the position from the line of polarity reversal versus the median linear stiffness (with interquartile ranges) for all the bundles tested in utricle 12. Also shown on these graphs are profiles of the bundles tested. A description of how the profiles were derived is provided in Chapter 3. It is apparent that as the position of the bundle in utricle 12 moves farther away from the line of polarity reversal, the linear stiffness of the bundle decreases.

The linear stiffness curves for all other utricles can be found in Appendix B.

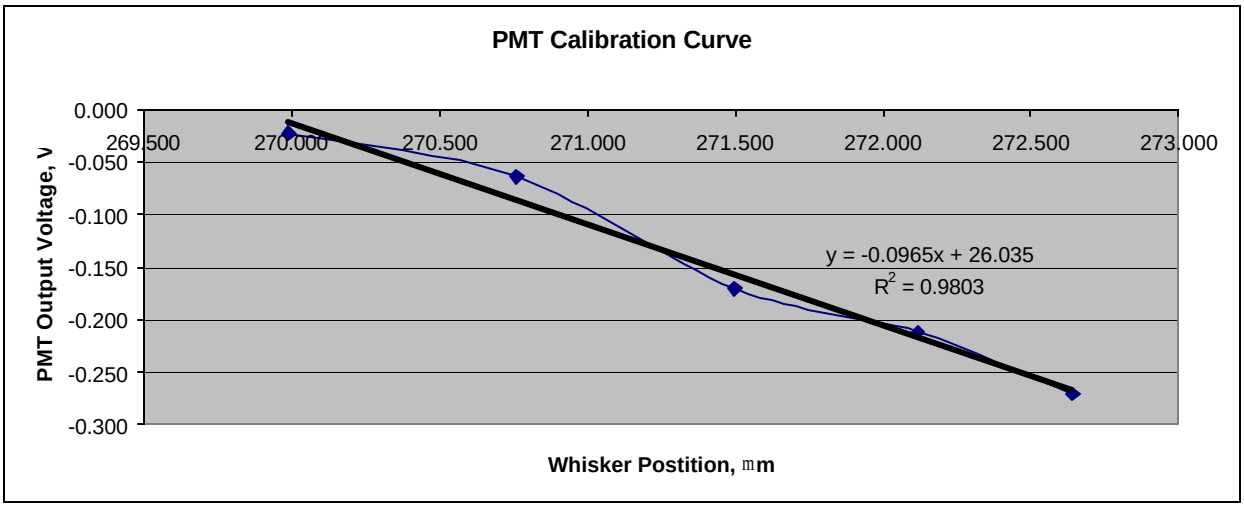

Trial	Whisker Displacement (? m)	Absolute PMT Voltage Change (V)	Bundle Displacement (? m)	Applied Force (pN)	Bundle Stiffness (N/m)
1	0.523	0.008	0.0829	4.24695	5.123 E-05
2	1.241	0.002	0.0207	11.77565	5.682 E-04
3	0.526	0.002	0.0207	4.8759	2.353 E-04
4	0.495	0.004	0.0415	4.37675	1.056 E-04
5	0.856	0.003	0.0311	7.9604	2.561 E-04
6	0.719	0.001	0.0104	6.83835	6.599 E-04
7	0.387	0.001	0.0104	3.63455	3.507 E-04

Figure 5.1 Tissue test results for test 12-9.
The whisker for this test had a stiffness of 9.65 E-06 N/m. The calibration factor determined from the calibration curve was 0.0965 V/μm. The mean stiffness was determined to be 3.181 E-04 N/m and the median stiffness was 2.56 E-04 N/m.

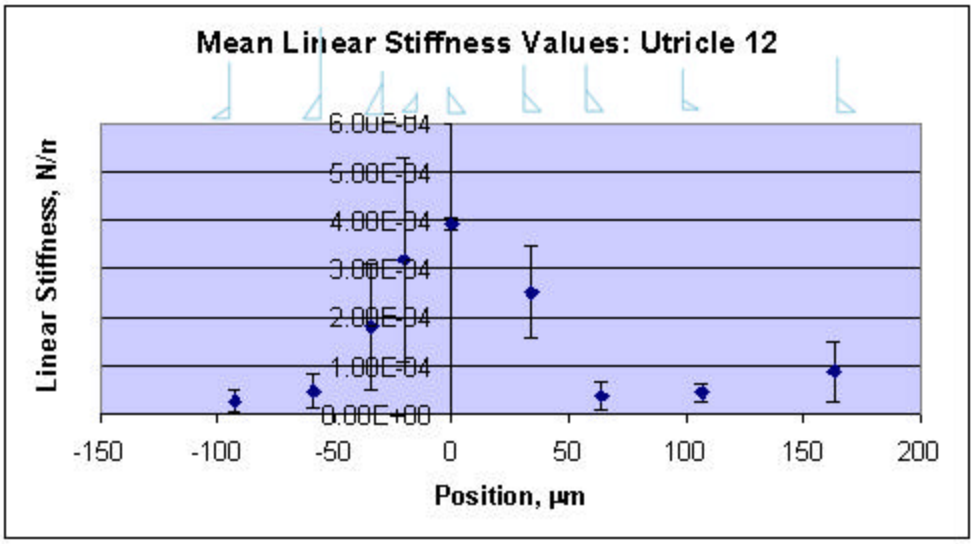

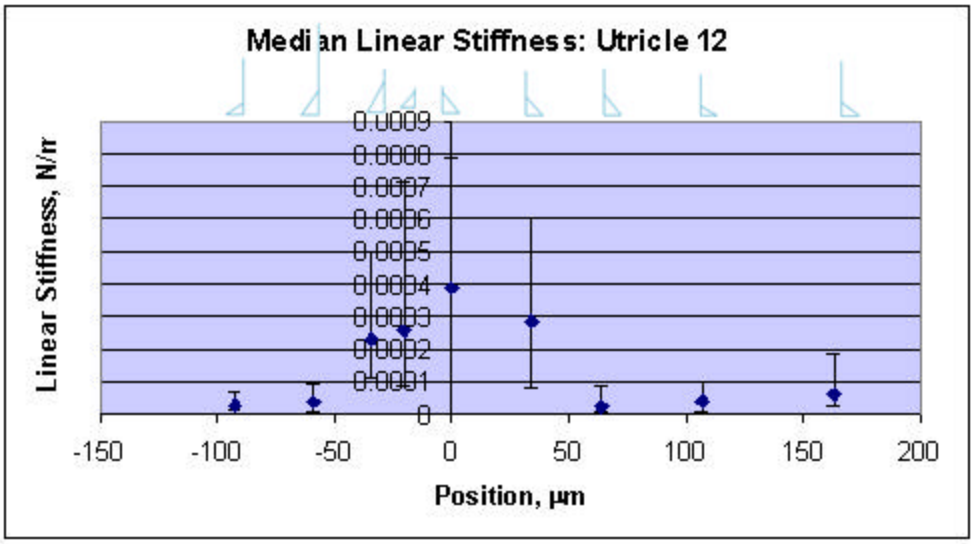

Figure 5.2 Mean and median linear stiffness versus position of the bundle from the line of polarity reversal (position=0) for utricle 12.
As the position of the bundle tested moves away from the line of polarity reversal, the stiffness of each bundle decreases.

TORSIONAL STIFFNESS

The torsional stiffnesses were also calculated for all of the bundles tested. Torsional stiffness is used to determine if the point of force application has an effect on the linear stiffness results. When the bundle is modeled as a rigid rod attached to a torsional spring at its base, the bundle's structural ability to resist an applied moment around the base can be expressed as torsional stiffness (Crawford and Fettiplace, 1985). Torsional stiffness, k_T, is calculated from the equation:

$$k_T = \frac{F_B \times h}{q} \quad \text{[N-m/rad]} \qquad [5.1]$$

where F_B is the force applied to the bundle, h is the height of the force application (in this study is the height of the kinocilium), and θ is the angular deflection of the bundle (Figure 5.3). The force is calculated using the stiffness and the deflection of the whisker as shown in equation 5.2.

$$F_B = k_W \times \Delta x_W \quad \text{[N]} \qquad [5.2]$$

The angular deflection is calculated using equation 5.3.

$$\theta = \text{ArcTan}\left(\frac{h}{\Delta x_B}\right) \quad \text{[rad]} \qquad [5.3]$$

Once the torsional stiffnesses were calculated, the mean and median torsional stiffnesses were plotted versus the position of the bundle from the line of polarity reversal, shown in Figure 5.4 for utricle 12. There was no trend found in the torsional stiffness versus position curves. At one time, it was thought that all bundles of similar structure would have similar torsional stiffnesses regardless of bundle height (Crawford et al, 1985). From the measurements in this study, this appears to not be the case.

The torsional stiffness curves for all other utricles can be found in Appendix C.

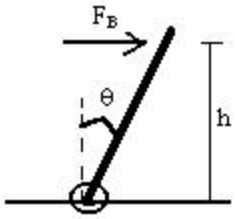

Figure 5.3 Torsional stiffness.
Angular deflection (θ) is calculated using the measured force applied to the bundle (F_B) and the height of force application (h).

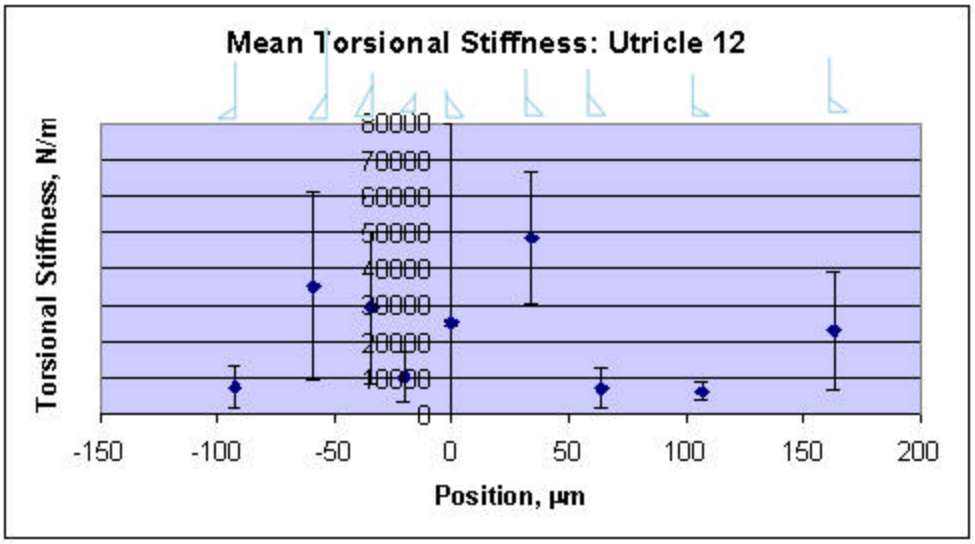

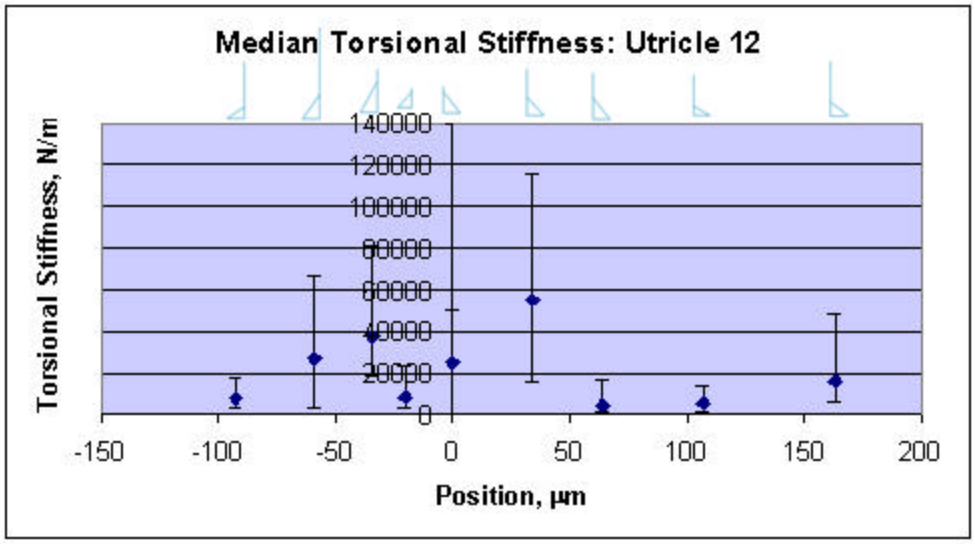

Figure 5.4 Mean and median torsional stiffness versus position of the bundle from line of polarity reversal (position=0) for utricle 12.
A trend is not apparent in these graphs.

APPLIED FORCE AND STIFFNESS

In Figure 5.5, the force versus linear stiffness slopes are shown for all bundles tested in utricle 12 as well as a plot of force versus linear stiffness for test 12-5. By observing the tests where the R^2 value is high, indicating a high correlation between the data points, it is shown that as the force applied to the bundle increases, the linear stiffness also increases. In almost all bundles tested in this study, the mean linear stiffness of a bundle increased with applied force, especially when the R^2 values were near one.

Test Number	Slope of Force/Mean Linear Stiffness Line	R^2
12-1	2 E-05	0.4874
12-2	1 E-06	0.031
12-3	2 E-05	0.5321
12-4	2 E-04	0.8624
12-5	1 E-04	1
12-6	6 E-05	0.9948
12-7	8 E-06	0.2201
12-8	4 E-06	1
12-9	5 E-05	0.3861

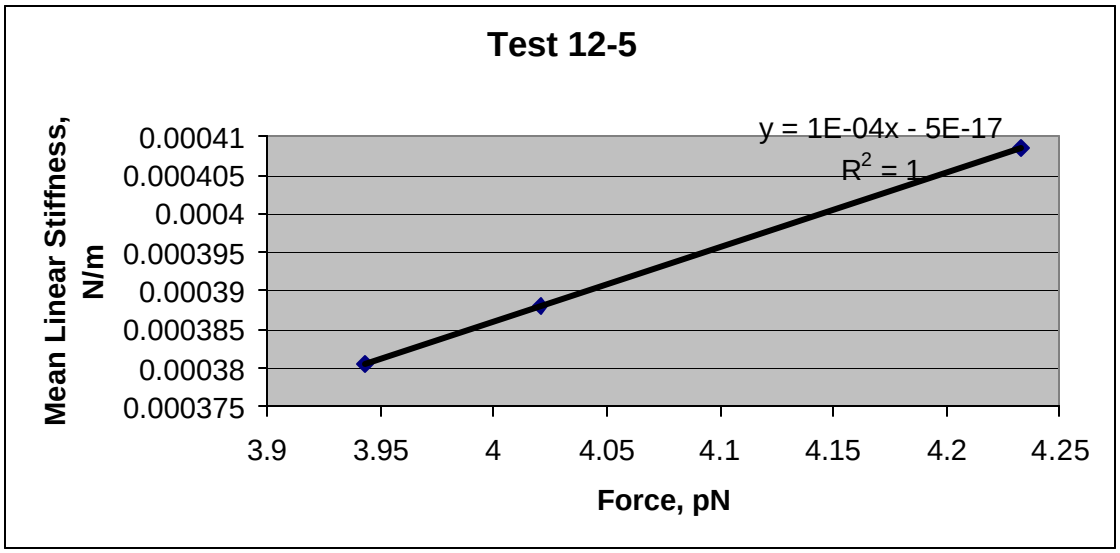

Figure 5.5 Relationship between force and mean linear stiffness for utricle 12.
As the force applied to the tip of the kinocilium increases, the measured linear stiffness value also increases.

This same type of general behavior is seen in computational models of bundles similar to the ones tested here (Silber, 2002). This result is considered to be one of the more significant results of this study. The increase in stiffness with applied force is most likely due to the fact that as the displacement of the bundle increases, more stereocilia in the bundle are being utilized. Plans are being made to compare these increases directly to the computer modeling effort. These comparisons will hopefully identify the structural contribution to this increasing stiffness.

DATA EXCLUSION

While analyzing the data, it was determined that some of the tests were erroneous. Numerous factors played into the decision to discard data. The first sets of data to be discarded were all the bundles tested on utricles 2, 3, and 4. It was determined that the stiffness of the whisker used during these tests was much higher than the stiffness range of the bundles tested, therefore the measurements were inaccurate. When the stiffness of the whisker is greater than the stiffness of the bundle, the whisker does not bend during the bundle displacement. Without a measurable whisker displacement, the stiffness of the bundle cannot be correctly determined. Test trials for a particular bundle that resulted in a negative stiffness value were also discarded. It was apparent that a mistake occurred during these trials. During testing, it is not possible to test the bundle and view the testing on the monitor simultaneously. Therefore, the whisker may have lost contact with the bundle and snapped back to its original position during the trials where the stiffness value was calculated as negative. Forces acting on the bundle due to convection flow of the fluid during testing may have caused motion in the bundle, eliciting a false response from the diodes. Another major source of error is the dual diode array. The diodes must be illuminated equally and require a very good light source. The voltages created by the diodes are so small that they are very susceptible to extraneous noise and interference. By comparing the raw data for each bundle tested, it was found that the direction of some of the PMT output voltages did not match the slope of the calibration curve for that utricle (i.e. a decrease in voltage when an increase was expected). This data was thrown out. Some of the calculated linear stiffnesses for a given bundle were out of the range of the other measurements (statistical outliers), causing the mean and median linear stiffnesses for a single bundle to be significantly different. These statistical outliers were also discarded. Finally, when the resulting data was compiled, bundles that were left with only one trial measurement were discarded. It was assumed that one measurement trial was not suitable for determining the stiffness of the bundle.

COMBINED UTRICLE RESULTS

The complete set of data from all utricles was used to produce the graphs shown in Figures 5.6, 5.7, and 5.8.

In Figure 5.6, the mean linear stiffness is plotted versus the position of the bundle from the line of polarity reversal for all bundles. A total of 83 bundles are included in the final data set. In the extended striolar region, defined by approximately from -50 μm to 150 μm, there is a significant increase in the overall stiffness of some bundles while others have the same stiffness as in the medial extrastriolar region. This increase in stiffness is what was originally thought to occur based on observed bundle structure and confirms previous research. Merkle (2000) found that most striolar bundles had higher stiffnesses than extrastriolar bundles. While there is an increase in stiffness of some bundles close to the line of polarity reversal, there is also an increase in stiffness of bundles lateral and medial to the line of polarity reversal. The classical definition of the striolar region includes bundles lateral to the line of polarity reversal (Werner, 1933). Observations made using a scanning electron microscope (SEM) have also found bundles with striolar like structure lateral to the line of polarity reversal (Peterson). The increased stiffness values found in the striolar region (mean of 2.27 E-04 ± 2.53 E-04 N/m) confirm these observations.

While the increase in the bundle stiffness in the striolar region was expected, the variance of stiffness in the medial region was unexpected. The stiffness of the bundles in this area averaged 1.16 E-04 ± 1.3 E-04 N/m. This wide range of medial bundle stiffnesses may be due to damage induced by dissection and folding, size variations (height and diameter) in the stereocilia between bundles, differences between maturity of the bundles which implies maturity of the link and actin materials, or a combination of these. The average of stiffness found in the region lateral to the striolar region was 6.30 E-05 ± 2.49 E-05 N/m.

In Figure 5.7, the mean torsional stiffness is plotted versus the position of the bundle from the line of polarity reversal for all 83 bundles. The relevance of the torsional stiffness to the results could not be determined. It has been hypothesized that all bundles have the same torsional stiffness, which is not confirmed from these results. There was no trend found in the torsional stiffness data.

Finally, Figure 5.8 shows the height of the kinocilium on each bundles plotted versus the mean linear stiffness for that bundle. It was thought that there is a direct relationship between the height of the kinocilium on a bundle and the bundle's stiffness. This plot shows no apparent relationship between the height and the stiffness. Computer models of bundles with varying heights also show little to no relationship between the height and stiffness of a bundle (Silber, 2002). There was also no correlation between height squared and stiffness. The conclusion that height is not a major factor in bundle stiffness leads to the assumption that other factors are involved in a bundle's stiffness. Other factors may include the number of stereocilia in a bundle, the arrangement of the stereocilia, and the diameters of each individual stereocilium. These are factors that were not measurable during this study. A study by Silber (2002) where bundles were modeled using Finite Element Modeling (FEM) shows that the diameter of the stereocilia does have an effect on the stiffness. The age of the turtle or the size of the turtle may also affect the bundle stiffness. Younger turtles may have less mature hair cells than older turtles and the maturity of the hair cell may have an effect on the measured stiffness of the bundle.

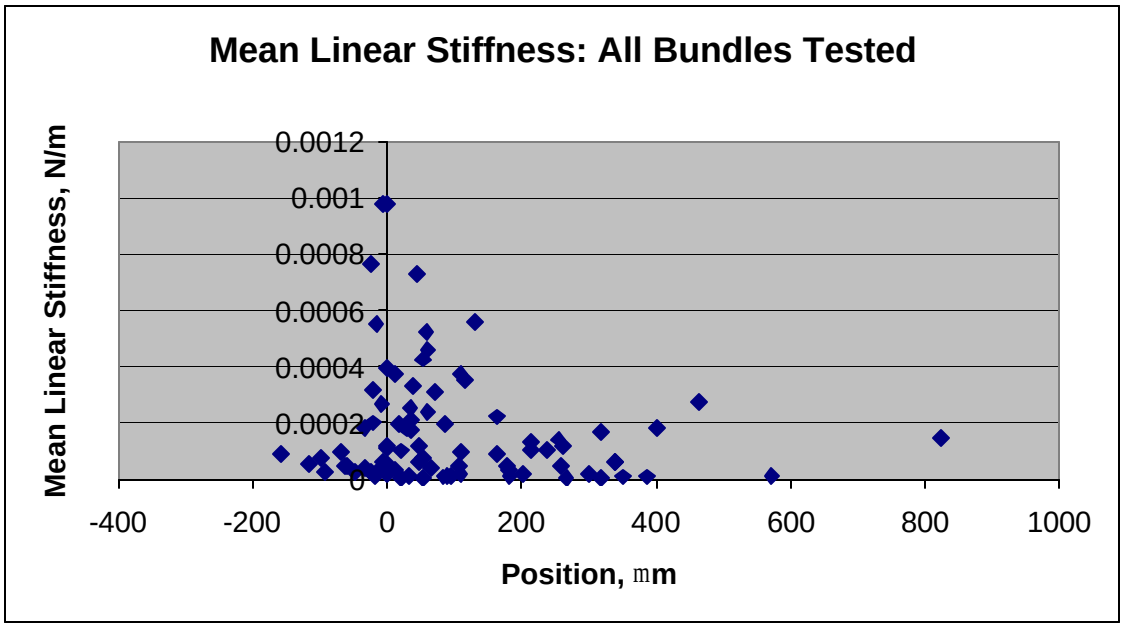

Figure 5.6 Mean linear stiffness versus position of the bundle.
The line of polarity reversal is indicated by a zero position. There is a significant increase in the stiffness of the bundles in the region surrounding the line of polarity reversal.

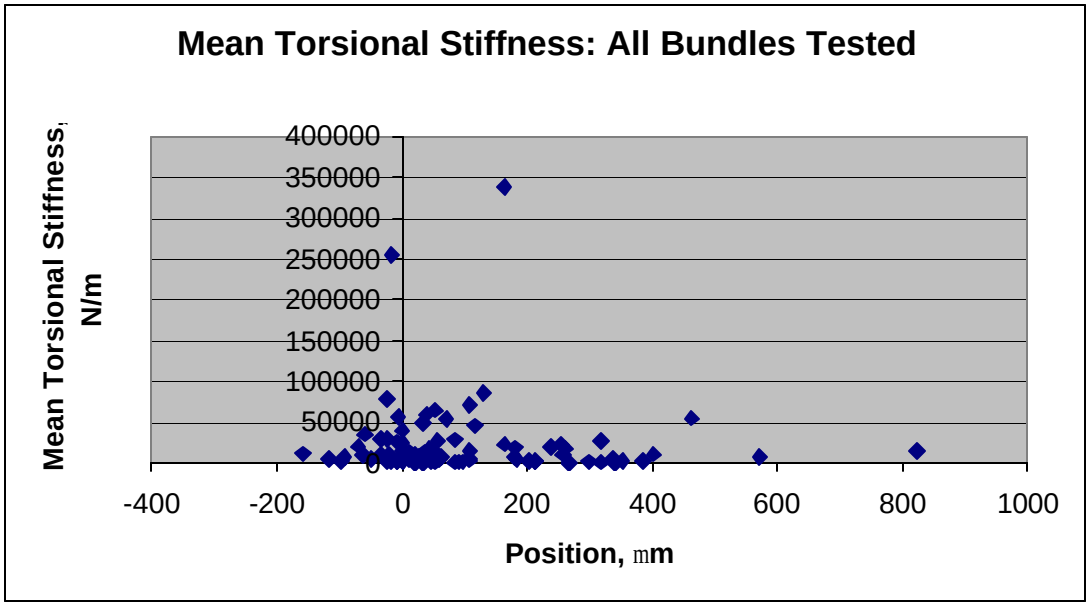

Figure 5.7 Mean torsional stiffness versus position of the bundle.
The line of polarity reversal is indicated by a zero position. There was no trend found between the position of the bundle and the torsional stiffness.

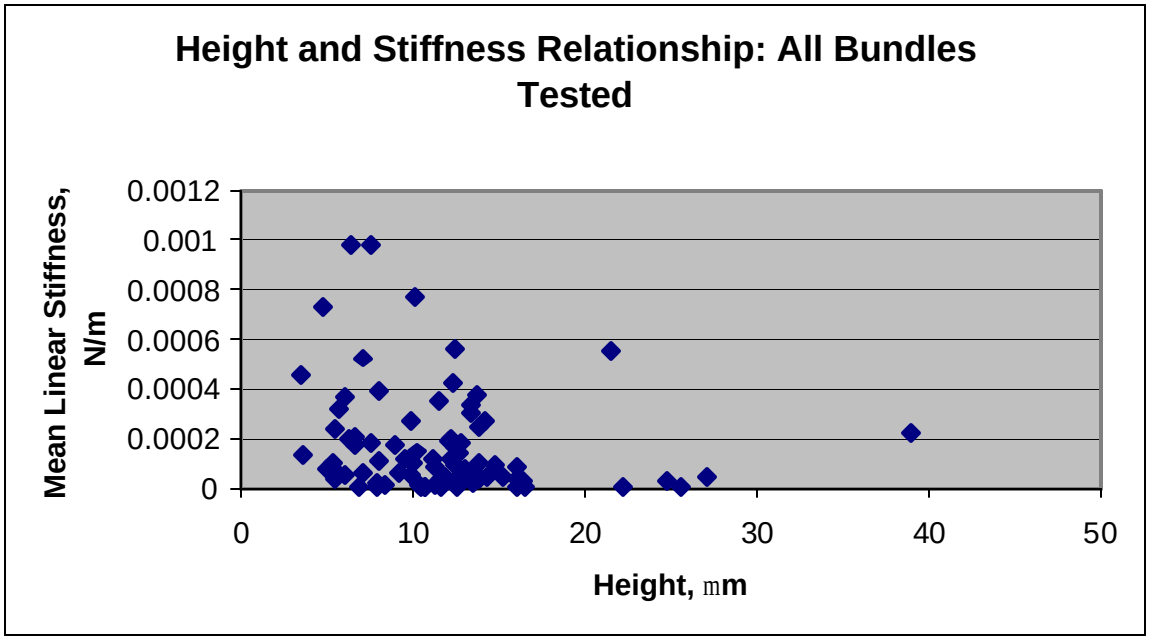

Figure 5.8 Mean linear stiffness versus height of a bundle.

SUMMARY OF CONCLUSIONS

Many factors may have lead to inaccurate stiffness measurements during this study. As previously mentioned, the PMT is very sensitive to the conditions it is exposed to and many errors can result from the use of this system. Damage to the hair bundles may have occurred during the dissection process resulting in erroneous stiffness measurements. While this study mainly investigated the relationship between the position of the bundle versus the stiffness of the bundle, there are many other factors that may affect the stiffness.

While numerous factors were investigated during this study, including height of hair bundles, location of hair bundles, linear stiffness, and torsional stiffness, the following conclusions have been made:

- Linear stiffness of a bundle increases in the area surrounding the line of polarity reversal including the striolar region.
- There is a wide range of linear stiffness found among the hair bundles in the medial range.
- Torsional stiffness of a bundle ranges drastically within a utricle.
- As the force applied to a hair bundle is increased, the stiffness of the bundle increases.

FUTURE WORK AND RECOMMENDATIONS

This study was very limited due to equipment constraints. The location of the bundles tested was measured from the line of polarity reversal. In future work, a more precise method for determining the exact location of the bundle can be developed. While the kinocilium and tallest stereocilium was measured during this study, determining the structure of the entire bundle, including the number and arrangement of the stereocilia, will paint a better picture of the bundle and allow for a better comparison between the structure of a bundle and its stiffness. An automated data recording system for the PMT and the EFPI would allow for more accurate data collection. Maintaining the viability of the hair cells during testing can be improved to allow for longer testing time.

REFERENCES

Barrett, M.D. (1995). Fiber Optic Interferometer for Measuring Sub-Micrometer Displacements of Ciliary Bundles. Thesis, Virginia Polytechnic Institute and State University.

Beer, F.P. & Johnston, Jr., E.R. (1992). Mechanics of Materials, Second Edition. New York: McGraw Hill.

Burleigh Manuals. (1997). Fishers, New York.

Crawford, A.C. & Fettiplace, R. (1985). "The mechanical properties of ciliary bundles of turtle cochlear hair cells." *Journal of Physiology* 364: 359-379.

EG&G Product Bulletin 1090. Montgomeryville: PA.

Engström, H. & Engström, B. (1981). "The Structure of the Vestibular Sensory Epithelia." The Vestibular System: Function and Morphology. Edited by T. Gualitierotti. New York: Springer-Verlag.

F&S, Inc. AFSS-PC v3 User's Manual, Revision B. (1999). Blacksburg, VA.

Felsted, K. (2002) "Analysis of Inner Ear Perilymph and Extracellular Fluid." Undergraduate Research, Virginia Tech.

Flanagan, J.L. (1972). Speech Analysis Synthesis and Perception, 2nd ed. New York: Springer-Verlag,.

Flock, Å. (1965). "Transducing mechanisms in the lateral line canal organ receptors." Cold Spring Harbor Symp. Quant. Biol. 30:133-145.

Geisler, D.C. (1998). From Sound to Synapse: Physiology of The Mammalian Ear. New York: Oxford University Press.

Gibbons, J.W. (1990). Life History and Ecology of the Slider Turtle. Washington D.C.: Smithsonian Institution Press.

Gillespie, D.G. (1995). "Molecular machinery of auditory and vestibular transduction." *Curr. Opin. Neurobiol*. 5:449-455.

Hudspeth, A.J. (1983). "The hair cells of the inner ear." *Scientific American* 248: 54-64.

Iurato, S. (1967). Submicroscopic Structure of the Inner Ear. Oxford: Pergamon.

Kachar, B., Parakkal, M., Fox, J. (1989). "Structural basis for mechanical transduction in the frog vestibular sensory apparatus: I. The otolithic membrane. *Hearing Research* 45: 179-190.

Kelly, J.P. (1981). "Vestibular System." Principles of Neural Science. Edited by E.R. Kandel and J.H. Schwartz. New York: Elsevier North Holland, Inc.

Klinke, R. (1986). "Physiology of Hearing." Fundamentals of Sensory Physiology. Edited by R.F. Schmidt. New York: Springer-Verlag.

Lewis, E.R., Leverenz, E.L., & Bialek, W.S. (1985). The Vertebrate Inner Ear. Boca Raton, FL: CRC Press, Inc.

Lim, D.J. (1976). "Morphological and Physiological Correlates in Cochlear and Vestibular Sensory Epithelia." Scanning Electron Microscopy. Chicago: IIT Research Institute.

Lindeman, H.H. (1973). "Anatomy of the otolith organs." Adv. Oto-Rhino-Laryngol., 20, 405.

Merkle, A.C. (2000). "Implementation of a Photoelectronic Motion Transducer for Measuring Sub-Micrometer Displacements of Vestibular Bundles." Master's Thesis, Virginia Tech.

Perkins, W.H., Kent, R.D. (1986). Functional Anatomy of Speech, Language, and Hearing. San Diego, CA: College-Hill Press

Silber, J. (2002). Personal Communication. Virginia Tech.

Singh, R.P. (1980). Anatomy of Hearing and Speech. New York: Oxford University Press.

Spoendlin, H. (1966). "Ultrastructure of the Vestibular Sense Organ." The Vestibular System and it Diseases. Philadelphia: University of Pennsylvania Press.

Streiloff, D. & Flock, Å. (1984) "Stiffness of sensory-cell hair bundles in the isolated guinea pig cochlea." *Hearing research* 15: 19-28.

Szymko, Y.M., Dimitri, P.S., & Saunders, J.C. (1991). "Stiffness of hair bundles in chick cochlea." *Hearing Research* 59: 241-249.

Werner, C.F. (1933) Die Differenzierung der Maculae im Labyrinth, insbesondere bei Säugetieren. Zeitschrift feur Anatomie und Entwicklungsgeschichte 99:696-709.

Wersall, J. Bagger-Sjoback, D. (1974) "Morphology of the vestibular sense organ." Handbook of Sensory Physiology. Kornhuber, H.H. Ed., Berlin: Springer-Verlag.

APPENDIX A: TABLE OF EXPERIMENTAL VALUES

position, µm	kino, .µm	stereo, µm	mean lin. stiffness, N/m	std dev, N/m	median lin. stiffness, N/m	quartile lower, N/m	quartile upper, N/m	utricle #
351.44	16.5	5.84	8.39369E-06	5.78847E-06	6.30128E-06	4.40123E-06	1.23123E-05	1
571.92	25.54	4.165	1.072E-05	6.68E-06	7.14433E-06	6.74817E-06	1.11206E-05	1
385.48	16.08	4.021	8.43E-06	1.61E-06	8.69731E-06	7.43838E-06	9.50654E-06	1
180.85	24.82	5.154	2.99E-05	2.91E-05	1.46121E-05	8.20658E-06	5.18382E-05	1
213.78	5.309	2.722	1.05E-04	6.21E-05	0.000105452	7.44202E-05	0.000136484	1
261.21	12.27	2.711	0.000119552	6.64E-05	0.000121163	8.76079E-05	0.000180685	5
213.48	3.647	2.177	0.000132972	1.11E-04	7.63868E-05	5.51674E-05	0.000182484	5
53.23	13.05	3.89	7.69689E-05	3.66538E-05	7.85048E-05	6.0722E-05	8.80755E-05	5
-157.83	11.26	2.593	8.96344E-05	7.62213E-05	0.000107461	9.35862E-06	0.000117867	5
338.06	9.144	3.161	6.12808E-05	4.50E-05	6.25762E-05	2.73754E-05	7.55596E-05	5
8.23E+02	1.02E+01	2.945	1.48E-04	9.80E-05	0.000108018	9.33212E-05	0.000162748	5
-98.34	4.987	3.132	7.72E-05	7.48E-05	6.18322E-05	2.02424E-05	9.04528E-05	6
60.37	5.5	5.21	0.000240646	0.000189864	0.00017085	0.000101326	0.000336022	6
34.89	6.664	5.087	0.000208351	9.17E-05	0.000188968	0.000120989	0.000299926	6
402.53	7.53	3.766	0.000184775	1.52E-04	0.000127296	6.45744E-05	0.000264672	6
48.36	9.539	5.487	0.000115387	3.73E-05	0.000141355	0.000102028	0.00014173	6
-18.02	10.3	8.121	1.29E-05	4.03E-06	1.28664E-05	1.04004E-05	1.53323E-05	7
95.75	10.5	2.357	1.05E-05	7.05E-06	1.05178E-05	1.40406E-05	8.41449E-05	7
163.43	38.97	2.068	0.000222082	1.39E-04	0.000151216	0.000123619	0.000262434	8
237.63	13.84	3.647	0.000104217	7.61E-05	5.95939E-05	5.06862E-05	0.000135436	8
339.75	13.59	4.417	5.99725E-05	3.07E-05	5.4911E-05	3.17479E-05	8.31356E-05	8
463.49	14.16	3.132	0.000273966	0.000111227	0.000278265	0.000217419	0.000300992	8
0	6.406	5.362	0.000980647	0.000565351	0.001114517	0.000644892	0.001450273	8
130.31	12.41	4.655	0.000558893	2.82E-04	0.000473274	0.000320363	0.000726461	8
2.54E+02	1.27E+01	3.305	1.42E-04	5.29E-05	0.000144242	0.000101396	0.000192155	8
70.68	13.35	4.769	3.08E-04	0.000157996	0.000239144	0.000219557	0.000395075	9
85.03	12.09	3.647	0.000194999	5.84E-05	0.000203206	0.000151955	0.000232814	9
108.74	12.42	2.432	9.43E-05	2.94E-05	9.00323E-05	7.32153E-05	0.000125572	9
1.08E+02	1.37E+01	3.031	3.75E-04	7.44E-05	3.76E-04	3.30E-04	4.21E-04	9
-24.62	10.11	2.566	0.000767421	0.000600302	0.000701363	0.000384412	0.0011174	9
-16.56	21.52	2.65	5.50E-04	0.000249531	0.000549984	0.000333764	0.000765929	9
317.71	12.41	3.287	0.000170329	1.04E-04	0.000183027	8.677E-05	0.000266586	10
53.55	12.31	4.333	0.000427476	8.14217E-05	0.000427476	0.000386765	0.000468187	10
38.53	13.41	3.571	0.000332976	0.000220622	0.000324951	0.000128597	0.00053371	10
35.94	8.906	8.274	0.000172346	0.000123558	0.000107913	7.89513E-05	0.000252797	11
57.73	7.068	6.185	0.000524995	0.000339039	0.000425866	0.00029708	0.000703345	11
11.7	11.64	8.322	3.61E-05	3.26E-05	1.89409E-05	1.72803E-05	3.90205E-05	11
-8.571	5.5	3.522	3.99E-05	1.60E-05	3.63482E-05	2.86066E-05	4.76334E-05	11
-24	7.925	4.793	2.34E-05	1.44739E-05	3.19051E-05	1.74754E-05	3.36075E-05	11
163.34	16.1	4.018	8.90E-05	6.29E-05	6.09901E-05	3.74933E-05	0.000126984	12
106.85	11.83	2.765	4.49E-05	1.76E-05	3.98213E-05	3.23549E-05	5.83837E-05	12
64.07	13.79	6.06E+00	3.81E-05	2.79E-05	2.29429E-05	1.74886E-05	6.57792E-05	12
34.1	13.88	5.236	0.000251869	9.44817E-05	0.000285548	0.000204299	0.000316279	12
0	8.03	6.415	0.000392329	1.18E-05	0.000387983	0.000384258	0.000398227	12
-34.17	12.74	8.934	0.000181182	0.000128945	0.00023014	0.000117358	0.000269485	12
-58.97	27.07	7.072	4.81E-05	3.52E-05	3.69319E-05	3.20792E-05	5.46278E-05	12
-92.71	16.43	3.325	2.79E-05	2.10E-05	2.78857E-05	1.73782E-05	3.83932E-05	12
-20.4	5.676	4.509	0.000318136	0.000209599	0.00025606	0.000170426	0.000459455	12

position, μm	kino, μm	stereo, μm	mean lin. stiffness, N/m	std dev, N/m	median lin. stiffness, N/m	quartile lower, N/m	quartile upper, N/m	utricle #
0	11.19	10.12	1.22E-04	7.69E-05	9.20084E-05	6.90667E-05	0.000159642	13
20.79	9.973	9.095	1.00E-04	6.99E-05	7.93756E-05	4.8747E-05	0.000159225	13
45.89	5.708	3.776	5.96E-05	3.64E-05	5.44079E-05	2.8025E-05	8.59601E-05	13
84.19	10.73	4.769	8.18E-06	4.22E-06	1.0348E-05	7.13019E-06	1.04314E-05	13
-6.846	7.055	5.979	6.50E-05	5.01E-06	6.49551E-05	6.24524E-05	6.74578E-05	13
-116.5	9.862	3.437	5.60E-05	3.928E-05	8.30826E-05	4.17616E-05	8.3762E-05	14
-61.73	14.26	6.74	4.70E-05	1.55E-05	4.69916E-05	3.92215E-05	5.47618E-05	14
-7.698	9.849	7.568	0.000269146	0.000162339	0.000213859	0.000149547	0.000355166	14
0	8.054	6.821	0.000110302	0.000105829	5.52289E-05	3.62747E-05	0.000156793	14
28.52	6.66	5.567	0.000177411	0.000152296	0.00015121	3.45119E-05	0.000294109	14
53.16	12.5	4.161	5.68E-06	5.58E-06	2.87772E-06	2.23709E-06	5.5988E-06	14
182.23	22.16	3.013	9.59501E-06	6.78733E-06	9.59501E-06	6.20134E-06	1.29887E-05	15
44.47	4.793	4.219	0.000728498	0.000413872	0.000771715	0.000587141	0.000795124	15
-6.279	7.562	5.565	0.000980879	0.000488903	0.000778318	0.000643984	0.001216493	15
-69.89	14.74	3.507	9.55E-05	7.98E-05	5.81872E-05	4.7068E-05	0.000123548	16
-22.25	12.23	5.211	0.000201013	0.000117955	0.000159749	0.000124178	0.00023639	16
-33.02	16.01	9.088	3.78E-05	1.42E-05	3.55048E-05	2.89876E-05	4.84705E-05	17
258.16	15.24	2.772	4.79E-05	4.08E-05	4.16624E-05	1.53464E-05	7.42126E-05	17
318.42	10.72	3.636	7.14E-06	4.60E-06	6.68696E-06	4.46762E-06	8.34098E-06	17
-48.28	13.55	4.914	2.36E-05	3.42744E-05	1.02765E-05	2.73236E-06	1.76534E-05	17
0	6.05	5.377	5.42E-05	2.31E-05	5.46694E-05	3.52818E-05	5.68272E-05	17
179.11	12.71	3.287	4.63E-05	4.51E-05	3.56905E-05	4.07552E-06	7.79509E-05	17
17.56	6.291	4.938	0.000197407	0.000198216	0.000136154	3.58834E-05	0.000313888	17
299.08	11.27	2.593	1.54471E-05	1.27575E-05	1.21576E-05	4.90613E-06	2.00626E-05	18
266.08	11.63	2.886	3.47227E-06	2.2629E-06	2.6516E-06	1.76136E-06	5.03489E-06	18
0	8.431	5.236	1.76037E-05	6.41285E-06	1.7994E-05	1.16672E-05	2.33747E-05	18
89.93	11.63	3.591	1.34801E-05	8.96829E-06	1.28094E-05	1.12523E-05	1.94908E-05	18
202.33	11.39	4.146	2.10365E-05	1.66742E-05	1.37872E-05	9.20752E-06	2.75612E-05	18
21.4	7.862	6.598	6.60625E-06	4.38135E-06	4.48813E-06	3.1172E-06	9.88628E-06	18
32.54	6.913	5.557	1.1219E-05	7.26006E-06	9.0435E-06	5.78218E-06	1.44803E-05	19
115.9	11.46	3.143	0.000350844	0.000167315	0.00044461	0.000280215	0.000468356	19
12.7	6.05	5.35	0.000371565	0.000240727	0.000371565	0.000251201	0.000491929	20
108.49	12.63	5.022	2.08727E-05	9.06406E-06	2.08727E-05	1.63407E-05	2.54047E-05	20
60.41	3.433	2.445	0.000457397	0.000285658	0.000482131	0.00027482	0.000664707	20

position, μm	kino, μm	stereo, μm	mean tors. stiffness, N/m	std dev, N/m	median tors. stiffness, N/m	quartile lower, N/m	quartile upper, N/m	utricle #
351.44	16.5	5.84	2293.841153	1577.12962	1722.405102	1216.959332	3360.211356	1
571.92	25.54	4.165	7020.690801	4345.00952	4696.943939	4414.848556	7302.786184	1
385.48	16.08	4.021	2203.998883	423.544279	2278.987984	1947.449239	2484.365793	1
180.85	24.82	5.154	18420.88119	17916.8122	9019.105087	5068.58526	31937.24819	1
213.78	5.309	2.722	2972.689223	1749.27763	2972.689223	2098.050409	3847.328038	1
261.21	12.27	2.711	17999.08601	9993.30065	18241.59307	13190.10435	27202.76009	5
213.48	3.647	2.177	1768.634006	1481.51653	1016.028781	733.7941675	2427.171232	5
53.23	13.05	3.89	13108.13315	6242.2658	13369.72717	10341.27966	14999.56721	5
-157.83	11.26	2.593	11364.92986	9663.64217	13624.8212	1188.047078	14944.2438	5
338.06	9.144	3.161	5123.998412	3760.03746	5232.358397	2289.121441	6317.850026	5
8.23E+02	1.02E+01	2.945	15524.38175	10273.1366	11326.63666	9785.586848	17065.43156	5
-98.34	4.987	3.132	1.92E+03	1860.08847	1538.010368	503.798066	2249.734571	6
60.37	5.5	5.21	7279.591591	5743.37714	5168.267741	3065.196745	10164.70301	6
34.89	6.664	5.087	9252.669352	4072.32662	8391.916519	5373.052033	13319.4073	6
402.53	7.53	3.766	10477.01926	8631.56917	7218.031831	3661.477524	15007.23513	6
48.36	9.539	5.487	10499.52472	3389.94039	12862.45769	9284.021913	12896.49401	6
-18.02	10.3	8.121	1365.003856	427.213492	1364.999789	1103.389073	1626.616606	7
95.75	10.5	2.357	1159.631059	776.822537	1159.631059	771.2197908	1548.042327	7
163.43	38.97	2.068	337268.7282	211614.246	229647.6225	187737.1988	398549.5912	8
237.63	13.84	3.647	19962.39481	14567.5347	11415.04542	9708.804531	25942.31039	8
339.75	13.59	4.417	5.99725E-05	3.0737E-05	14202.56985	6080.409889	18810.48859	8
463.49	14.16	3.132	54932.6116	22301.5341	55794.50416	43594.24665	60351.95779	8
0	6.406	5.362	40243.37451	23200.1227	45737.08615	26464.9904	59515.47027	8
130.31	12.41	4.655	86075.45789	43455.8363	72890.63082	49340.49768	111881.6597	8
2.54E+02	1.27E+01	3.305	22963.54748	8538.58477	23267.51827	16356.01636	30994.14448	8
70.68	13.35	4.769	54699.9643	28032.1664	42430.68556	38955.03222	70096.23566	9
85.03	12.09	3.647	28503.80369	8531.73134	29703.31361	22211.73101	34031.64839	9
108.74	12.42	2.432	14549.82489	4532.85077	12051.03739	11295.62272	19370.38644	9
1.08E+02	1.37E+01	3.031	7.07E+04	1.40E+04	7.09E+04	6.22E+04	7.93E+04	9
-24.62	10.11	2.566	78440.19276	61358.2047	71688.93294	39292.20132	114212.5543	9
-16.56	21.52	2.65	254576.99	115559.657	254703.4469	154570.5231	354709.9137	9
317.71	12.41	3.287	2.623E+04	15979.5485	28190.52262	13364.90689	41059.47615	10
53.55	12.31	4.333	64778.4802	12338.2537	64778.4802	58609.35337	70947.60703	10
38.53	13.41	3.571	5.99E+04	39673.5856	58435.67209	23125.6999	95976.0661	10
35.94	8.906	8.274	13670.05673	9800.16362	8559.484004	6262.298244	20051.13996	11
57.73	7.068	6.185	26226.99742	16937.2492	21274.85166	14841.14344	35136.77852	11
11.7	11.64	8.322	4897.998794	4411.02803	2732.118413	2341.450441	5287.092722	11
-8.571	5.5	3.522	1206.843352	484.837263	1099.672254	865.4592139	1441.056391	11
-24	7.925	4.793	1470.958703	909.053891	2003.893607	1097.597483	2110.787374	11
163.34	16.1	4.018	23060.14047	16301.3773	15809.34246	9718.650856	32915.61686	12
106.85	11.83	2.765	6278.966487	2466.53125	5573.024029	4528.410751	8170.916132	12
64.07	13.79	6.06E+00	7239.001101	5302.11692	4362.914461	3325.726403	12508.85654	12
34.1	13.88	5.236	48523.68851	18202.3202	55012.15145	39359.10435	60932.50414	12
0	8.03	6.415	25297.72763	761.638667	25017.51175	24777.32671	25678.0206	12
-34.17	12.74	8.934	2.94E+04	20928.7455	37353.57503	19048.15648	43739.45246	12
-58.97	27.07	7.072	35215.27728	25814.1618	27063.2394	23507.28191	40030.67177	12
-92.71	16.43	3.325	7528.1953	5673.32685	7528.1953	4691.531876	10364.85872	12
-20.4	5.676	4.509	1.02E+04	6752.63393	8249.546331	5490.645651	14802.28457	12
0	11.19	10.12	15251.78621	9628.69343	11521.13503	8648.380806	19989.86603	13
20.79	9.973	9.095	9946.069694	6949.72273	7894.927765	4848.512984	15836.67358	13

position, μm	kino, μm	stereo, μm	mean tors. stiffness, N/m	std dev, N/m	median tors. stiffness, N/m	quartile lower, N/m	quartile upper, N/m	utricle #
45.89	5.708	3.776	1.94E+03	1187.19651	1772.89843	913.3344447	2800.833099	13
84.19	10.73	4.769	942.0639788	486.275356	1191.95863	821.3091052	1201.818603	13
-6.846	7.055	5.979	3233.105386	249.196705	3233.105386	3108.507033	3357.703738	13
-116.5	9.862	3.437	5445.461012	3820.51283	8080.627544	4061.803111	8146.702179	14
-61.73	14.26	6.74	9555.924089	3160.07719	9555.924089	7975.885493	11135.96269	14
-7.698	9.849	7.568	26108.18755	15747.2552	20745.48249	14506.72441	34452.22341	14
0	8.054	6.821	7.16E+03	6864.75779	3582.586551	2353.11821	10170.7558	14
28.52	6.66	5.567	7.87E+03	6755.08132	6707.359571	1531.302257	13045.45319	14
53.16	12.5	4.161	888.5344043	871.175968	449.8461676	349.9158015	875.9897225	14
182.23	22.16	3.013	4711.866478	3333.10862	4711.866478	3045.312168	6378.420787	15
44.47	4.793	4.219	16735.71619	9507.84242	17728.54293	13488.34541	20975.91371	15
-6.279	7.562	5.565	56090.73219	27957.1566	44507.24979	36825.90385	69563.81933	15
-69.89	14.74	3.507	2.08E+04	17331.3266	1.26E+04	10226.7872	26843.45042	16
-22.25	12.23	5.211	30066.30126	17642.811	23894.36591	18574.22644	35357.48917	16
-33.02	16.01	9.088	9680.584057	3629.7389	9100.911193	7430.442358	12424.19481	17
258.16	15.24	2.772	11125.20761	9480.02558	9677.837685	3566.01952	17237.02577	17
318.42	10.72	3.636	820.3336434	528.889765	769.134105	513.7711965	958.7461443	17
-48.28	13.55	4.914	4326.974736	6293.3485	1887.089608	501.809877	3242.308181	17
0	6.05	5.377	1985.682116	847.062284	2001.066535	1291.624776	2080.202976	17
179.11	12.71	3.287	7485.39846	7280.04735	5765.775669	658.659266	12592.51486	17
17.56	6.291	4.938	7812.813038	7844.73514	5388.824907	1420.199808	12422.78345	17
299.08	11.27	2.593	1962.398651	1620.40926	1544.344301	623.4617182	2549.132916	18
266.08	11.63	2.886	469.7777259	306.073814	358.7530529	238.4105788	681.252086	18
0	8.431	5.236	1251.651328	455.676245	1279.79158	829.7220256	1661.623982	18
89.93	11.63	3.591	1.823E+03	1213.12816	1651.772424	1194.465284	2270.865069	18
202.33	11.39	4.146	2729.341894	2163.23511	1788.712742	1194.716517	3575.986485	18
21.4	7.862	6.598	408.5650464	270.828209	277.5501212	193.0635405	611.4923923	18
32.54	6.913	5.557	536.2508411	346.959659	432.336489	276.4674276	692.1199026	19
115.9	11.46	3.143	4.592E+04	21897.0368	58187.80532	36672.8328	61295.55319	19
12.7	6.05	5.35	13600.24365	8811.23113	13600.24365	9194.628089	18005.85922	20
108.49	12.63	5.022	3329.838414	1445.90979	3329.838414	2606.883519	4052.79331	20
60.41	3.433	2.445	5.391E+03	3366.61934	5682.152885	3238.895744	7833.908021	20

APPENDIX B: STIFFNESS VERSUS POSITION PLOTS FOR ALL UTRICLES TESTED

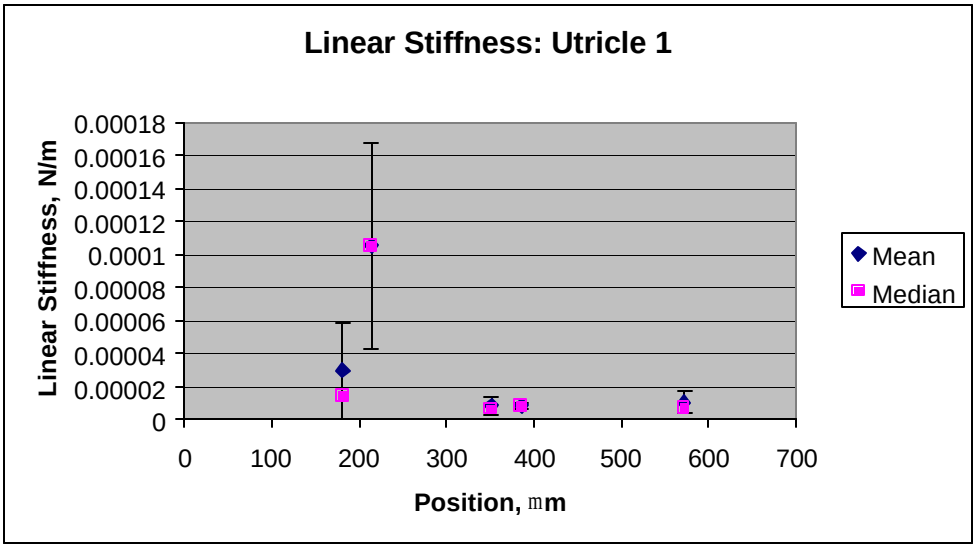

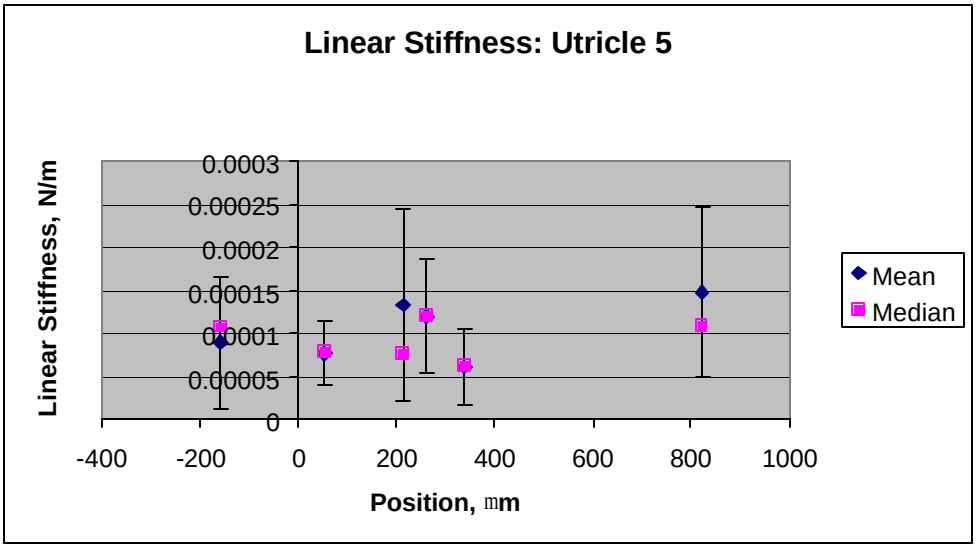

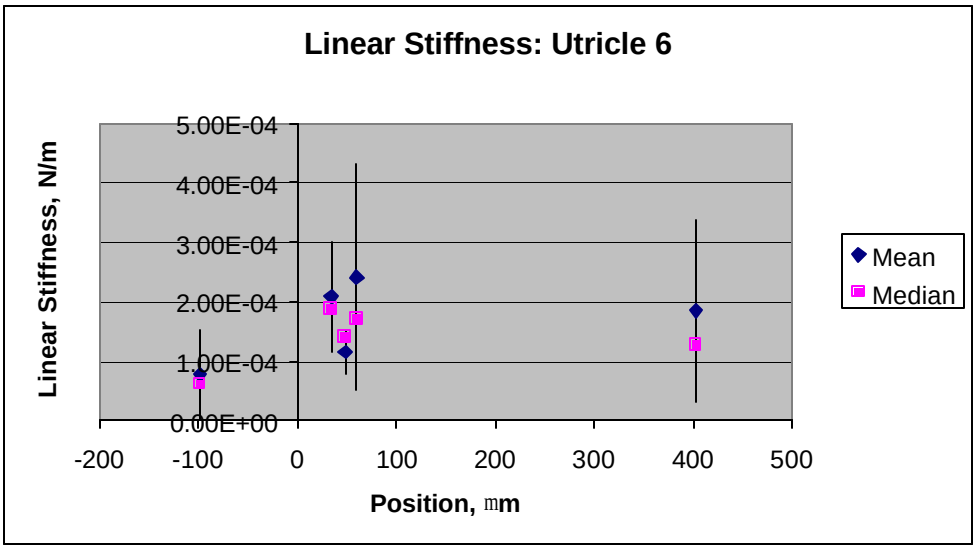
Linear Stiffness: Utricle 6
Linear Stiffness, N/m
5.00E-04
4.00E-04
3.00E-04
2.00E-04
1.00E-04
0.00E+00
-200
-100
0
100
200
300
400
500
Position, mm
Mean
Median

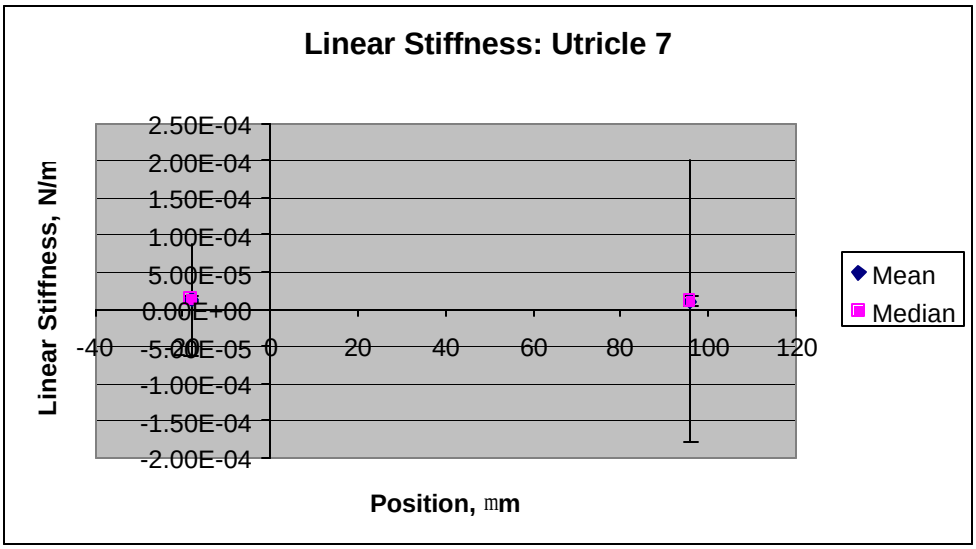
Linear Stiffness: Utricle 7
Linear Stiffness, N/m
2.50E-04
2.00E-04
1.50E-04
1.00E-04
5.00E-05
0.00E+00
-5.00E-05
-1.00E-04
-1.50E-04
-2.00E-04
-40
-20
0
20
40
60
80
100
120
Position, mm
Mean
Median

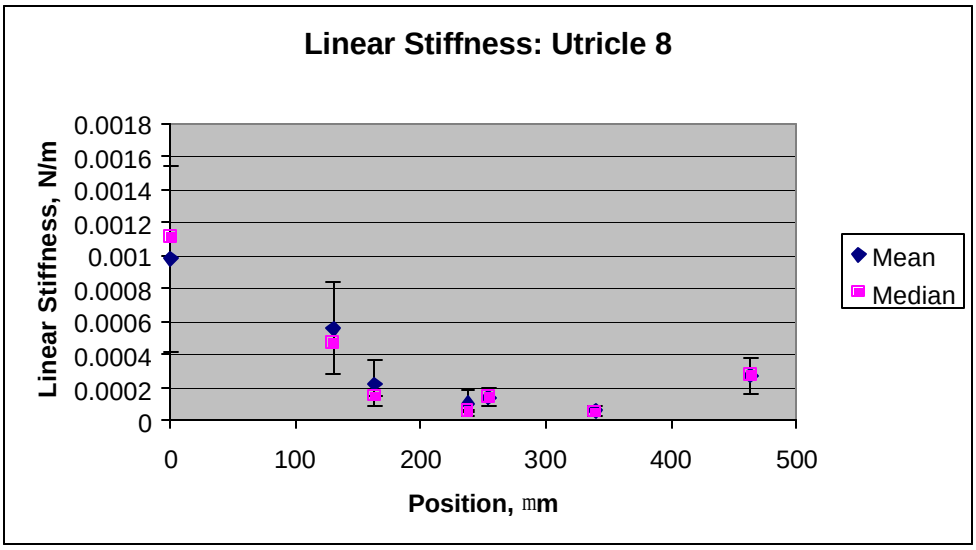
Linear Stiffness: Utricle 8
Linear Stiffness, N/m
0.0018
0.0016
0.0014
0.0012
0.001
0.0008
0.0006
0.0004
0.0002
0
0
100
200
300
400
500
Position, mm
Mean
Median

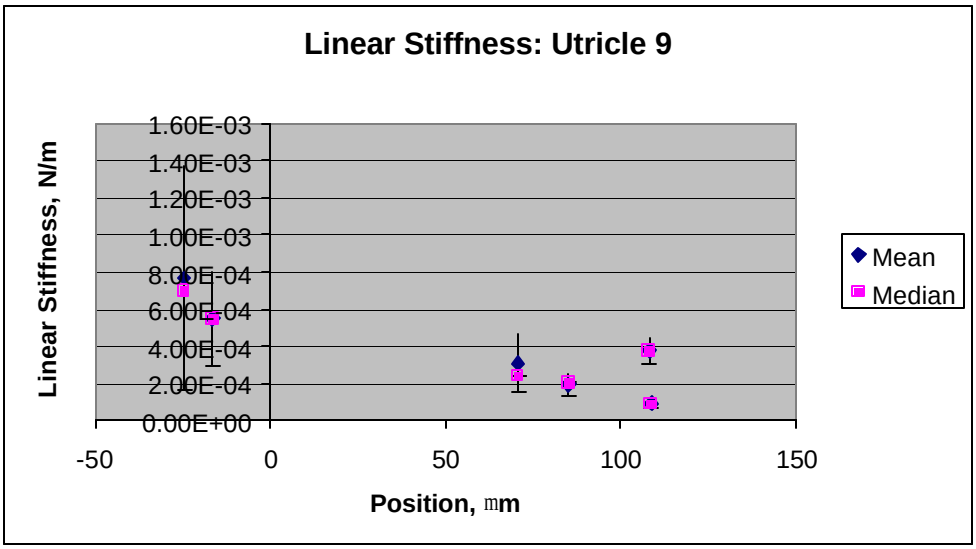
Linear Stiffness: Utricle 9
Linear Stiffness, N/m
1.60E-03
1.40E-03
1.20E-03
1.00E-03
8.00E-04
6.00E-04
4.00E-04
2.00E-04
0.00E+00
-50
0
50
100
150
Position, mm
Mean
Median

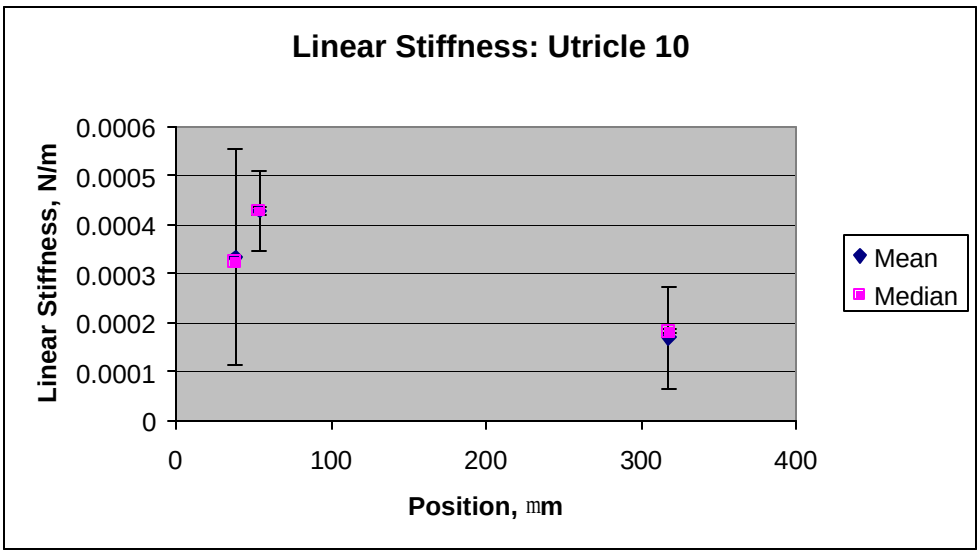
Linear Stiffness: Utricle 10
Linear Stiffness, N/m
0.0006
0.0005
0.0004
0.0003
0.0002
0.0001
0
0
100
200
300
400
Position, mm
Mean
Median

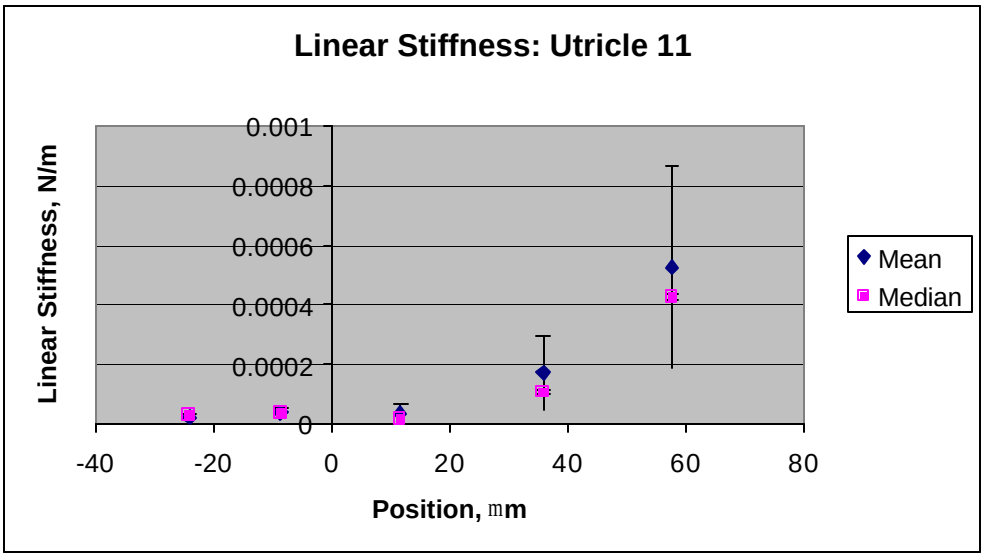
Linear Stiffness: Utricle 11
Linear Stiffness, N/m
0.001
0.0008
0.0006
0.0004
0.0002
0
-40
-20
0
20
40
60
80
Position, mm
Mean
Median

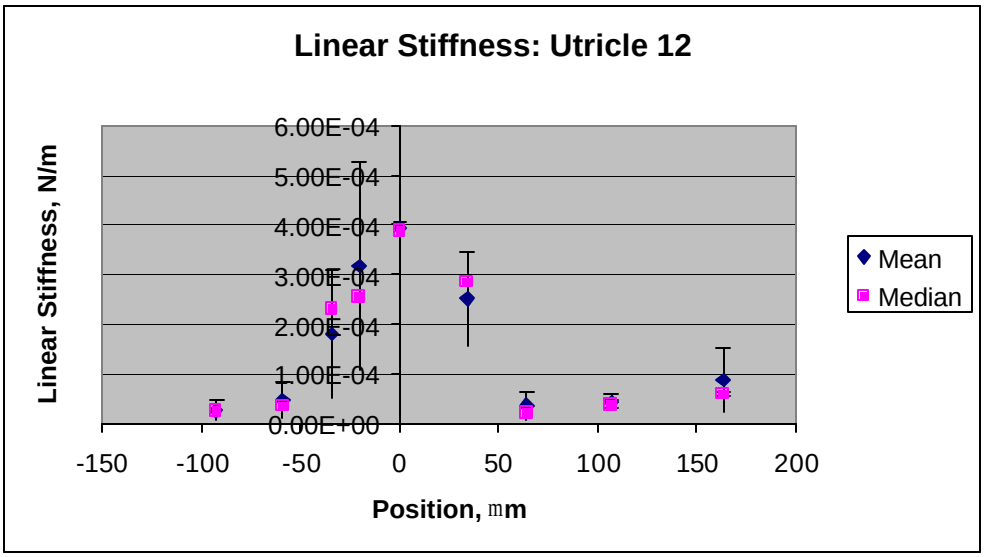
Linear Stiffness: Utricle 12
Linear Stiffness, N/m
6.00E-04
5.00E-04
4.00E-04
3.00E-04
2.00E-04
1.00E-04
0.00E+00
-150
-100
-50
0
50
100
150
200
Position, mm
Mean
Median

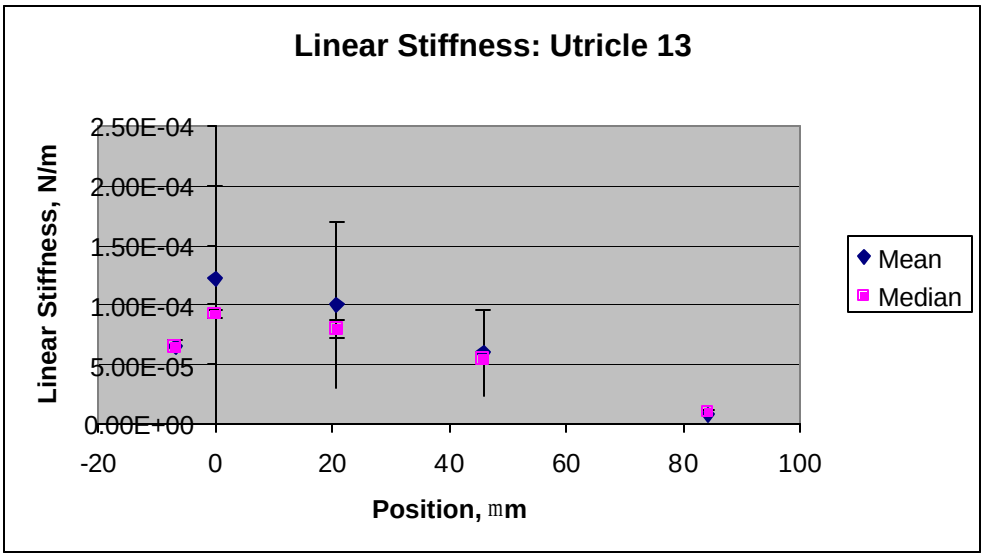
Linear Stiffness: Utricle 13
Linear Stiffness, N/m
2.50E-04
2.00E-04
1.50E-04
1.00E-04
5.00E-05
0.00E+00
-20
0
20
40
60
80
100
Position, mm
Mean
Median

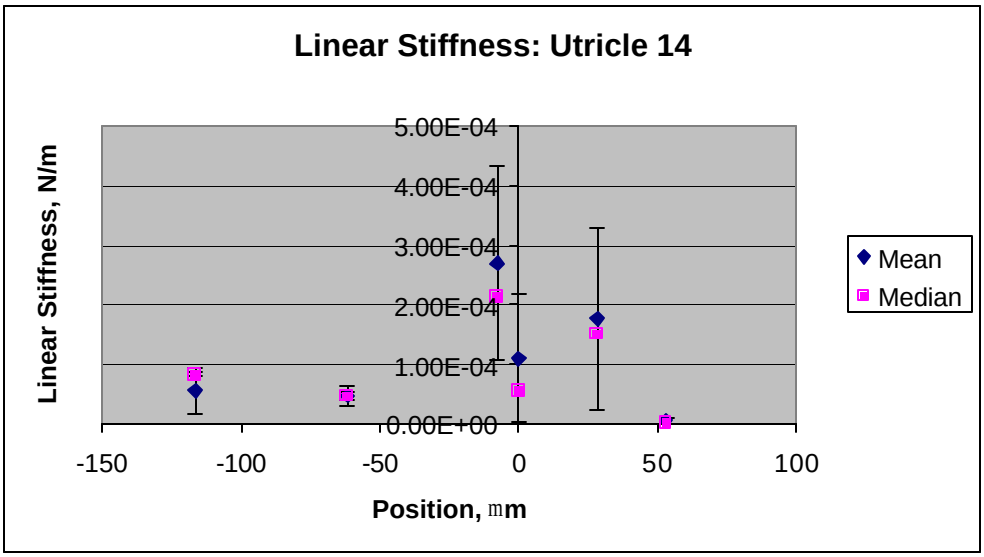
Linear Stiffness: Utricle 14
Linear Stiffness, N/m
5.00E-04
4.00E-04
3.00E-04
2.00E-04
1.00E-04
0.00E+00
-150
-100
-50
0
50
100
Position, mm
Mean
Median

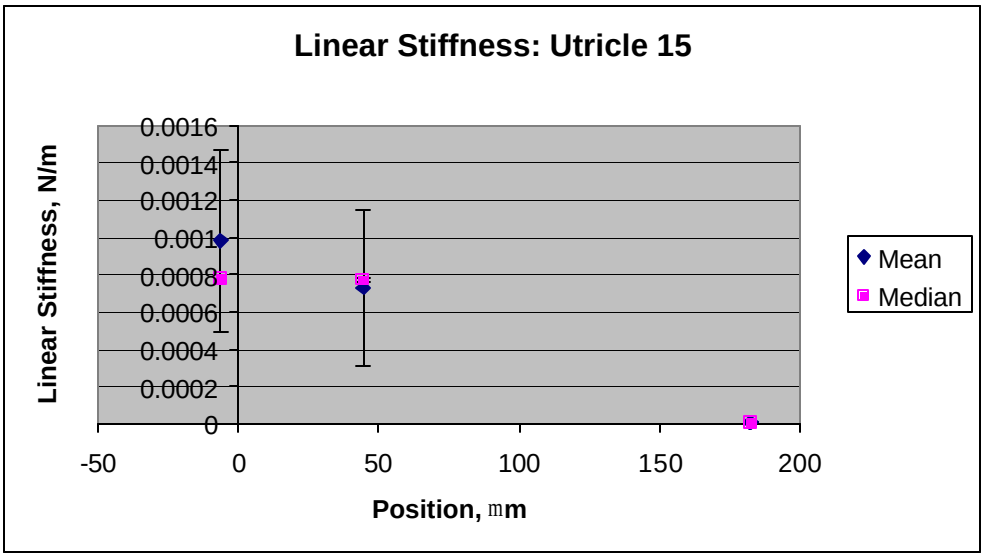
Linear Stiffness: Utricle 15
Linear Stiffness, N/m
0.0016
0.0014
0.0012
0.001
0.0008
0.0006
0.0004
0.0002
0
-50
0
50
100
150
200
Position, mm
Mean
Median

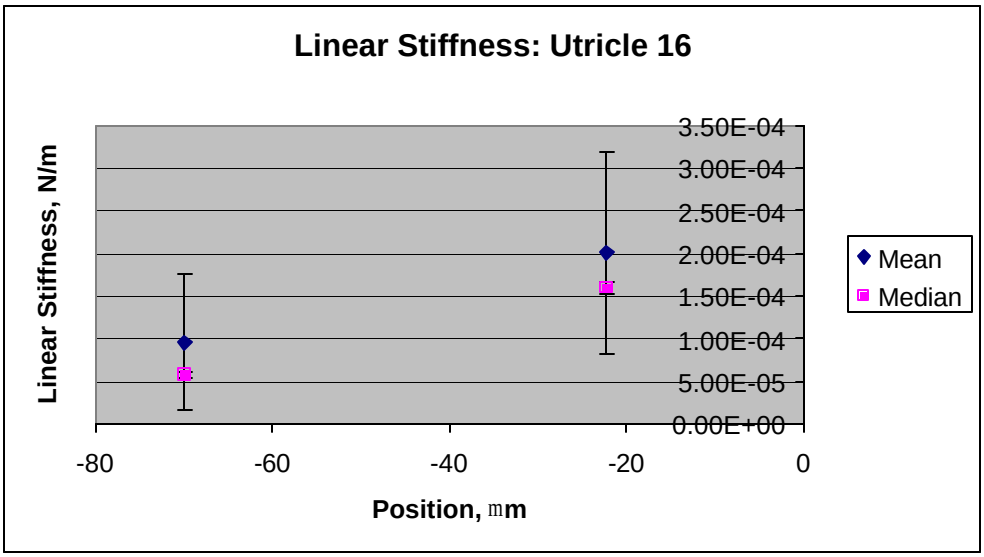
Linear Stiffness: Utricle 16
Linear Stiffness, N/m
3.50E-04
3.00E-04
2.50E-04
2.00E-04
1.50E-04
1.00E-04
5.00E-05
0.00E+00
-80
-60
-40
-20
0
Position, mm
Mean
Median

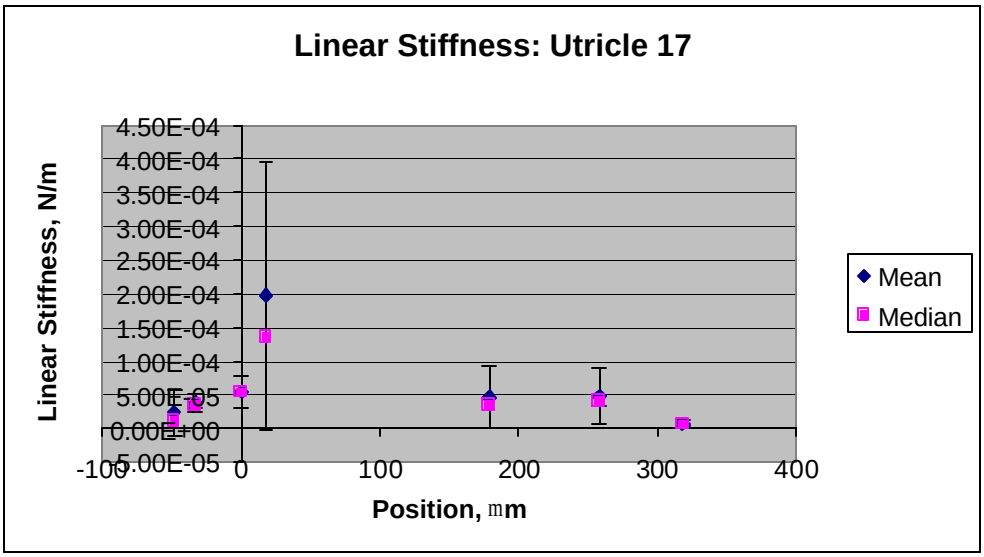
Linear Stiffness: Utricle 17
Linear Stiffness, N/m
4.50E-04
4.00E-04
3.50E-04
3.00E-04
2.50E-04
2.00E-04
1.50E-04
1.00E-04
5.00E-05
0.00E+00
-5.00E-05
-100
0
100
200
300
400
Position, mm
Mean
Median

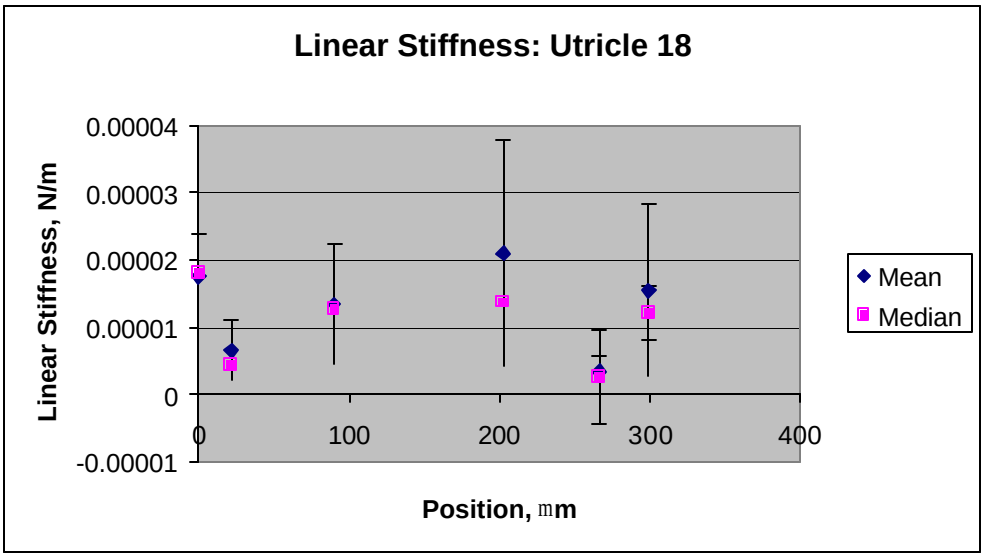
Linear Stiffness: Utricle 18
Linear Stiffness, N/m
0.00004
0.00003
0.00002
0.00001
0
-0.00001
0
100
200
300
400
Position, mm
Mean
Median

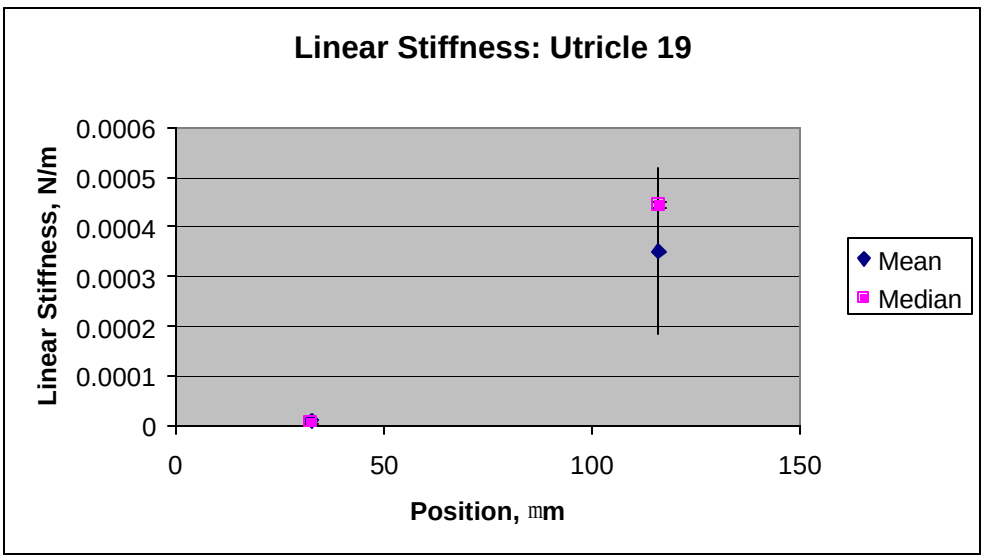
Linear Stiffness: Utricle 19
Linear Stiffness, N/m
0.0006
0.0005
0.0004
0.0003
0.0002
0.0001
0
0
50
100
150
Position, mm
Mean
Median

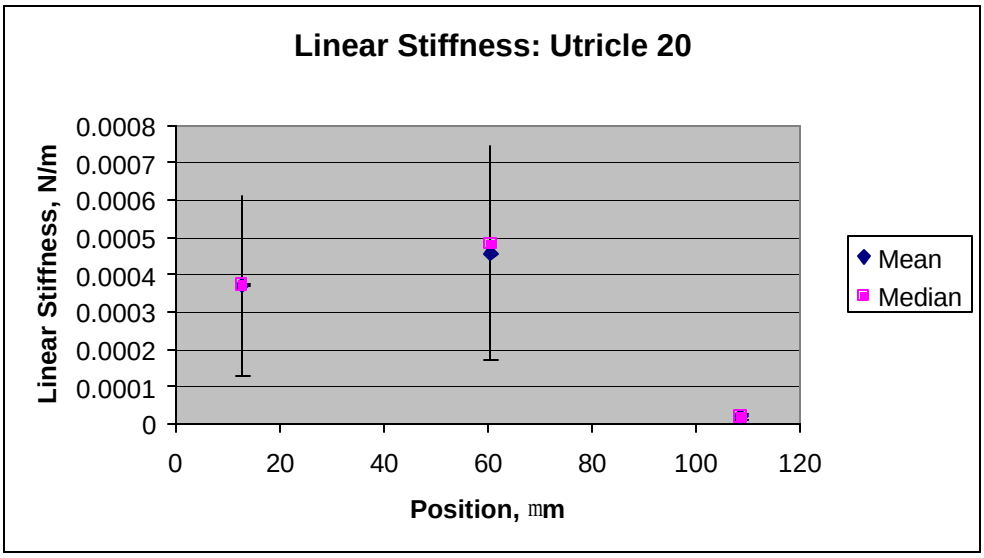
Linear Stiffness: Utricle 20
Linear Stiffness, N/m
0.0008
0.0007
0.0006
0.0005
0.0004
0.0003
0.0002
0.0001
0
0
20
40
60
80
100
120
Position, mm
Mean
Median

APPENDIX C: TORSIONAL STIFFNESS VERSUS POSITION PLOTS FOR ALL UTRICLES TESTED

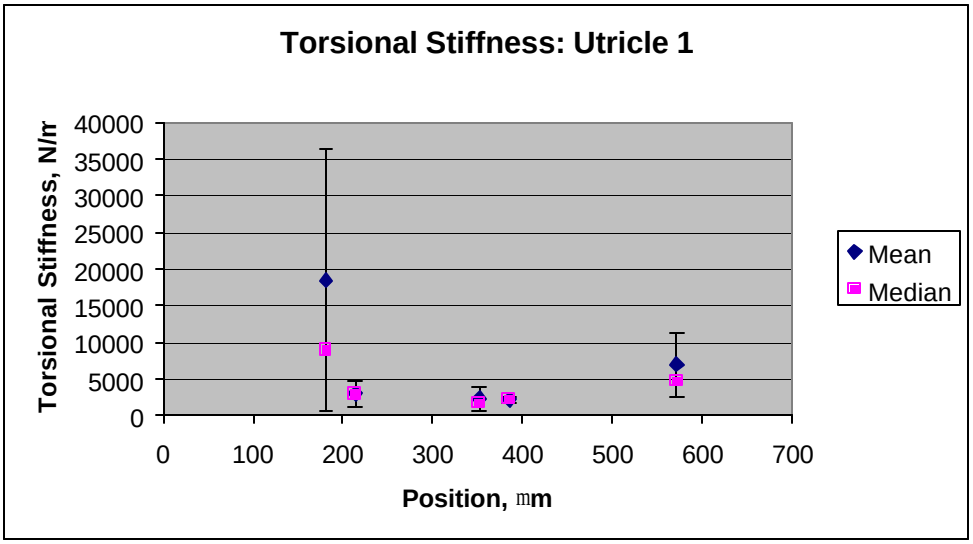

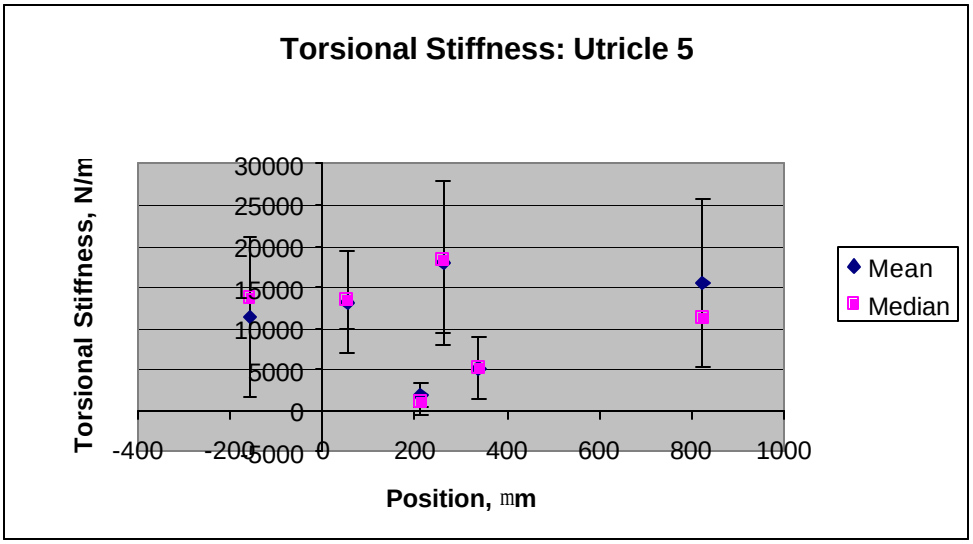

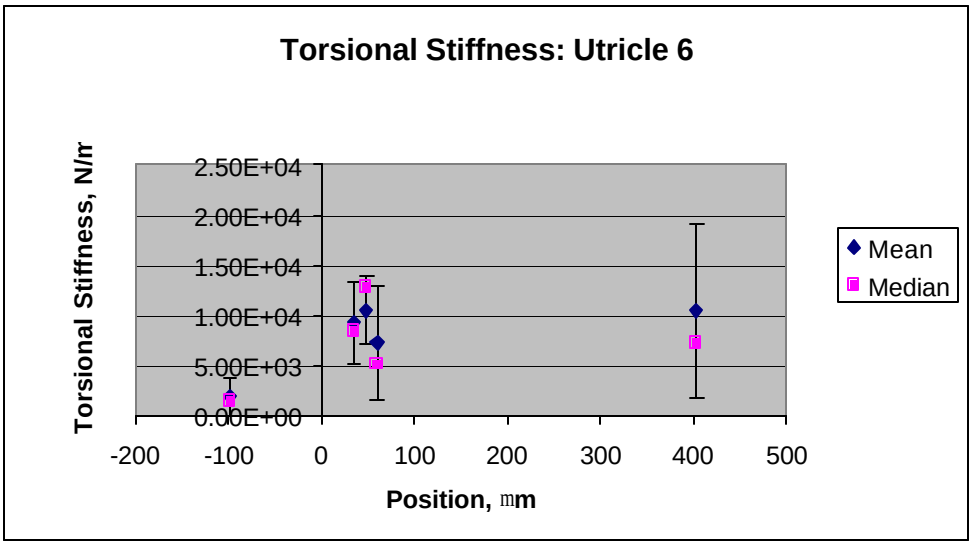
Torsional Stiffness: Utricle 6
Torsional Stiffness, N/m
2.50E+04
2.00E+04
1.50E+04
1.00E+04
5.00E+03
0.00E+00
-200
-100
0
100
200
300
400
500
Position, mm
Mean
Median

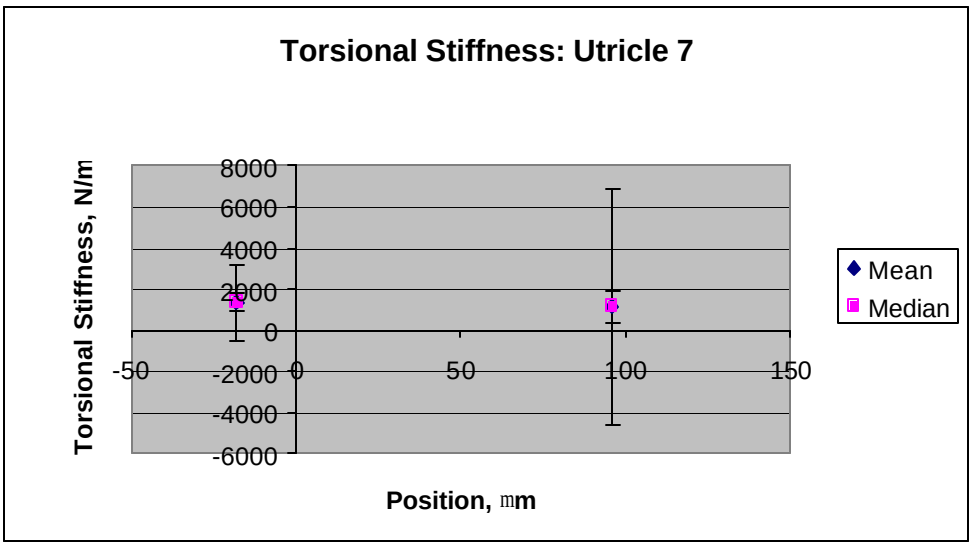
Torsional Stiffness: Utricle 7
Torsional Stiffness, N/m
8000
6000
4000
2000
0
-2000
-4000
-6000
-50
0
50
100
150
Position, mm
Mean
Median

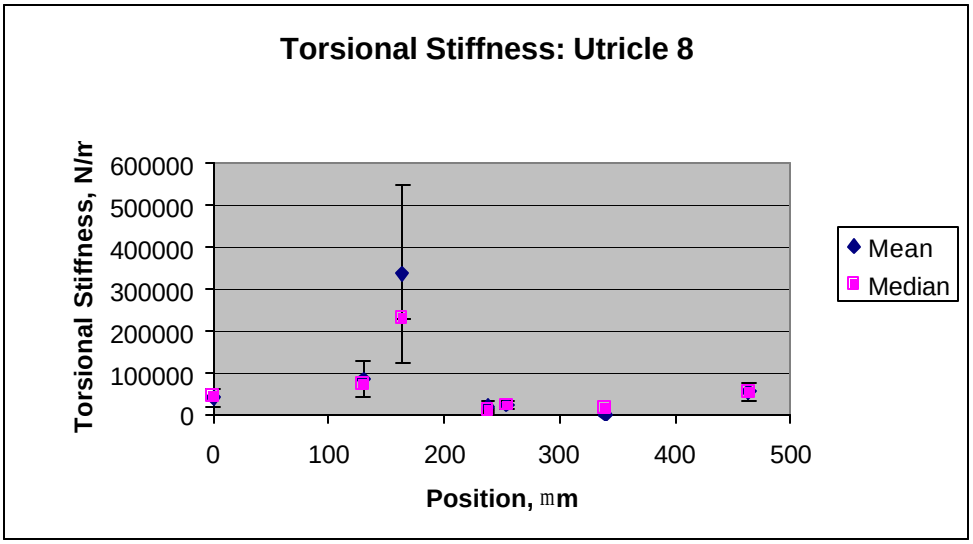
Torsional Stiffness: Utricle 8
Torsional Stiffness, N/m
600000
500000
400000
300000
200000
100000
0
0
100
200
300
400
500
Position, mm
Mean
Median

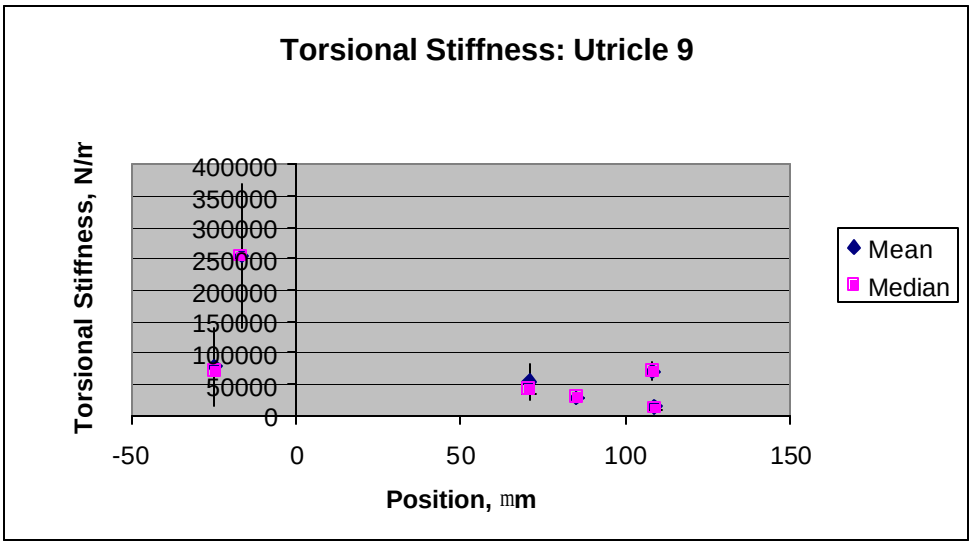
Torsional Stiffness: Utricle 9
Torsional Stiffness, N/m
400000
350000
300000
250000
200000
150000
100000
50000
0
-50
0
50
100
150
Position, mm
Mean
Median

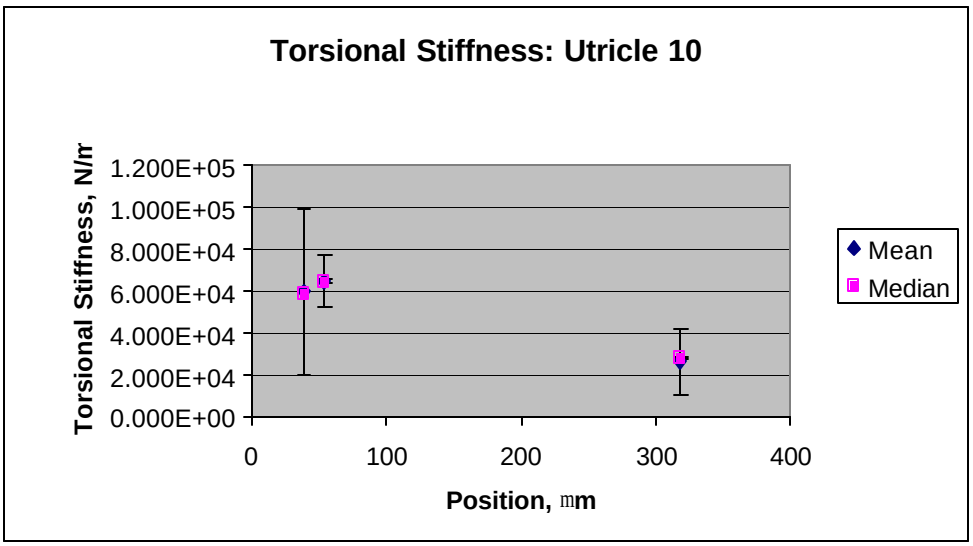
Torsional Stiffness: Utricle 10
Torsional Stiffness, N/m
1.200E+05
1.000E+05
8.000E+04
6.000E+04
4.000E+04
2.000E+04
0.000E+00
0
100
200
300
400
Position, mm
Mean
Median

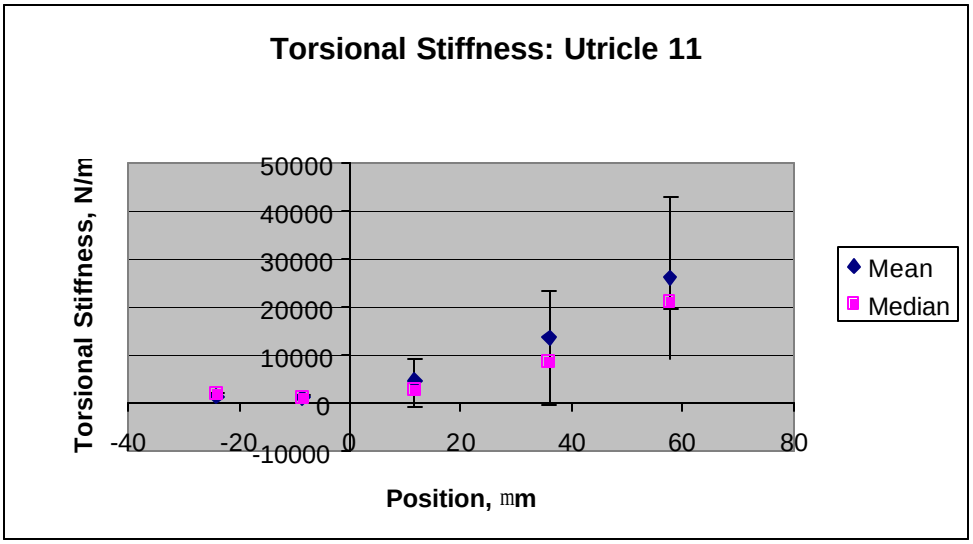
Torsional Stiffness: Utricle 11
Torsional Stiffness, N/m
50000
40000
30000
20000
10000
0
-10000
-40
-20
0
20
40
60
80
Position, mm
Mean
Median

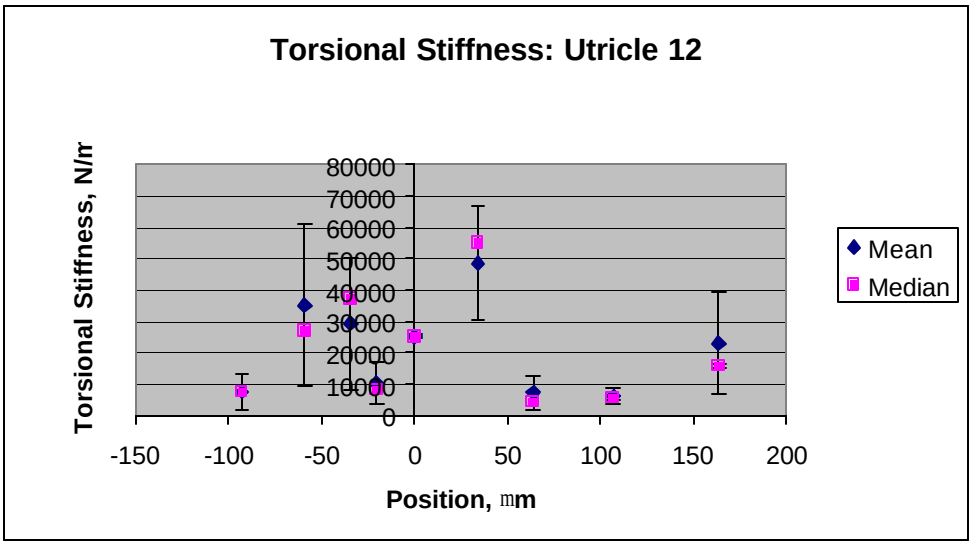
Torsional Stiffness: Utricle 12
Torsional Stiffness, N/m
80000
70000
60000
50000
40000
30000
20000
10000
0
-150
-100
-50
0
50
100
150
200
Position, mm
Mean
Median

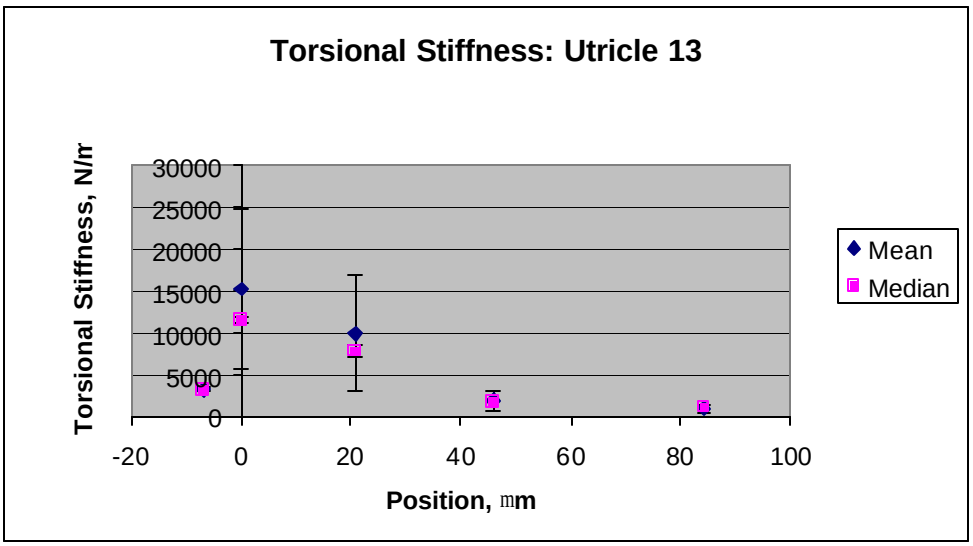
Torsional Stiffness: Utricle 13
Torsional Stiffness, N/m
30000
25000
20000
15000
10000
5000
0
-20
0
20
40
60
80
100
Position, mm
Mean
Median

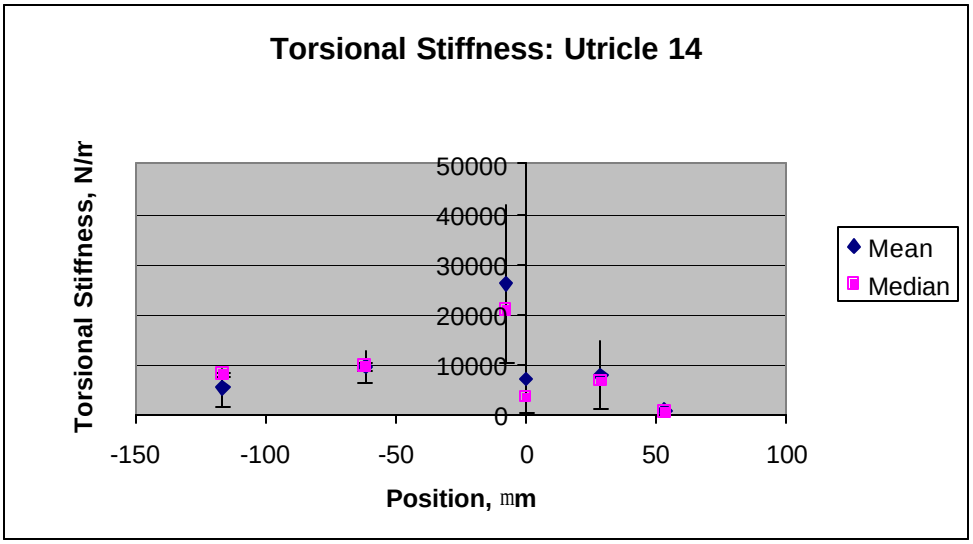
Torsional Stiffness: Utricle 14
Torsional Stiffness, N/m
50000
40000
30000
20000
10000
0
-150
-100
-50
0
50
100
Position, mm
Mean
Median

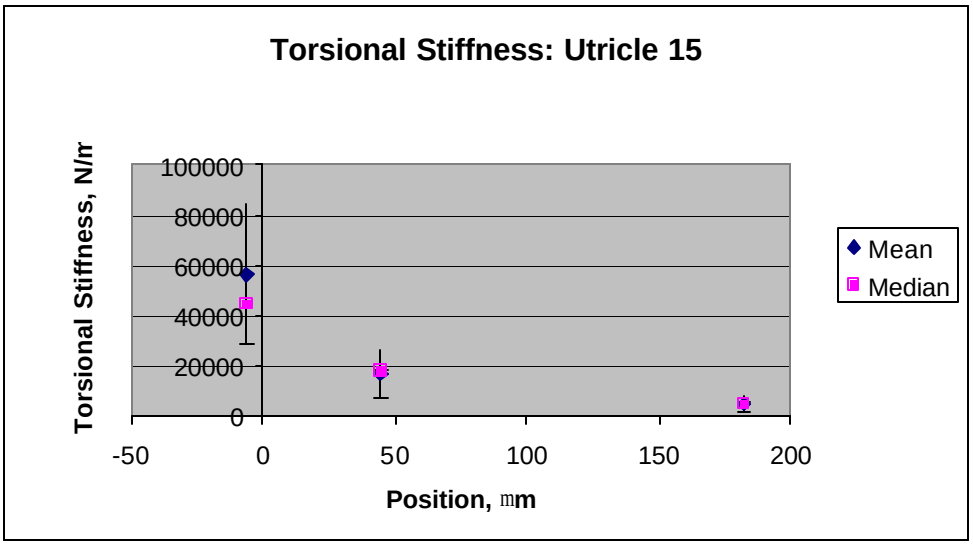
Torsional Stiffness: Utricle 15
Torsional Stiffness, N/m
100000
80000
60000
40000
20000
0
-50
0
50
100
150
200
Position, mm
Mean
Median

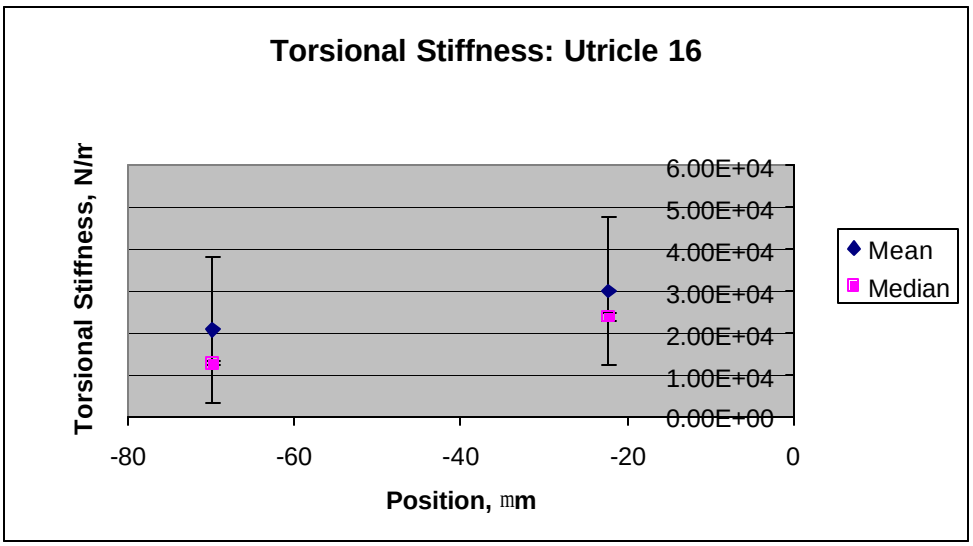
Torsional Stiffness: Utricle 16
Torsional Stiffness, N/m
6.00E+04
5.00E+04
4.00E+04
3.00E+04
2.00E+04
1.00E+04
0.00E+00
-80
-60
-40
-20
0
Position, mm
Mean
Median

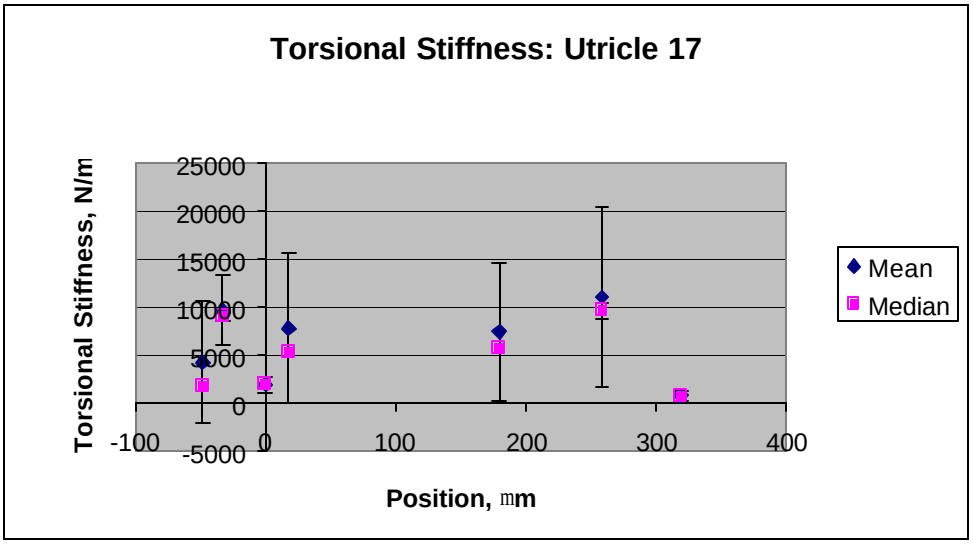
Torsional Stiffness: Utricle 17
Torsional Stiffness, N/m
25000
20000
15000
10000
5000
0
-5000
-100
0
100
200
300
400
Position, mm
Mean
Median

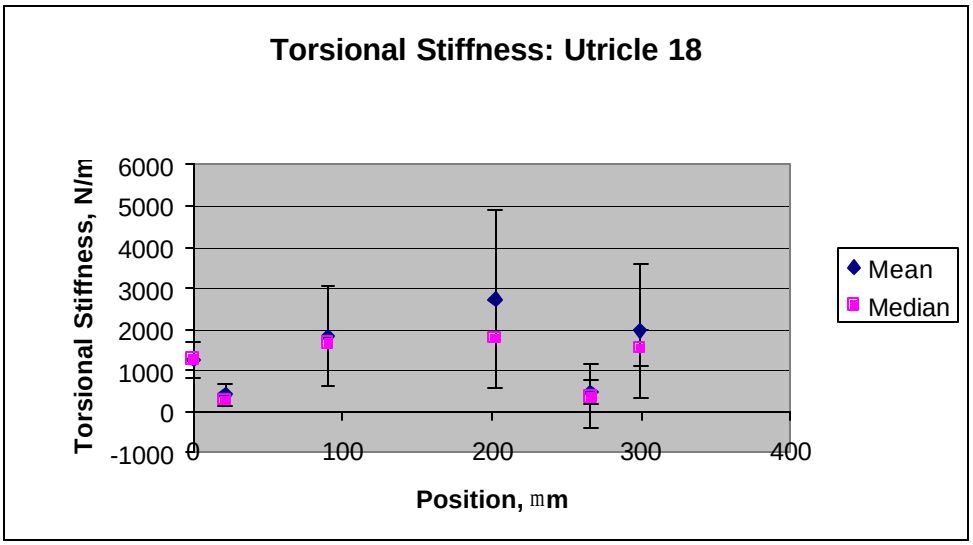
Torsional Stiffness: Utricle 18
Torsional Stiffness, N/m
6000
5000
4000
3000
2000
1000
0
-1000
0
100
200
300
400
Position, mm
Mean
Median

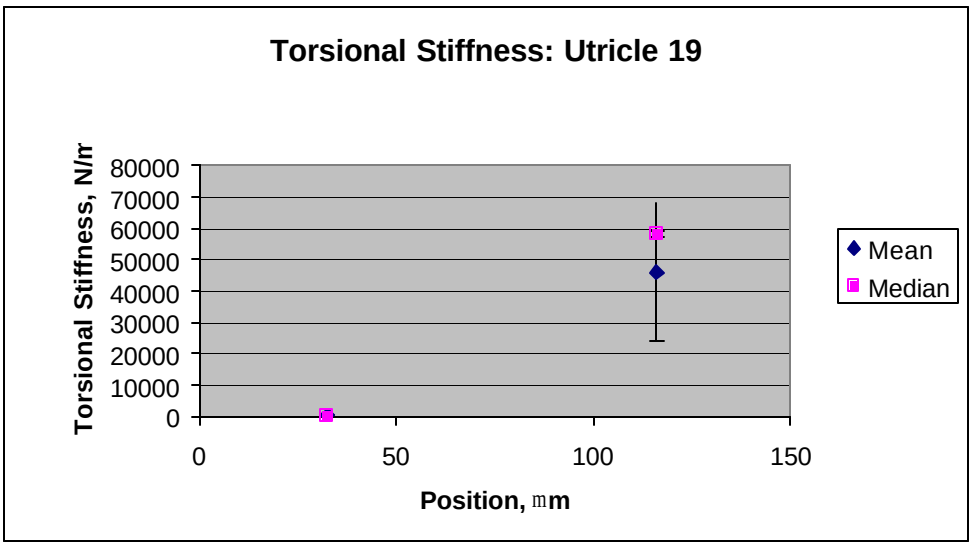
Torsional Stiffness: Utricle 19
Torsional Stiffness, N/m
80000
70000
60000
50000
40000
30000
20000
10000
0
0
50
100
150
Position, mm
Mean
Median

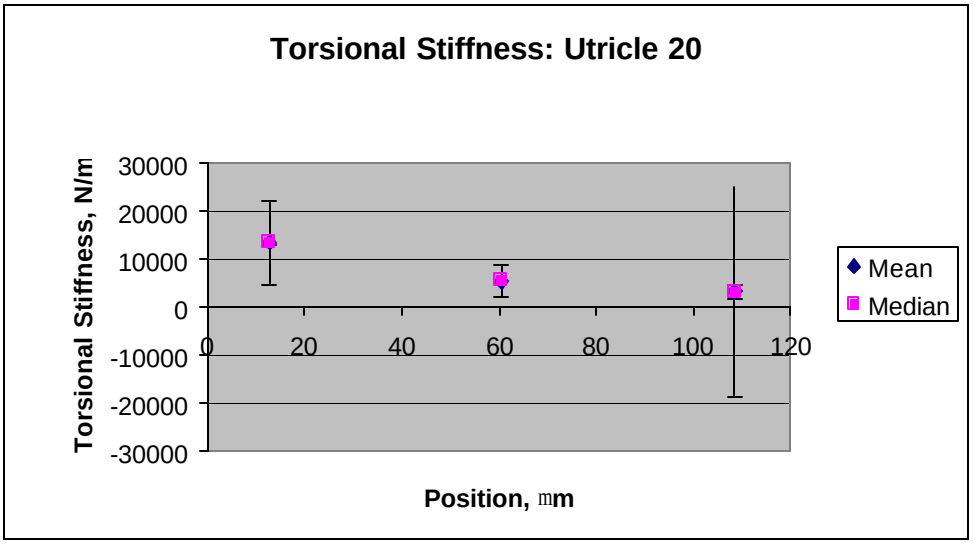
Torsional Stiffness: Utricle 20
Torsional Stiffness, N/m
30000
20000
10000
0
-10000
-20000
-30000
0
20
40
60
80
100
120
Position, mm
Mean
Median

VITA

Jennifer Mary Silverman was born in Washington D.C. on May 10, 1979. She spent her childhood in Myersville, Maryland and graduated as valedictorian of Middletown High School in 1997. In May of 2001, she received her Bachelor of Science majoring in Engineering Science and Mechanics, minoring in Mathematics and Chemistry, and concentrating in Biomechanics. In addition to her academic studies, Ms. Silverman enjoys volunteering in the community. Upon graduation with her Master of Science in Engineering Mechanics and a concentration in Biomedical Engineering, she will attend the Medical College of Virginia School of Medicine.